

2014-04-23

Digital Pre-distortion for Interference Reduction in Dynamic Spectrum Access Networks

Zhu Fu

Worcester Polytechnic Institute

Follow this and additional works at: <https://digitalcommons.wpi.edu/etd-dissertations>

Repository Citation

Fu, Z. (2014). *Digital Pre-distortion for Interference Reduction in Dynamic Spectrum Access Networks*. Retrieved from <https://digitalcommons.wpi.edu/etd-dissertations/152>

This dissertation is brought to you for free and open access by [Digital WPI](#). It has been accepted for inclusion in Doctoral Dissertations (All Dissertations, All Years) by an authorized administrator of Digital WPI. For more information, please contact wpi-etd@wpi.edu.

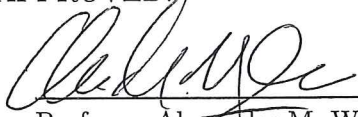
Digital Pre-distortion for Interference Reduction in Dynamic Spectrum Access Networks

Zhu Fu

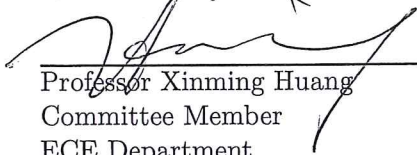
A Dissertation
Submitted to the Faculty
of the
WORCESTER POLYTECHNIC INSTITUTE
in partial fulfillment of the requirements for the
Degree of Doctor of Philosophy
in
Electrical and Computer Engineering

May 2014

APPROVED:



Professor Alexander M. Wyglinski
Primary Advisor
ECE Department
Worcester Polytechnic Institute



Professor Xinming Huang
Committee Member
ECE Department
Worcester Polytechnic Institute



Professor Donald R. Brown III
Committee Member
ECE Department
Worcester Polytechnic Institute



Professor Mikko Valkama
Committee Member
Department of Communications Engineering
Tampere University of Technology

Abstract

Given the ever increasing reliance of today's society on ubiquitous wireless access, the paradigm of dynamic spectrum access (DSA) as been proposed and implemented for utilizing the limited wireless spectrum more efficiently. Orthogonal frequency division multiplexing (OFDM) is growing in popularity for adoption into wireless services employing DSA framework, due to its high bandwidth efficiency and resiliency to multipath fading. While these advantages have been proven for many wireless applications, including LTE-Advanced and numerous IEEE wireless standards, one potential drawback of OFDM or its non-contiguous variant, NC-OFDM, is that it exhibits high peak-to-average power ratios (PAPR), which can induce in-band and out-of-band (OOB) distortions when the peaks of the waveform enter the compression region of the transmitter power amplifier (PA). Such OOB emissions can interfere with existing neighboring transmissions, and thereby severely deteriorate the reliability of the DSA network.

A performance-enhancing digital pre-distortion (DPD) technique compensating for PA and in-phase/quadrature (I/Q) modulator distortions is proposed in this dissertation. Although substantial research efforts into designing DPD schemes have already been presented in the open literature, there still exists numerous opportunities to further improve upon the performance of OOB suppression for NC-OFDM transmission in the presence of RF front-end impairments. A set of orthogonal polynomial basis functions is proposed in this dissertation together with a simplified joint DPD structure. A performance analysis is presented to show that the OOB emissions is reduced to approximately 50 dBc with proposed algorithms employed during NC-OFDM transmission.

Furthermore, a novel and intuitive DPD solution that can minimize the power regrowth at any pre-specified frequency in the spurious domain is proposed in this dissertation. Conventional DPD methods have been proven to be able to effectively reduce the OOB emissions that fall on top of adjacent channels. However more spectral emissions in more distant frequency ranges are generated by employing such DPD solutions, which are potentially in violation of the spurious emission limit. At the same time, the emissions in adjacent chan-

nel must be kept under the OOB limit. To the best of the author's knowledge, there has not been extensive research conducted on this topic. Mathematical derivation procedures of the proposed algorithm are provided for both memoryless nonlinear model and memory-based nonlinear model. Simulation results show that the proposed method is able to provide a good balance of OOB emissions and emissions in the far out spurious domain, by reducing the spurious emissions by 4–5 dB while maintaining the adjacent channel leakage ratio (ACLR) improvement by at least 10 dB, comparing to the PA output spectrum without any DPD.

Acknowledgements

The work for this thesis was carried out over the years 2011-2014 at the Department of Electrical and Computer Engineering (ECE), Worcester Polytechnic Institute, Worcester, MA, USA. Several individuals have contributed to the thesis process and the final outcome, and they all deserve a special mention.

First and foremost, I would like to express my deepest gratitude to my supervisor Professor Alexander Wyglinski for his excellent guidance, continual encouragement and support, and actually being the best supervisor I have ever expected. I feel very grateful that Professor Wyglinski decided to take me as his student four years ago, my life path, which I am very happy with, wouldn't be the same without him. It is truly my honor to have worked for him.

I also wish to extend my sincere thanks to Professor D. Richard Brown, Professor Xinming Huang and Professor Mikko Valkama, for agreeing to be my committee members and being so responsible by providing all the great advices to guide my study. I would also like to express my gratitude to Lauri Anttila, who is working for Professor Mikko Valkama in Tampere University of Technology, Tampere, Finland, for introducing me to the details of my research area and continually giving me great advices in my research and paper writing process. I also would like to thank all the professors in WPI who I have been working with as their teaching assistants, I have learned a lot from all of them.

During the four years, Professor Wyglinski was kind enough to allow me doing two internships first in Broadcom and then in Qualcomm. I would like to say thank you to my managers and mentors Dan English, Adam Bezanson, Jeremy Dunworth, Vladimir Aparin and Sameer Vora, for offering the great work opportunities both of which are helpful to my research.

I am also grateful that I have known many good friends during my stay in WPI. I would like to thank my best friend Sean Rocke, who offered me great help adjusting to the pace of study and research in WPI and always encouraging me when I was under stress. I also wish to thank Le Wang, for being an excellent friend by tolerating my temper and taking great care of me during the last year of my stay in WPI. I am also thankful to all the students in

our research lab for keeping me good company.

As always, I am deeply indebted to my grandparents, my parents and the rest of my family in China, for their love, tolerance and unwavering belief in me throughout this degree and my life. Especially I would like to dedicate all my achievement to my grandma who passed away in 2012 when I was in US, she was the best grandma and had great impacts in my life. Thank you for everything.

Finally, I would like to thank Zhengyang Luo for his love, understanding, sharing and support, thank you for making my life so much easier than it could be.

Contents

List of Figures	vii
List of Tables	ix
List of Abbreviations	x
1 Introduction	1
1.1 Spectrum Interference in Wireless Networks	1
1.2 Research Objectives	4
1.3 Related Work	5
1.4 Thesis Contributions	7
1.5 Thesis Outline	8
1.6 List of Publications	9
2 Practical Considerations of Wireless Transceivers	11
2.1 Chapter Introduction	11
2.2 Overview of Reconfigurable Multi-standard RF Transmitters	12
2.2.1 Typical Architectures of RF Transceivers	12
2.2.2 Characteristics of RF Power Amplifiers	15
2.2.3 Impairments of Other Key Components on the RF Front-end	25
2.3 Spectrally Agile Transmission in Cognitive Radio (CR) Networks	26
2.3.1 Overview of CR Networks	26
2.3.2 First-step in CR Realization: Carrier Aggregation in LTE-Advanced	27
2.3.3 Regulations for Operating Dynamic Spectrum Access (DSA) Networks in TVWS	29
2.3.4 Potential Spectral Interference in DSA Network	32
2.4 Chapter Summary	35
3 Power Amplifier Linearization Techniques for Distortion Reduction	36
3.1 Chapter Introduction	36
3.2 An Overview of Common Techniques for Power Amplifier Linearization	37
3.2.1 Feedback and Feedforward Method	37
3.2.2 Predistortion Method	38
3.2.3 Outphasing PA System	40

3.2.4	Summary of PA linearization methods	42
3.3	Adaptive Digital Pre-distortion	43
3.3.1	DPD Structure-identification	44
3.3.2	DPD Parameter-identification	48
3.3.3	Iterative Steps for DPD System Identification	53
3.3.4	Features and Drawbacks of Current DPD techniques	54
3.4	Chapter Summary	56
4	Proposed DPD Method for OOB Emission Reduction	57
4.1	Chapter Introduction	57
4.2	Proposed DPD System Identification Solutions	59
4.2.1	DPD Structure for PA	59
4.2.2	Parameter Identification with Proposed Orthogonal Basis Functions	61
4.2.3	Simplified DPD Structure for Joint PA and I/Q Modulator	65
4.3	Simulation and Measurement Results	68
4.3.1	Mathematical Simulation	68
4.3.2	Hardware Experiment	74
4.4	Chapter Summary	77
5	Proposed DPD method for Spurious Emission Reduction	79
5.1	Chapter Introduction	79
5.2	Problem Statement and Motivation	80
5.3	Mathematical Analysis of the Proposed Digital Predistortion Solutions	83
5.4	Parameter Estimation of the Proposed Predistorter	85
5.5	Examples and Simulation Results	88
5.6	Chapter Summary	95
6	Conclusion	97
6.1	Research Achievements	97
6.2	Future Work	98
6.3	List of Publications	98
	Bibliography	100

List of Figures

1.1	A concept diagram showing the growing data rates of IEEE 802.11 standards over time [1, 2].	2
1.2	An illustration showing how NC-OFDM works in a DSA environment. . .	3
1.3	A typical transceiver architecture with DPD function employed on a SDR platform.	4
2.1	Typical transmitter and receiver structures.	13
2.2	DC and AC load lines with equivalent circuits.	16
2.3	Signal clipping determined by location of Q-point.	17
2.4	PA output power and IMP power versus input power.	18
2.5	Output current of different class operations of the PA.	20
2.6	Nonlinear effects caused by power amplifier.	21
2.7	Illustration of the error vector.	22
2.8	Intermodulation products in a two-tone transmission.	24
2.9	Examples of AM/AM and AM/PM plots.	25
2.10	General review of Adjacent Channel Power Ratio (ACPR).	26
2.11	LTE-Advanced Carrier Aggregation (CC) operating in FDD mode, with three CCs aggregated. The CCs can be of different bandwidths.	28
2.12	VHF and UHF television channels and frequencies.	30
2.13	Example spectrum of Dynamic Spectrum Access network with interference.	33
3.1	A typical Cartesian Feedback System.	38
3.2	Illustration of Analog PD and DPD.	39
3.3	A typical Adaptive DPD System.	40
3.4	Illustration of different complex signal representations.	41
3.5	General architecture of PA with Digital Pre-distortion employed.	43
3.6	Some common nonlinear nonorthogonal models.	46
3.7	Direct Learning Architecture (DLA).	49
3.8	Indirect Learning Architecture (ILA).	49
3.9	A general DPD parameter identification architecture.	50
3.10	Illustration of MSE surface of LMS and block LS methods.	52
3.11	Illustration of iterative steps in ILA structure.	54
3.12	Illustration of possible spectrum interference caused by employing DPD. . .	55

4.1	Proposed parallel Hammerstein predistorter structure based on orthogonal polynomials.	63
4.2	A general overview of the NC-OFDM transmitting system with proposed digital PD approach employed.	66
4.3	ILA for joint DPD parameter identification.	67
4.4	Normalized AM/AM for nonlinear and linearized PA model (16-QAM. . . .	70
4.5	Output PSD of PA model with DPD employed tested on 16-QAM input signal.	71
4.6	Output spectra of the direct-conversion transmitter model.	71
4.7	Schematic of NC-OFDM transmitter employing cascaded band reject filters	72
4.8	Output spectra of the direct-conversion transmitter model without DPD technique.	72
4.9	Normalized output magnitudes (AM/AM) and phase shift (AM/PM) versus input magnitudes. Including nonlinear and linearized direct-conversion transmitter models.	73
4.10	Measured power levels on Rx end by sweeping Tx power gain from Tx end, over a range of frequencies supported by XCVR2450 dual-band transceiver daughter cards.	75
4.11	Block diagram of elements on USRP 2 hardware.	76
4.12	Hardware test-bed setup for experimental measurements on USRP 2.	77
4.13	PSD of NC-OFDM signals output from USRP2 with and without DPD. . . .	78
5.1	Transmitter RF spectrum. It is composed of channel bandwidth, OOB emissions and the spurious domain.	81
5.2	Output spectrum of a transmitter (a) with no DPD, (b) with conventional DPD, (c) employing FDD mode with power limit and (d) with proposed DPD.	81
5.3	Block diagram showing signal processing procedures in the proposed DPD method.	85
5.4	Implementation of Newton-Raphson method in the proposed DPD method for parameter optimization.	86
5.5	The proposed combined predistorter based on ILA. A multiplexer is used to determine whether the parameters of the proposed DPD algorithm or the conventional LS method is selected for the next ILA iteration.	87
5.6	PA output PSD plots of 16-QAM baseband waveform in the fourth ILA iteration with no DPD, proposed DPD, combined DPD and conventional DPD methods employed.	91
5.7	PA output PSD plots of 20 MHz baseband LTE waveform in the fourth ILA iteration with no DPD, proposed DPD, combined DPD and conventional DPD methods employed.	93
5.8	PA output PSD plots of baseband NC-OFDM waveform in the fourth ILA iteration with no DPD, proposed DPD, combined DPD and conventional DPD methods employed.	94

List of Tables

2.1	Comparisons of different Tx architectures.	15
2.2	Illustration of intermodulation products.	23
3.1	Summary of common PA linearization methods.	42
4.1	Principal notations used in the chapter	59
4.2	1-dB compression points of RF frequencies supported by XCVR2450	74
5.1	Values of SER at 2 MHz and ACLR with Different DPD Methods Employed on Quasi-memoryless Models and 16-QAM Baseband Waveform.	92
5.2	Values of SER at 34 MHz and ACLR with Different DPD Method Employed on Quasi-memoryless Models and 20 MHz baseband LTE waveform.	93
5.3	Values of SER at 2 MHz and ACLR with Different DPD Method Employed on Quasi-memoryless Models and 1 MHz baseband NC-OFDM waveform. .	95

List of Abbreviations

3GPP	Third Generation Partnership Project
A/D	Analog-to-digital
ACLR	Adjacent channel leakage power Ratio
ACPR	Adjacent channel power ratio
AM/AM	Amplitude-to-amplitude modulation
AM/PM	Amplitude-to-phase modulation
BRFs	Band reject filters
BS	Base station
CA	Carrier aggregation
CC	Component carrier
D/A	Digital-to-analog
DBPSK	Differential binary phase shift keying
DFT	Discrete Fourier Transform
DL	Downlink
DLA	Direct learning architecture
DPD	Digital predistortion
DSA	Dynamic spectrum access
DSP	Digital signal processor
eNB	Evolved NodeB
EPS	Evolved Packet System
E-UTRA	Evolved Universal Terrestrial Radio Access
E-UTRAN	Evolved Universal Terrestrial Access Network

EVM	Error vector magnitude
FCC	Federal Communications Commission
FDD	Frequency division duplexing
FDM	Frequency division multiplexing
FM	Frequency modulation
FPGA	Field programmable gate array
GSM	Global System for Mobile Communications
HF	High frequency
IF	Intermediate frequency
ILA	Indirect learning architecture
IM	Intermodulation IMD
Intermodulation distortion	
IMPs	Intermodulation products
IMT-A	International Mobile Telecommunications-Advanced
I/Q	Inphase and quadrature
ISI	Intersymbol interference
ISM	Industrial, Scientific and Medical
LINC	Linear amplification using nonlinear component
LMS	Least mean squares
LNA	Low-noise amplifier
LO	Local oscillator
LPFs	Lowpass filters
LS	Least squares
LTE	Long Term Evolution
LTE-A	Long Term Evolution Advanced
LTI	Linear time-invariant
MCM	Multicarrier modulation
MP	emory polynomial
M-PSK	M-ary phase shift keying

M-QAM	M-ary quadrature amplitude modulation
MSE	Mean-square error
NC-MCM	Non-contiguous multicarrier modulation
NC-OFDM	Non-contiguous orthogonal frequency division multiplexing
NLP	Nonlinear program
OFDM	Orthogonal frequency-division multiplexing
OFDMA	Orthogonal Frequency Division Multiple Access
OOB	Out-of-band
PA	Power amplifier
PAPR	Peak-to-average power ratio
PD	Predistortion
PGA	Programmable-gain amplifier
PH	Parallel Hammerstein
PSD	Power spectral density
RF	Radio frequency
RLS	Recursive least squares
Rx	Receiver
SC-FDMA	Single carrier - frequency division multiple access
SDR	Software-defined-radio
SER	Spurious emission ratio
TDD	Time division duplexing
TVWS	Television white spaces
Tx	Transmitter
UE	User equipment
UHF	Ultra-high-frequency
UL	Uplink
USRP	Universal Software Radio Peripheral
VHF	Very-high-frequency
WCDMA	Wideband Code Division Multiple Access

Wi-Fi

Wireless fidelity

WLANs

Wireless local area networks

Chapter 1

Introduction

1.1 Spectrum Interference in Wireless Networks

“Everything will be wireless!” This statement was publicly made during the 2012’s Intel Developer Forum event in San Francisco, California [3]. Wireless communications have enabled us to realize ubiquitous information access almost anywhere around the world. Everyday actions, such as watching a live football game on your tablet, placing an online order with your laptop, and paying your account balance over a cellphone, all involve wireless data transmissions. Over the last several months, the first batch of 5G Wi-Fi 802.11ac devices have started to enter the market. The latest IEEE 802.11ac standard [4] can provide up to 1.3 gigabit per second throughput [5] for wireless local area networks (WLANs) [6] in the 5 GHz band, which is triple the throughput provided by today’s most widely implemented form WiFi, IEEE 802.11n [2], as shown in Fig. 1.1. In the future, the wired gigabit ethernet networking at home and in the office may eventually be replaced by Wi-Fi.

With these ever increasing demands for new wireless services, coupled with limited radio frequency (RF) spectrum resources, a potential spectrum scarcity problem has emerged due to the fact that most of the spectrum has already been exclusively assigned to licensed users with traditional wireless spectrum regulatory processes [7]. The Industrial, Scientific and Medical (ISM) bands have been extensively used by various unlicensed wireless applications

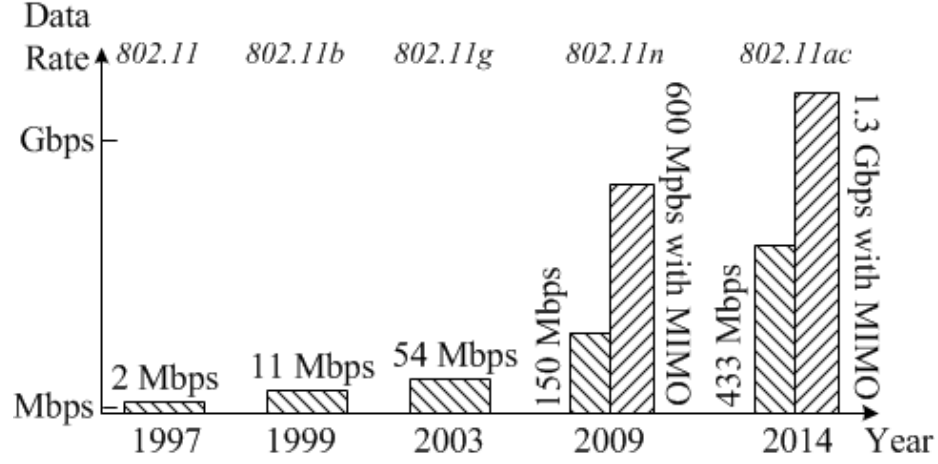


Figure 1.1: A concept diagram showing the growing data rates of IEEE 802.11 standards over time [1,2].

for decades. Examples of applications in these bands include bluetooth, microwave ovens, and Wi-Fi networks. However, these various transmissions generate spectral emissions, and potentially interfere with each other. In order to avoid further interference, the Federal Communications Commission (FCC) [8,9] has approved spectrum allocation policy in US for exploitation in television white spaces (TVWS), which include several noncontinuous portions of the radio spectrum across the very-high-frequency (VHF) (54 - 216 MHz) and ultra-high-frequency (UHF) (470 - 806 MHz) bands.

A spectrum allocation paradigm called dynamic spectrum access (DSA) [10] has been proposed and implemented for TVWS access, where unlicensed devices can temporarily access unoccupied bands of licensed spectrum while simultaneously respecting the rights of the incumbent license holders following a unified rule. In a DSA environment, it is difficult to obtain a contiguous block of spectrum. Orthogonal frequency division multiplexing (OFDM)-based transceivers that are capable of deactivating the subcarriers based on the spectrum sensing methods are employed as shown in Figure. 1.2, which are referred to as non-contiguous OFDM (NC-OFDM)-based transceivers. OFDM is a typical realization of Multicarrier modulation (MCM) [11], which is a form of frequency division multiplexing (FDM), where data is transmitted in several narrowband streams at adjacent carrier frequencies. The main drawback of MCM is that it exhibits a high peak-to-average power

ratio (PAPR).

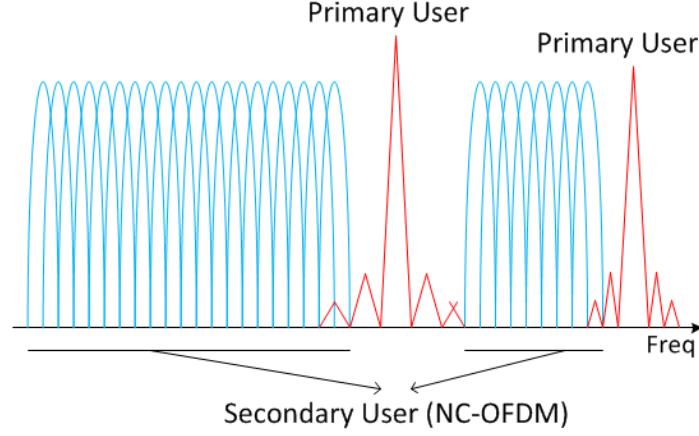


Figure 1.2: An illustration showing how NC-OFDM works in a DSA environment.

RF front-end of transmitters is a necessary enabler for delivery of wireless services, where a significant amount of the impairments and degradation of a wireless system are introduced. Power amplifiers (PA), inphase and quadrature (I/Q) modulators, and local oscillators (LO) are examples of components that constitute the RF front-end and introduce non-idealities to the signal. In particular, the PA is known for generating nonlinear distortion of the transmitting signals when combined with a high PAPR associated with multicarrier transmissions, this will create large spectral leakage that can potentially interfere with existing neighboring transmissions, and thus severely deteriorate the reliability of the DSA network.

Linearization is a systematic procedure for reducing a PA's distortion. A substantial amount of research has been conducted into PA linearization approaches ever since 1980s. Among all the approaches, digital predistortion (DPD) [12, 13] has been recognized by the researchers as the most promising linearization technique due to its good performance and cost efficiency, and is thus being extensively used and steadily improved upon by the industry.

A generic implementation of DPD in a wireless transceiver using software-defined radio (SDR) technology is shown in Figure. 1.3, where the digital signal processing (DSP) (including DPD) and digital communication parts are implemented in the software along

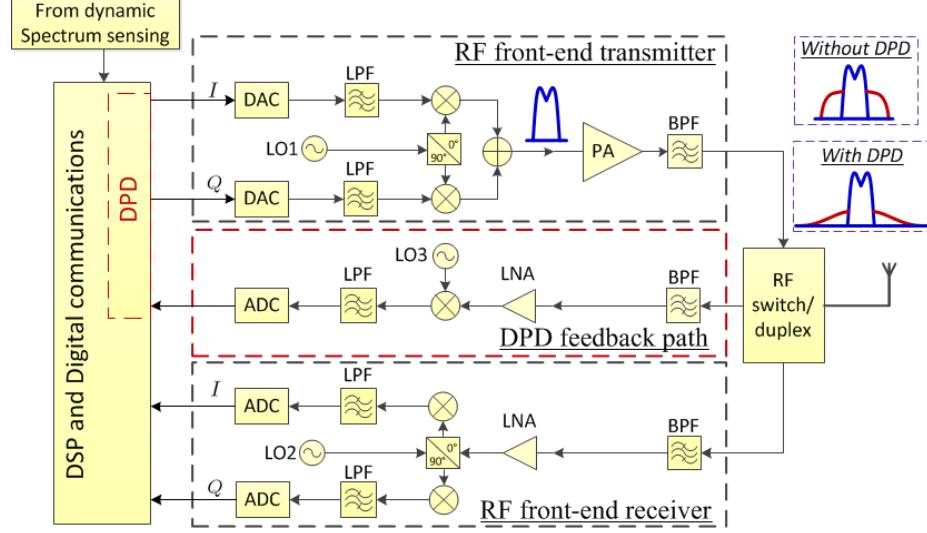


Figure 1.3: A typical transceiver architecture with DPD function employed on a SDR platform.

with dynamic spectrum sensing function, and the RF front-end consists of transmitting path, receiving path and DPD feedback path. The effects of the RF front-end with and without employing DPD techniques are also presented in the figure, where the suppression of emissions in adjacent channels can be observed when DPD is employed.

1.2 Research Objectives

The main objective of this dissertation research is to develop performance-enhancing DPD techniques that are capable of suppressing the spectral emissions on not only adjacent channels but also the far out spurious domain in the output RF spectrum. This spectral emission problem is particularly severe for wireless networks based on multicarrier transmission, such as a DSA network.

Therefore, to reach this primary objective, several sub-objectives have been established in this dissertation, namely:

- Investigation of the spectrum emission problem resulting from the RF front-end distortion in DSA networks, as well as the PA linearization techniques found in the literature in order to reduce these spectral regrowth. The worst case scenario occurs

when dealing with nonlinear distortion of the PA in multicarrier transmissions, which possess high PAPR.

- Enhancements of the DPD method for NC-OFDM transmissions in order to reduce OOB emissions on top of adjacent channels caused by major RF front-end components. Instead of only studying PA nonlinearity, the effects caused by the I/Q modulator and LO will also be considered.
- The design of orthogonal polynomial basis functions for predistorter modeling with the purpose of alleviating the numerical instability problem associated with the conventional polynomials. Theoretically, the conventional and orthogonal polynomial models are “equivalent”, and thus should behave similarly. However, in practice, the two approaches can perform quite differently in the presence of finite precision processing.
- The design of an enhanced DPD method aiming to reduce the spectral emissions in the far out frequency range, which is called spurious domain. Employing conventional DPD approaches will actually result in more power emissions in spurious domain, for the reason that it increases the order of nonlinearity on the transmitter.

1.3 Related Work

Linearization is a systematic procedure for reducing an amplifiers distortion. A substantial amount of research has been conducted into PA linearization approaches including those by Akawa [14] on Catesian feedback method and Cavers [12, 13, 15–17] on DPD schemes. There are many different ways of linearizing an amplifier. Such as approaches include power backoff, feedforward [18], polar feedback [19, 20], catesian feedback [21, 22], analog predistortion [23] and digital predistortion [12, 24, 25]. Among all the approaches, the DPD method (especially adaptive DPD method) is being extensively used and steadily improved upon at the same time in current wireless communication systems [26, 27]. DPD considers both nonlinearity and memory effects have appeared in the late 1980s [28], using Volterra filters as models for the nonlinear channel and also the pre-equalizer [29].

Many types of DPD techniques for PAs have been proposed and previously used (see [30] for a review). From performance and flexibility points of view, adaptive DPD is currently seen as the most promising linearization technique [31], especially given the adaptive DPD approach proposed for linearizing amplifiers [12, 13]. As a result, researchers' attentions have been drawn to making further improvements on DPD techniques.

A vast amount of research work has focused on a polynomial-based DPD approaches [32–35]. More recently, several DPD approaches were proposed for multicarrier transmission schemes such as in [36, 37]. As a proof-of-concept, FPGA or DSP implementation of DPD methods have been investigated and presented in the open literatures [38–40].

In addition to the PA DPD problem, I/Q imbalance and LO leakage are known to weaken the performance of adaptive PA predistorters in direct-conversion radios. To further suppress spectrum leakage, these impacts should also be considered. For narrowband inputs, the gain/phase imbalance can be considered as frequency independent, and its impacts on DPD have been analyzed (*e.g.*, [16]), and various remedy techniques have been proposed (*e.g.*, [15, 17]). The techniques described in [17, 41] focus only on I/Q modulator errors. Several publications discuss these two problems, such as references [26, 42] that focus on joint PA and I/Q modulator calibration in wideband direct-conversion transmitters, assuming frequency-dependent behavior for PA nonlinearities and modulator I/Q imbalance. However, these papers did not take into account spectrally agile transmissions.

After the FCC approved a spectrum allocation policy for more efficient television broadcast channel usage, NC-OFDM has become the ideal candidate for enabling DSA for unlicensed users. Sidelobe emission of second user transmissions becomes one of the crucial factors that determines the reliability of a DSA network. Authors in [10, 43] proposed approaches for cognitive radio-based OFDM sidelobe suppression with simulation results presented. However, they did not address the issue of spectral distortion introduced by the PA.

Furthermore, conventional DPD methods have been proved to be able to effectively reduce the OOB emissions that fall within adjacent channels. However, the implementation of DPD results in the distant spurious emissions and thus expands the transmission bandwidth. Moreover, when deploying frequency division duplexing (FDD) [44], one challenge

is also to protect its own receiving band, which can be affected by the spurious emissions from the transmitter. Although a duplex filter is usually implemented to provide adequate rejection of transmitter noise occurring at the receive frequency, one challenge is to obtain enough attenuation for the emissions on the receiver band when the duplexing gap is small. Therefore, there is a need to investigate on an enhancement to conventional DPD approach that can keep both OOB emissions and spurious emissions under the corresponding power limits. There has been several publications on this topic, for example, references [45, 46] proposed enhanced DPD method to reduce the OOB emissions more effectively, the work in [47] was with the objective of generally suppressing intermodulation distortion (IMD) in LTE-Advanced network [48]. The published patent presented in [49] proposed systems and methods for spurious emission cancellation, but not many results are provided to show the effectiveness of the method.

1.4 Thesis Contributions

This dissertation presents the following novel contributions in the design and performance-enhancement of DPD techniques:

- A simplified digital predistorter designed to compensate for impairments from either a PA only structure or a joint ‘PA + I/Q modulator’ structure in direct-conversion radio transmitters during NC-OFDM transmission. The proposed mechanism can effectively reduce the OOB emissions that occur during the transmissions of both untreated NC-OFDM waveforms and NC-OFDM waveforms processed using sidelobe suppression algorithms.
- A set of orthogonal polynomial basis functions proposed for PA and DPD modeling with the purpose of alleviating the numerical instability problem associated with non-orthogonal polynomials. Unlike in the literature, the proposed algorithm is *not* based on the assumptions of knowing the statistics of the PA input waveform. In fact, the distribution of the transmit waveform is not always known.
- A novel DPD method that can reduce the spectral regrowth at any pre-specified

component in the spurious domain of the output RF spectrum. The implementation of conventional DPD results in less OOB emissions but more spurious emissions. The proposed algorithm serves as an enhancement to conventional DPD approach that can keep both OOB and spurious emissions under the corresponding power emission limits.

1.5 Thesis Outline

Chapter 2 presents an extensive literature survey and tutorial of several topics covered in this dissertation. Specifically, an overview of the RF transceiver architecture and the characteristics of major RF front-end components is presented. The spectral emissions resulted from PA impairments are covered. Also studied is the basic concept of CR networks with two examples: Carrier aggregation (CA) in LTE-A and DSA operations in TVWS. Also included is the regulations approved by FCC to enable the coexistence of incumbent users and secondary users in TVWS. Finally, the potential spectral interference between separate multicarrier transmissions caused by nonideal performance of RF front-end components, especially PA, is presented.

Chapter 3 introduces the reader to all common techniques for PA linearization in the literature, focusing more on fundamental knowledge of DPD algorithm, which includes both Current-of-the-Art and insight to mathematical system identification procedures for adaptive DPD. Finally, the potential emissions at far out frequencies caused by employing conventional DPD methods are also presented, which are increasingly drawing more attention from both researchers and industry recently.

Chapter 4 studies both PA only, and joint PA and I/Q modulator effects for a NC-OFDM transceiver with sidelobe suppression algorithms employed. A DPD method that can simultaneously compensate for PA and I/Q modulator impairments is proposed. Also studied is a set of orthogonal polynomial basis functions which, combined with the proposed pre-distorter structure, is better suited for NC-OFDM transmission. Finally, the performance analysis of our proposed method is presented to support the theoretical explanation.

Chapter 5 presents the proposed frequency-selective DPD method that can reduce the

spectral regrowth at any pre-specified component in the spurious domain of the output RF spectrum while at the same time maintaining the OOB under its emission limit. The mathematical derivation procedures of our proposed DPD solution are presented for both memoryless nonlinear model and memory-based nonlinear model. The corresponding simulation results are provided and compared in the end.

In Chapter 6, the research achievements of this work are outlined and topics for future work are presented.

1.6 List of Publications

The work presented in this thesis is based on the following articles:

- [P1] Zhu Fu, Lauri Anttila, Mikko Valkama, and Alexander M. Wyglinski. “Digital pre-distortion of power amplifier impairments in spectrally agile transmissions,” in *Sarnoff Symposium (SARNOFF)*, 2012 35th IEEE, pages 16, May 2012.
- [P2] Zhu Fu, and Alexander M. Wyglinski. “Digital Pre-distortion of Radio Frequency Front-end Impairments in the Design of Spectrally Agile Multicarrier Transmission,” 2013 *Conference Record of the Forty Seventh Asilomar Conference on Signals, Systems and Computers (ASILOMAR)*, Nov. 2013
- [P3] Zhu Fu, and Alexander M. Wyglinski. “Digital Pre-distortion of Power Amplifier Impairments on Software-defined Radio Platforms”, *Electronics Letters, IET*, Dec 2013 [Submitted]
- [P4] Zhu Fu, Amit Sail, and Alexander M. Wyglinski. “Digital pre-distortion for power amplifier and I/Q modulator impairments in spectrally agile transmissions”, *EURASIP Journal on Wireless Communications and Networking*, Jan 2014 [Submitted]
- [P5] Zhu Fu, Lauri Anttila, Mikko Valkama, and Alexander M. Wyglinski. “Frequency-Selective Digital Predistortion for Spectrum Emission Reduction”, *IEEE Transactions on Communications*, April 2014 [Submitted]

- [P6] Zhu Fu, Lauri Anttila, Mahmoud Abdelaziz, Mikko Valkama, and Alexander M. Wyglinski. “On Digital Predistortion for Next Generation Wireless Networks: Improving Emission Mitigation in Spectrally Agile Waveforms”, *IEEE Communications Magazine*, April 2014 [Submitted]

Chapter 2

Practical Considerations of Wireless Transceivers

2.1 Chapter Introduction

The objective of this work is to reduce the interference in the radio frequency (RF) spectrum between different transmissions by proposing enhanced digital predistortion (DPD) methods to correct imperfections of radio front-end at the transmitter, thereby guaranteeing the reliability of the wireless networks, especially Dynamic Spectrum Access (DSA) networks based on spectrally agile transmission. To fully understand how impairments caused by RF front-end components can be compensated in a DSA environment, one must understand the characteristics of these components, the regulation in cognitive radio (CR) networks and the nature of the multicarrier waveforms transmitted in the CR network. Hence, this chapter will provide some insights into the RF transceiver architecture, the properties of multicarrier transmission, and the working order of DSA networks.

This chapter is organized as follows: An overview of the architecture of RF transceivers and the characteristics of major RF front-end components is presented. The out-of-band (OOB) emissions caused by power amplifier (PA) impairments are discussed followed by an introduction to the RF front-end structure of a prototyping software-defined-radio (SDR) platform. The basic concept of CR networks is presented followed by two examples of CR

network realization: Carrier aggregation (CA) in LTE-A and DSA operations in TV white space (TVWS) bands. The regulations approved by Federal Communications Commission (FCC) are covered to enable the coexistence of incumbent users and secondary users in TVWS. Finally, the possible spectral interference between separate multicarrier transmissions caused by nonideal performance of RF front-end components, especially the PA, is emphasized.

2.2 Overview of Reconfigurable Multi-standard RF Transmitters

2.2.1 Typical Architectures of RF Transceivers

Data transmission has become an ubiquitous component of today's world which can be performed either over a wireline infrastructure or a wireless network. Wireless methods do not use electrical or optical conductors. Rather, they use the Earth's electromagnetic frequency spectrum. There are three main types of wireless media: Radio wave, microwave, and infrared. The range of the electromagnetic spectrum between 10 KHz and 1 GHz is called RF. Radio waves include: short wave, very-high-frequency (VHF) television and Frequency Modulation (FM) radio, and ultra-high-frequency (UHF) radio and television. Most radio frequencies are regulated, and to use these frequencies you must receive a license from the Federal Communications Commission (FCC). In this research work, we focus on correcting the wireless front-end non-ideal behaviors of transmitters operating in the RF frequency range.

The trend of wireless communications is toward creating a network-ubiquitous era in the upcoming years. Major wireless communication standards such as Global System for Mobile Communications (GSM), Wideband Code Division Multiple Access (WCDMA) and Orthogonal frequency-division multiplexing (OFDM) have constantly been developed over decades with the purpose of achieving higher data rates of data transmission. In order to allow users to switch seamlessly among different standards, achieving so-called global roaming, a multi-standard transceiver is required in order to operate a wireless device under

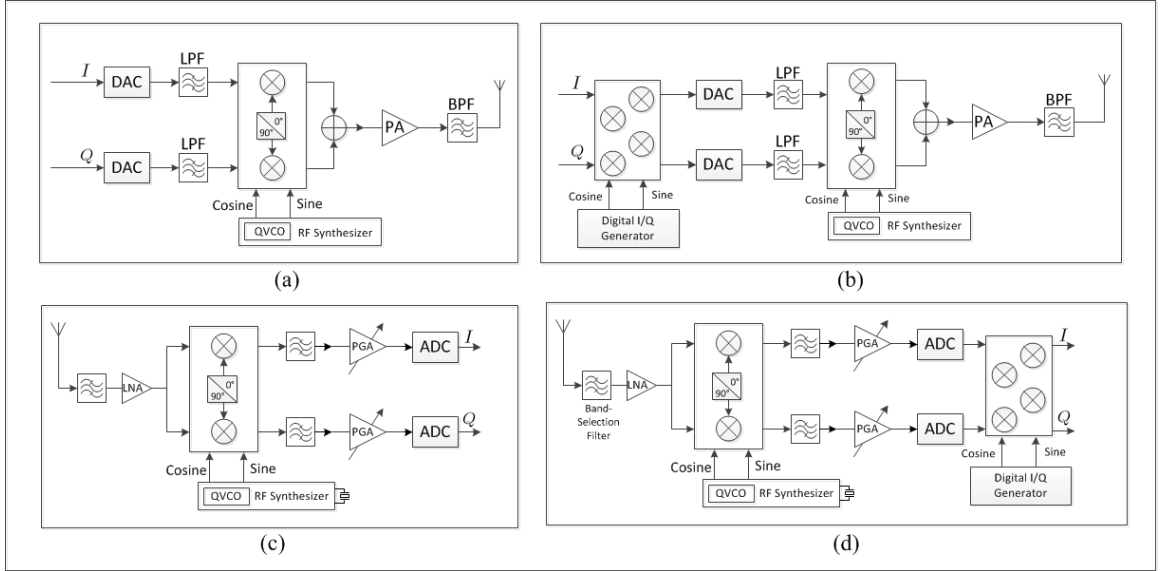


Figure 2.1: Typical transmitter and receiver structures.

different network protocols. Although a multi-standard device can be designed simply by duplicating more than one transceiver, the growing economic impact of wireless communication hardware platform, along with the evolution of different standards for voice and data, is driving worldwide research towards the implementation of fully-integrated multi-standard transceivers. For example, a fully reconfigurable transceiver (*e.g.*, software-defined radio) implementing the network protocols via block reconfiguration can effectively minimize the cost [50–52].

The basic set-up for any radio communication system consists of either a transmitter together with an associated receiver, or a transceiver comprising both a transmitter (Tx) and a receiver (Rx) which are combined and share common circuitry or a single housing. There are mainly two types of architectures for transmitters, namely direct-conversion transmitters and two-step transmitters. Similarly, there are homodyne (zero-IF) receivers and low-IF receivers, categorized depending on whether intermediate frequency (IF) is a transition state between RF and baseband [50]. Figure. 2.1 shows examples of transmitter and receiver architectures.

An example of a low-IF Rx is shown in Figure. 2.1 (a), with a band-selection filter elimi-

nating the out-of-band (OOB) interference, the in-band RF channels are free from amplification by a low-noise amplifier (LNA). This is followed by a RF-to-IF down-conversion through inphase and quadrature (I/Q) channels. The signal level is adjusted by a programmable-gain amplifier (PGA) prior to baseband lowpass filters (LPFs). The baseband PGAs adjust the signal swing for an optimum-scale analog-to-digital (A/D) conversion. After that, the IF-to-baseband downconversion is performed digitally. Figure 2.1 (c) shows the structure of a zero-IF Rx, the desired channel is translated directly to DC through the I and Q channels, with similar layout for other components.

Architecturally, the low-IF Tx, as seen in Figure 2.1 (b), is a reverse of operation from its Rx counterpart (low-IF Rx) with the A/D conversion replaced by a digital-to-analog (D/A) conversion. However, they are very different in the design specification. For instance, in transmission, only one channel will be upconverted in the Tx. Its power level is well-determined throughout the Tx path. There are differences in the signal reception, the power of the incoming signals is variable, and the desired channel is surrounded with numerous unknown-power in-band and OOB interferences. Thus, PGAs are essential for the Rx to relax the dynamic range of the A/D converter, but can be omitted in the Tx if the power control could be fully implemented by the power amplifier (PA). Similarly, since the channel in the TX is progressively amplified toward the antenna and finally radiated by a PA, the linearity of the whole TX is dominated by the PA. On the other hand, the noise contribution of the LNA is what dominates the entire Rx noise figure.

The direct-up Tx as in Figure 2.1 (a) features an equal integratability as the zero-IF Rx. Note that although the functional blocks in Rx and Tx look identical, their design specifications are largely different. For instance, the Rx-LPF has to feature a high OOB linearity due to the co-existence of adjacent channels, whereas it is not demanded from Tx-LPF [50].

Table 2.1 summarizes the advantages and disadvantages of different Tx structures. The most appealing feature of applying the direct-up Tx architecture is its cost effectiveness. However, its major drawback is that it introduces I/Q imbalance in the RF front-end properties.

Table 2.1: Comparisons of different Tx architectures.

Tx Architecture	Advantages	Disadvantages
Direct-Up	1. Low cost 2. Simple frequency plan for multi-standard 3. High integratability	1. Power amplifier nonlinearity 2. I/Q imbalance 3. LO leakage
Two-Step-Up	1. Better I/Q matching 2. Carrier far from LOs frequency	1. Power amplifier nonlinearity 2. High quadrature factor

2.2.2 Characterstics of RF Power Amplifiers

A technical definition of power amplifiers (PA) is given as an amplifier designed to deliver the maximum output power for a wireless transmitter. RF PAs are extremely used in wireless and wireline communication area [53]. The power efficiency of PAs can greatly influence overall power efficiency of the transmitter, and so is the output transmitted power of PA to the total power consumption.

Every amplifier as a DC equivalent circuit and an AC equivalent circuit. Because of this, it has two load lines: a *DC load line* and an *AC load line*, as shown in Figure. 2.2. For DC load line, with reference to Figure. 2.2(a), one way to move the Q point is by varying the value of R_2 . For very high resistance of R_2 , the transistor reaches saturation level and the current is given by:

$$I_{C(SAT)} = \frac{V_{CC}}{R_C + R_E}. \quad (2.1)$$

On the other hand, a small R_2 will run the transistor into cutoff level. Its voltage can be written as:

$$V_{CE(CUTOFF)} = V_{CC}. \quad (2.2)$$

Figure. 2.2(b) shows the DC load line with the Q point.

Figure. 2.2(c) is the AC equivalent circuit of Figure. 2.2(a). When an AC signal comes in, the instantaneous operating point moves along the AC load line of Figure. 2.2(d). In other words, the peak-to-peak sinusoidal current and voltage are determined by the AC load lind. Referring to Figure. 2.2(d), the saturation current of the AC load line is:

$$i_c(\text{sat}) = I_{CQ} + \frac{V_{CEQ}}{r_c}. \quad (2.3)$$

where I_{CQ} is DC collector current, V_{CEQ} is DC collector-emitter voltage and r_c is AC resistance seen by collector. And the AC voltage cutoff is given by:

$$v_{ce(\text{cutoff})} = V_{CEQ} + I_{CQ}r_c. \quad (2.4)$$

After introducing the two lines, note that since the slope of AC load line is higher than DC one, the maximum peak-to-peak output is always less than DC supply voltage [54].

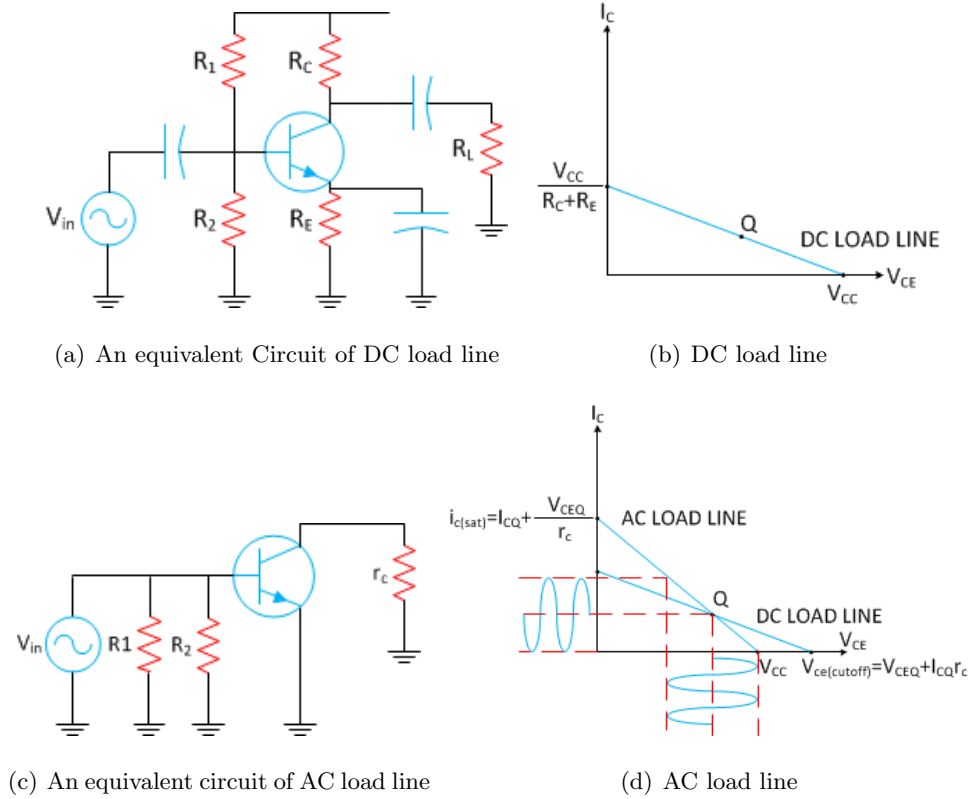


Figure 2.2: DC and AC load lines with equivalent circuits.

Input signals to PA can be divided into two categories by signal level: *Small signal* and *large signal*. A small signal is defined as the one with peak-to-peak swing in current less than 10% of maximum collector current. On the other hand, a large signal is with peak-to-peak AC voltage using most of the load line.

The location of Q-point is not too critical for small signal operation, but it is for large signal operation. If Q-point is closer to saturation current, we get saturation clipping as

shown in Figure. 2.3(b), and if Q-point is moved to the right closer to cutoff voltage, we get cutoff clipping as shown in Figure. 2.3(a). Both cutoff and saturation clipping are unwanted since they can cause distortion to the signal. Also, when the Q-point is centered on the DC load line (Figure. 2.2(d)), the AC load line can be fully used without clipping. Hence, a well-designed power amplifier for large signal should have Q-point at the centre of AC load line as in Figure. 2.3(c).

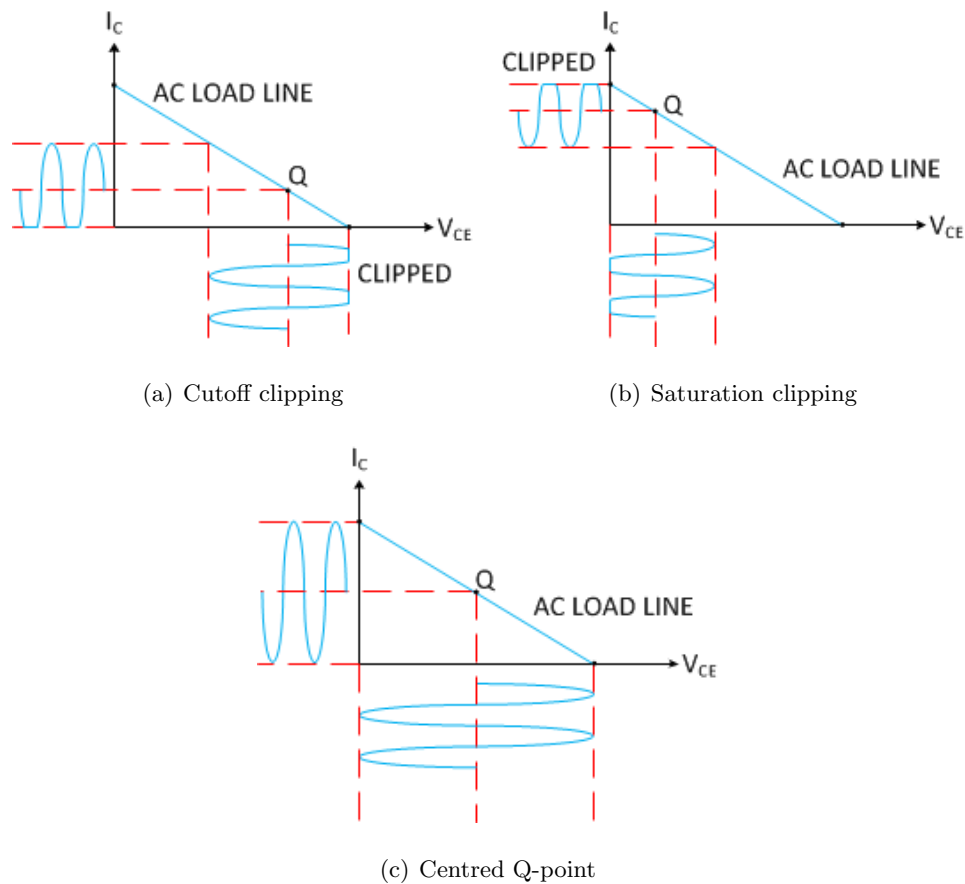


Figure 2.3: Signal clipping determined by location of Q-point.

One of the most important characteristics of a high-power amplifier is the so-called **gain compression** for large-signal. At low drive levels, the output is linear to the input power with a **constant small-signal gain** G_0 . However, as the power increases beyond a certain point, the gain of the transistor decreases, and the output power saturates eventually [55] as

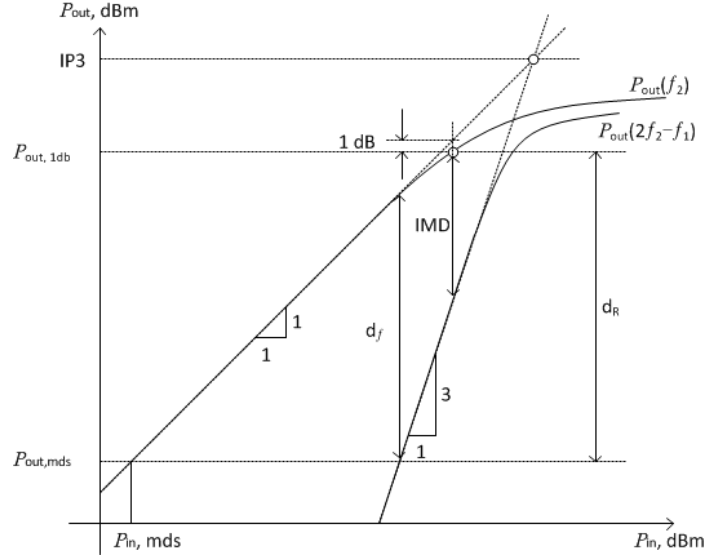


Figure 2.4: PA output power and IMP power versus input power.

seen in Figure. 2.4. The point where the gain of the amplifier deviates from the linear gain by 1 dB is called the **1 dB compression point**, and it is referred to as $G_{1\text{dB}} = G_0 - 1\text{dB}$. Denoting **input power** and **output power** of the amplifier with P_{in} and P_{out} , $P_{\text{out},1\text{dB}}$ can be related to the corresponding $P_{\text{in},1\text{dB}}$ at the 1 dB compression point by:

$$\begin{aligned} P_{\text{out},1\text{dB}}[\text{dBm}] &= G_{1\text{dB}}[\text{dB}] + P_{\text{in},1\text{dB}}[\text{dBm}] \\ &= G_0[\text{dB}] - 1\text{dB} + P_{\text{in},1\text{dB}}[\text{dBm}]. \end{aligned} \quad (2.5)$$

Another important characteristic of an amplifier is its **dynamic range**, d_R , which indicates the region of the amplifier with a linear power gain as the difference between $P_{\text{out},1\text{dB}}$ and $P_{\text{out},\text{mds}}$. where $P_{\text{out},\text{mds}}$ is the output power of the minimum detectable signal.

An unwanted property of power amplifier is the occurrence of **intermodulation distortion** (IMD). Due to the third-order nonlinearities of the amplifier, the input signals $P_{\text{in}}(f_1)$ and $P_{\text{in}}(f_2)$ create besides $P_{\text{out}}(f_1)$ and $P_{\text{out}}(f_2)$ as expected, additional tones known as third-order **Intermodulation products** (IMPs) $P_{\text{out}}(2f_1 - f_2)$ and $P_{\text{out}}(2f_2 - f_1)$. The difference between the desired and the undesired power level in dBm at the output port is normally defined as IMD in dB [55], that is:

$$\text{IMD}[\text{dB}] = P_{\text{out}}(f_2)[\text{dBm}] - P_{\text{out}}(2f_2 - f_1)[\text{dBm}]. \quad (2.6)$$

In Figure. 2.4, projecting the linear region of $P_{out}(f_2)$ and $P_{out}(2f_2 - f_1)$ leads to the third order **intercept point** (IP3). Consequently, a PA with better linearization achieves a higher IP3. Also shown in Figure. 2.4 is a parameter named **spurious free dynamic range** d_f , which is expressed as:

$$d_f[\text{dB}] = \frac{2}{3}(IP3[\text{dBm}] - G_0[\text{dB}] - P_{in,mds}[\text{dBm}]). \quad (2.7)$$

Theoretically, no spurious emissions will be generated when keeping the input power within $d_f[\text{dB}]$.

Furthermore, there are various ways of classifying PAs, such as from perspective of their mode of operation and supported frequency range. For instance, amplifiers that generally classified according to their mode of operation are the ones driven by large signals with the output signal either cut-off or in saturation region. This classification is based on the amount of transistor bias and amplitude of the input signal either cut-off or is in saturation region. They are mainly classified as below:

- **Class A Operation:** This type of PAs has its transistor operate in the active region at all times with conduction angle of 2π . It is normally shown as current flows versus time as (see Figure. 2.5(a)). Such amplifiers are used where freedom from distortion is prime aim.
- **Class B Operation:** In this case, output current flows only during positive half cycle of the input signal as seen in Figure. 2.5(b). Comparing to class A PAs, average current and power dissipation are less, hence overall efficiency is increased.
- **Class AB Operation:** For class AB operation the output signal swing occurs between π and 2π . (Figure. 2.5(c))
- **Class C Operation:** A Class C PA is biased to operate for less than π of the input signal cycle as shown in Figure. 2.5(d). Such power amplifiers are employed in special areas of tuned circuits.

Class A is generally for small signal operating on direct current, the rest of classification works for large signals, among which, RF PAs are mostly implemented as Class AB and Class C, and Class B is more for operations on Audio frequencies.

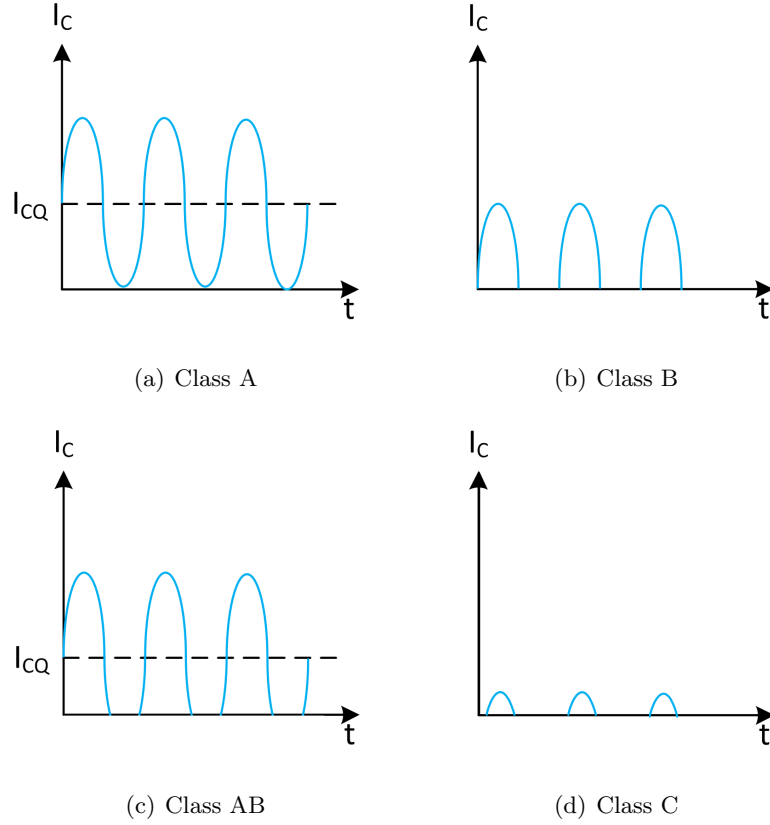


Figure 2.5: Output current of different class operations of the PA.

There are mainly two broad categories of PAs by frequency range they operate on: audio power amplifiers and radio-frequency power amplifiers. An *audio amplifier* is designed to operate between 20 Hz and 20 kHz. It is usually used to amplify signals to deliver music or speech. On the other hand, a *radio-frequency power amplifier* refers to an amplifier that is designed to amplify frequencies much higher than but above 20 kHz, such as HF (High frequency), VHF and UHF frequency bands.

PA's can also be classified by bandwidth as *narrowband* or *wideband*. A narrowband amplifier or tuned RF amplifier is designed to amplify signals with a small bandwidth, for instance, signal tune signals. A wideband amplifier can be operated over a larger bandwidth up to 200 MHz technically, which is more difficult to design.

RF front-end components each possess different characteristics, one such RF front-end component is the PA. PA is known for its non-linearity, which translate to spectral regrowth

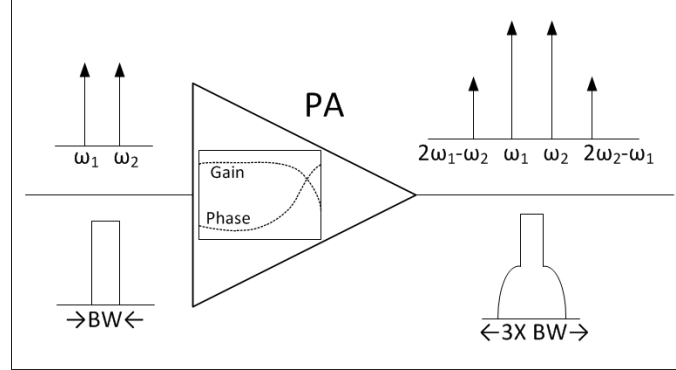


Figure 2.6: Nonlinear effects caused by power amplifier.

in frequency domain. The primary issue associated with the PA is its nonlinear distortion characteristic, which combined with the high peak-to-average power ratio (PAPR) often associated with multicarrier transmissions, generates large OOB sidelobe spectral leakage that can potentially interfere with existing neighboring transmissions.

Power amplifiers are mainly presented in the transmitters, and are designed to raise the power level of the signal before passing it to the antenna, which is usually the last active block in any transmitter system. This power boost is crucial to achieve the desired signal to noise ratio at the receiver, and without which received signals would not be detectable. For the power amplifier it is necessary to have as high gain as possible, while adding as little distortion to the signal as possible *i.e.* be as linear as possible. For small and mobile transmitters, there is usually another factor not less important which is power efficiency, since these devices are usually battery driven. [56,57] Unfortunately, from the circuit design point of view, increasing the power efficiency would drive the device more and more into nonlinearity region which means that the amount of distortion will increase.

The reason why the linearity is so important is the varying signal envelopes in spectrum efficient modulation types used in new generation mobile communication systems. If signals have constant envelopes like in FM then PA linearity may not be a crucial issue because the instantaneous input power stays constant and therefore there are no gain and phase variations for a specific operation point. However, newer transmission standards, such as WCDMA and OFDM used in 3G communication systems, the envelope of the signal

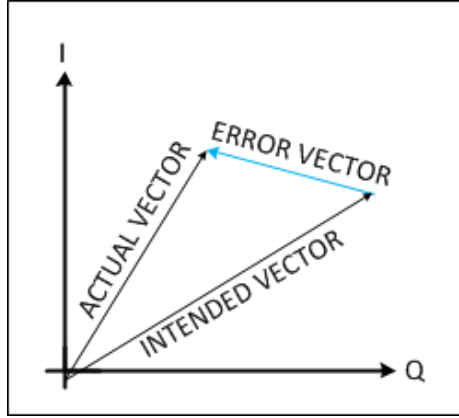


Figure 2.7: Illustration of the error vector.

continuously varies and hence the instantaneous input power changes continuously. As a result the signal at the PA output contains inter-modulation products, if the amplifier gain and phase response are not linear. IMPs interfere with adjacent and alternate channels and affects the error vector magnitude (EVM) defined as the distance between the desired and actual signal vectors (error vector) as shown in Figure. 2.7, normalized to a fraction of the signal amplitude.

IMD is the unwanted amplitude modulation of signals containing two or more different frequencies in a system with non-linearity, and it is caused by frequency harmonic or products. The harmonic of a wave is a component frequency of the signal that is an integer multiple of the fundamental frequency. Intermodulation products occur when the input to a non-linear system is composed of two or more frequencies. Of all the harmonics and intermodulation components produced, we should be cautious in those which fall in the passband of our equipment and, in the case of the intermodulation components, those which happen to be closest to our fundamental frequencies [58].

Take a two-tone transmission for example, as seen in Table. 2.2, one third order product ($2f_1 - f_2$) is 1 kHz lower in frequency than f_1 and another ($2f_2 - f_1$) is 1 kHz above f_2 . One fifth order product ($3f_1 - 2f_2$) is 2 kHz below f_1 and another ($3f_2 - 2f_1$) is 2 kHz above f_2 . Thus, it is the odd order products which are closest to the fundamental frequencies f_1 and f_2 . A typical spectrum produced could be depicted as shown Figure. 2.8(a). As

Table 2.2: Illustration of intermodulation products.

1 st Order	f_1	f_2	500 kHz	501 kHz
2 nd Order	$f_1 + f_2$	$f_2 - f_1$	1001 kHz	1 kHz
3 rd Order	$2f_1 - f_2$	$2f_2 - f_1$	499 kHz	501 kHz
	$2f_1 + f_2$	$2f_2 + f_1$	1501 kHz	1502 kHz
4 th Order	$2f_1 + 2f_2$	$2f_2 - 2f_1$	2001 kHz	2 kHz
5 th Order	$3f_1 - 2f_2$	$3f_2 - 2f_1$	498 kHz	502 kHz
	$3f_1 + 2f_2$	$3f_2 + 2f_1$	2502 kHz	2503 kHz

a result, quite a number of the IMPs will be generated by multi-carrier transmissions and thus become OOB sidelobe spectral leakage. Referring to Figure. 2.6, the bandwidth of output signal from PA is normally three times of input signal bandwidth, since the third order components are the closest and also usually the highest in amplitude. Therefore, they are usually the products of most concern and are those which are commonly measured and defined in transmitter and receiver performance specifications.

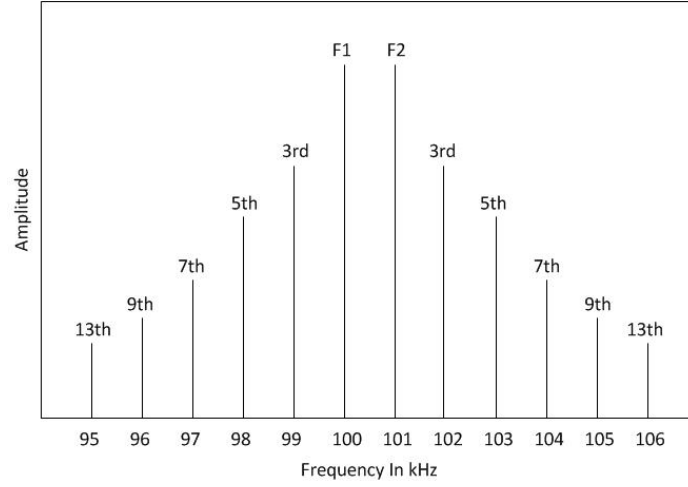
Operating these PAs near saturation increases signal distortion but improves efficiency, justifying the effort spent on an accurate PA nonlinear characterization to optimize that tradeoff. In order to estimate the impact that the power amplification has in narrow-band communication systems, the nonlinear behaviour of a PA is usually described using the amplitude-to-amplitude modulation (AM/AM) and amplitude-to-phase modulation (AM/PM) [59], examples of AM/AM and AM/PM plots are shown in Figure. 2.9. with reference to Figure. 2.4.

Adjacent channel Power Ratio (ACPR) is another figure-of-merit to characterize how nonlinearity affects adjacent channels and is widely used with modern shaped pulse digital signals. As shown in Figure. 2.10, ACPR is defined as the ratio between the total power of adjacent channels (sum of IMD) and the main channel's power as:

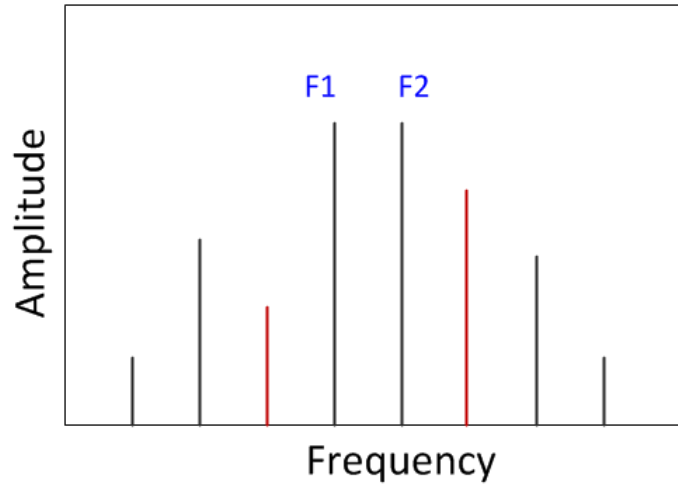
$$ACPR[\text{dB}] = 10 \lg \frac{P_{\text{adj}}}{P_{\text{ref}}} \quad (2.8)$$

with P_{adj} and P_{ref} denoting the power spectral density (PSD) of adjacent channel and desired channel, respectively.

Memory effects are defined as distortion phase and amplitude changes over the modulation bandwidth, which obvious character is spectrum asymmetry as shown in Figure. 2.8(b).



(a) Without memory effects.



(b) With memory effects.

Figure 2.8: Intermodulation products in a two-tone transmission.

It can not be ignored especially in wideband signal processing.

Two categories of memory effects have been identified, *i.e.*, **electrical memory effects** and **thermal memory effects**. The predominant factor that causes the electrical memory effect is the variation of terminal impedances (biasing and matching circuits impedances) over the input signal bandwidth around the carrier frequency and its harmonics, as well as at baseband frequencies. Careful design of the matching and biasing circuit would min-

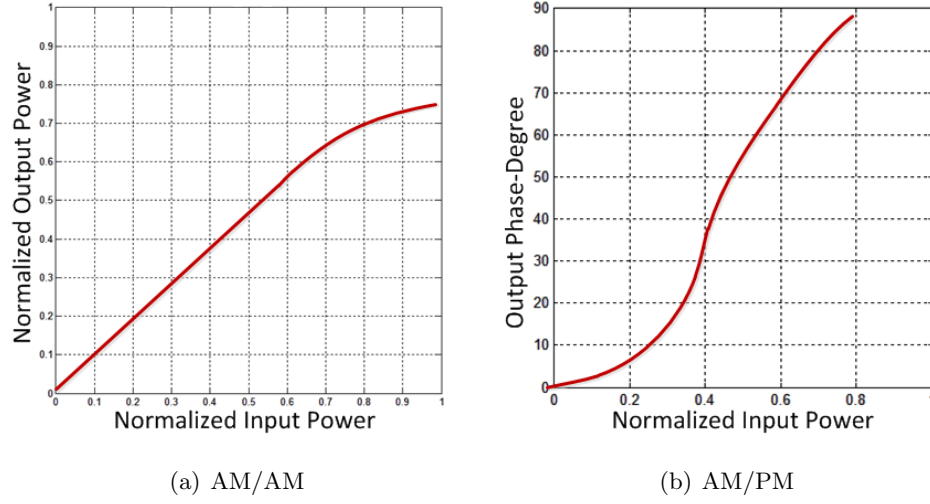


Figure 2.9: Examples of AM/AM and AM/PM plots.

imize these effects, especially in the case of FET-based amplifiers [60]. Variations in the envelope of the signal produce rapid changes in temperature in the active device of the amplifier caused by transistor temperature-dependent electrical parameters. Changes in the temperature of the active device affect its nonlinear gain, and it is unavoidable.

2.2.3 Impairments of Other Key Components on the RF Front-end

Inphase and Quadrature (I/Q) imbalance and Local Oscillator (LO) Leakage are typical effects caused by I/Q modulator and LO, respectively. The I/Q imbalance is commonly seen in any RF front-end that exploits analog quadrature up-mixing. This imbalance mainly attributes to the mismatched components in the in-phase (I) and the quadrature (Q) branches. Examples include but not limited to an imperfectly balanced local oscillator (LO) and/or baseband LPF with mismatched frequency responses. Although the I/Q imbalance introduced by the LO may be assumed constant over the signal bandwidth, the mismatches in the subsequent baseband I/Q amplifiers and filters tend to vary with frequencies. Such frequency dependent I/Q imbalance is particularly severe in a wideband direct-conversion transceiver and the corresponding estimation and compensation process becomes more challenging [26, 61].

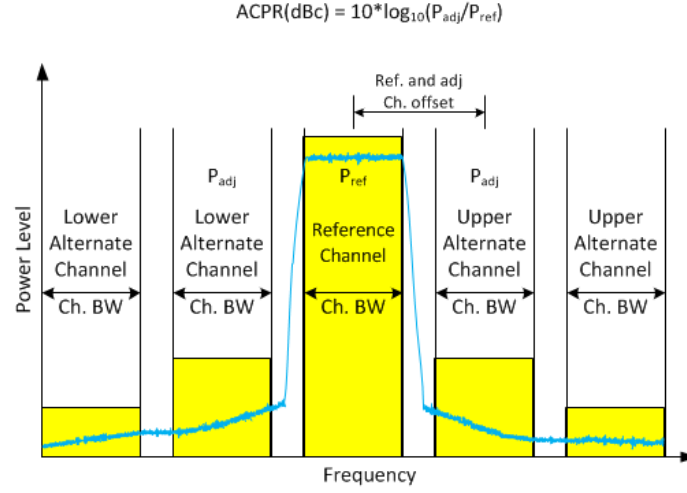


Figure 2.10: General review of Adjacent Channel Power Ratio (ACPR).

In addition to nonlinearity and memory effects of PA, I/Q imbalance and LO leakage are known to weaken the performance of adaptive PA predistorters. Under severe I/Q imbalance and/or LO leakage, the PA predistorter coefficient estimates become biased and PD can, in some cases, even worsen the spectral regrowth.

2.3 Spectrally Agile Transmission in Cognitive Radio (CR) Networks

2.3.1 Overview of CR Networks

cognitive radio (CR) is proposed and recognized as a key technical evolution toward the exploitation of the future wireless communication systems, where efficient utilization of the spectrum is maximized by dynamically sensing the wireless environment and modifying the parameters, such as frequency, power, and modulation. As the first step to realize CR implementation, carrier aggregation (CA) is employed in Long term Evolution Advanced (LTE-Advanced) [62] in order to increase the bandwidth, and thereby the data rates by aggregating a maximum of five fragmented component carriers. Moreover, a spectrum allocation paradigm called dynamic spectrum access (DSA) has been proposed as a CR-based feature, where unlicensed devices can temporarily access unoccupied bands of licensed

spectrum while simultaneously respecting the rights of the incumbent license holders [63]. Due to the ubiquitous conversion to digital television, FCC approved rules for exploitation in television white spaces (TVWS) [64]. Several standards based on DSA scheme are designed or reformed to work on TVWS bands, one such rule is IEEE 802.22 [65] which aims to provide a wireless broadband access in rural areas.

2.3.2 First-step in CR Realization: Carrier Aggregation in LTE-Advanced

Long Term Evolution (LTE) or the Evolved Universal Terrestrial Access Network (E-UTRAN), introduced in the Third Generation Partnership Project (3GPP) Release 8, is the access part of the Evolved Packet System (EPS). The LTE access network is a network of base stations, evolved NodeB (eNB), generating a flat architecture, without a centralized intelligent controller. This distributed solution is aimed to speed up the connection set-up and reduce the time required for a handover [48, 66].

To achieve high radio spectral efficiency, a multicarrier approach for multiple access was chosen by 3GPP. For the downlink (DL) (user equipment (UE) to base station), Orthogonal Frequency Division Multiple Access (OFDMA) was selected and for the uplink (UL) (base station to UE) Single Carrier - Frequency Division Multiple Access (SC-FDMA) also known as DFT (Discrete Fourier Transform) spread OFDMA is employed. OFDM is a multicarrier modulation scheme, such that in OFDMA the subcarriers can be shared between multiple users. Nevertheless, the OFDMA solution possesses high PAPR which results in high requirements on linearity of PAs on the Tx. This is less of a problem in the eNB, but would lead to a very expensive UE. Hence, a different solution – SC-FDMA was selected for the UL, which generates a signal with single carrier characteristics, and thus with a low PAPR [48, 66].

As defined in [67], LTE is developed to support E-UTRA operating bands range from 700 MHz up to 2.7 GHz currently. In the 3GPP technology family, it is also required that the system supports flexible frequency allocation, such that a single carrier can have the bandwidths of 1.4 MHz, 3 MHz, 5 MHz, 10 MHz, 15 MHz or 20 MHz, with the actual bandwidth values slightly adjusted. LTE supports both frequency division duplexing (FDD) and time division duplexing (TDD), which are typically used in different geographical areas

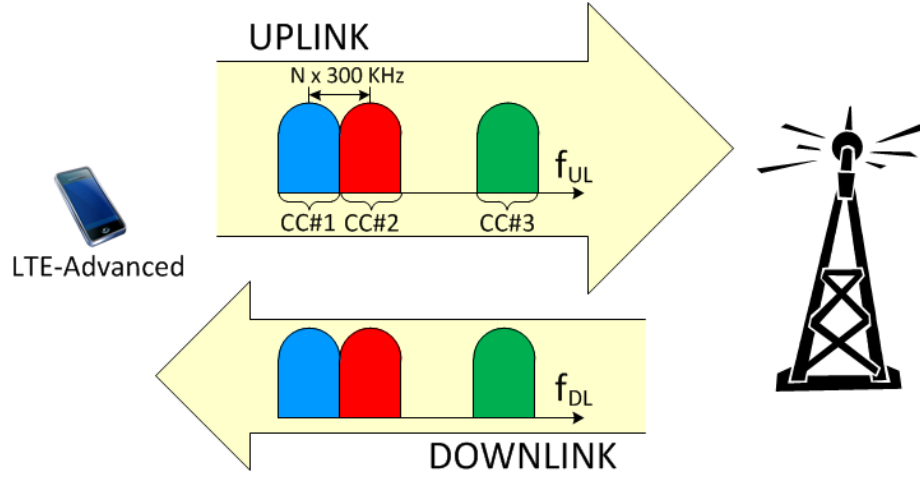


Figure 2.11: LTE-Advanced Carrier Aggregation (CC) operating in FDD mode, with three CCs aggregated. The CCs can be of different bandwidths.

but can also coexist. For instance, in Release 11 there are 29 bands specified for FDD and twelve bands for TDD. The FDD mode of LTE enables full duplex operation, meaning that UL and DL can be operated simultaneously on separate frequencies. In TDD mode UL and DL are operated on the same frequency bands but are alternating in time domain. FDD mode is more challenging for the mobile because UL transmission can interfere with DL reception with a small frequency gap [68].

In order to meet the requirements of the International Mobile Telecommunications-Advanced (IMT-A), the key of which is to support enhanced user and service demands with 100 MHz bandwidth for high mobility, LTE-A defines a novel technique – CA in Release 10, which proposed aggregation of both continuous and discontinuous spectrum. The LTE-A UE can be allocated DL and UL resources on the aggregated resource consisting of two or more component carriers (CCs), the R8/R9 UEs can be allocated resources on any one of the CCs. The CC can have a bandwidth of any single carrier defined in LTE and a maximum of five component carriers can be aggregated, and thus the maximum aggregated bandwidth is 100 MHz. The simplest way to arrange aggregation is to use contiguous CCs within the same operating frequency band, which is called intra-band contiguous. However, this might not always be feasible due to operator frequency allocation scenarios. For non-contiguous allocation it could either be intra-band, *i.e.*, the component carriers belong to

the same operating frequency band, but with one or more frequency gaps in between, or it could be inter-band, in which case the CCs belong to different operating frequency bands. For instance, in the UL transmission as shown in Figure. 2.11, CC3 can be either within the same operating band as in CC1 and CC2 or in the neighboring band. The spacing between the centre frequencies of two contiguous CCs is $N \times 300$ kHz, where N is an integer. This is in order to be compatible with the 100 kHz frequency raster of Release-8/9 and at the same time preserve orthogonality of the subcarriers with 15 kHz spacing. For non-contiguous cases the CCs are separated by frequency gaps [62, 69]. The list of operating frequency bands supporting CA can be found in [67]. Furthermore, in the context of CR, available spectrum resources can be dynamically used on an opportunistic and non-interfering basis, which provides more flexibility in the aggregation of spectrum resources, enhancing both data rate and spectrum efficiency. [70]

Although for the LTE UL, SC-FDMA is employed for the reason that it is a single carrier mechanism with a low PAPR, the limitation of implementing CA is that aggregating a number of CCs results in a high PAPR which often is associated with multicarrier transmissions [71]. Hence, based on the discussion in the last section, the output spectrum is highly likely to carry large OOB spectral leakage due to the PA nonlinearity that can potentially interfere with neighboring transmissions.

2.3.3 Regulations for Operating Dynamic Spectrum Access (DSA) Networks in TVWS

With the demand for extra bandwidth increasing due to existing and new services, both spectrum policy makers and communication technologists are seeking solutions for the spectrum scarcity. Meanwhile, measurement studies have shown that much of the licensed spectrum is relatively unused across time and frequency [72]. Nevertheless, current regulatory requirements prohibit unlicensed transmissions in these bands, constraining them instead to several heavily populated, interference-prone frequency bands. To provide the necessary bandwidth required by current and future wireless services and applications, the FCC has commenced work on the concept of unlicensed users borrowing spectrum from spectrum licensees [73]. This approach to spectral usage is known as DSA.

TV stations operate on 6 MHz channels designated channels 2 to 69 in four bands of frequencies including 54 – 72 MHz, 76 – 88 MHz, 174 – 216 MHz and 470 – 806 MHz) in the VHF (54–216 MHz) and UHF (470–806 MHz) regions of the radio spectrum [8,9] as shown in Figure. 2.12. Due to the ubiquitous conversion to digital television, the FCC approved rules in November 2008 for exploitation in TVWS, which include several noncontinuous portions of the radio spectrum across the VHF and UHF bands, thus that unlicensed radio transmitters are allowed to operate in the broadcast television spectrum at locations where that spectrum is not being used by licensed services [74]. The Commission decided to rely on a combination of spectrum sensing and geo-location combined with access to a database of existing spectrum use to determine if a channel is available [75].

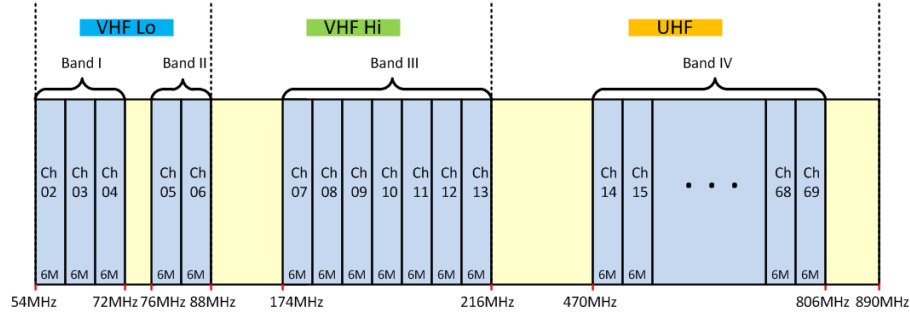


Figure 2.12: VHF and UHF television channels and frequencies.

To enable unlicensed user operate in the TV spectrum without interfering licensed transmitters, the Commission proposed several rules for all unlicensed transmitters to follow:

- The unlicensed devices must first access the database to obtain a list of the permitted channels before operating and re-check the database at least once daily.
- Adopting power spectral density limits for unlicensed TV bands devices.
- Minimizing adjacent channel emissions to certain level.
- Restricting fixed TV bands devices from operating at locations where the height above average terrain of the ground level is greater than 76 meters

The Commission required all TV bands devices to access a publicly available database to obtain information on the available channels at their location and required all unlicensed fixed TV bands devices to register their operations in this database [8]. A database system that maintains records of all authorized services in the TV frequency bands, is capable of determining the available channels using the interference protection requirements as a specific geographic location and provides lists of available channels to this database system that have been certified under the Commissions equipment authorization procedures. According to [9], a TV bands device is permitted to begin operating on a TV channel if no wireless microphone or other low power auxiliary device signals above the detection threshold are detected within a minimum time interval of 30 seconds, and it must also perform in-service monitoring of channels on which it operates a minimum of once every 60 seconds. If a device detects a wireless microphone or other low power auxiliary device signal on a channel it is using, the device must cease all transmissions on that channel within 2 seconds.

Several standards based on the CR networks principle are designed or reformed to work on TVWS bands, typical ones are IEEE 802.22 [65, 76] and IEEE 802.11af [77, 78]. The two IEEE standards define international specifications with different characteristics on operating architecture and mechanisms for spectrum sharing among unlicensed devices and licensed services in the TVWS bands, the main difference is that 802.11af is designed for Wi-Fi in TVWS and 802.22 is aimed at providing a wireless broadband access in rural areas [79]. After IEEE has proposed standardization to enable operation within TVWS bands, 3GPP LTE-A operators are following with an effort to be performed in secondary usage scenario with minor modifications to existing LTE-A CA framework, which allows aggregating multiple channels of different bandwidths [80].

The FCC has strict OOB emission requirements in order to prevent interference with licensed transmissions in other channels. According to the following statement made in 2012 [64]: “In the television channels immediately adjacent to the channel in which a TVBD is operating, emissions from the TVBD shall be at least 55 dB below the highest average power in the TV channel in which the device is operating.” and “Emission measurements in the adjacent channels shall be performed using a minimum resolution bandwidth of 100 kHz with an average detector.” At frequencies beyond the TV channels immediately adjacent

to the channel, the radiated emission limits from TVBDs are 69 dB for fixed devices and 53 dB for portable devices [81].

After being overlooked by the broadband revolution for decades, rural broadband access has recently received significant attention from the telecommunications sector. The FCC finalized rules in [82] to make the unused spectrum in TV bands available for unlicensed broadband wireless devices, which possess suitable propagation characteristics for enabling signals to reach substantial distances. IEEE Standard 802.22 is designed for enabling wireless regional area networks (WRAN), the goal of which is to use CR techniques in order to share underused TVWS on a non-interfering basis, thus providing broadband access to rural environments. Proposed to set aside TV channels in rural areas for fixed licensed backhaul, especially due to the inability of the 4G wireless service infrastructure to reach out to rural areas, WRAN technology has a much larger coverage within a transmission range of 10 – 40 kilometers due to its higher power, which will result in larger OOB emissions that may be right at the emission limits.

A substantial amount of work has been done to guarantee reliable working order between licensed TV bands users and unlicensed users [83, 84], and FCC certifies TVWS solution with Google TV White Space database in 2013 [85]. The coexistence challenges for multiple transmission standards with different characteristics between different unlicensed usage adds complexity to the problem, which attracted more research efforts recently [80, 86]. Nevertheless, even after a unified standard is developed and settled, one of the conditions to achieve the coordination in the TVWS is that all unlicensed services follow strictly the specifications in the regulation, which can be problematic because of potential interference between transmissions in neighboring bands.

2.3.4 Potential Spectral Interference in DSA Network

With the rapid evolution of microelectronics, wireless transceivers are becoming more versatile, powerful, and portable. This has enabled the development of SDR technology, where the radio transceivers perform the baseband processing entirely in software, *e.g.*, modulation/demodulation. The ease and speed of programming baseband operations in an SDR makes this technology a prime candidate for DSA implementation. SDR transceivers

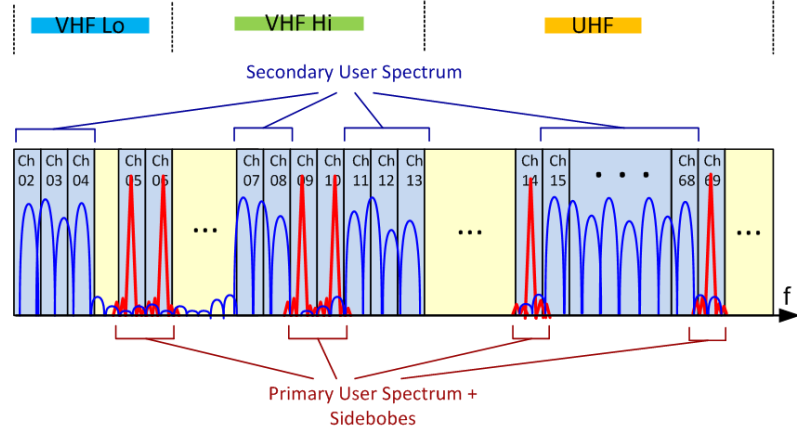


Figure 2.13: Example spectrum of Dynamic Spectrum Access network with interference.

that can rapidly reconfigure operating parameters due to changing requirements and conditions which are known as CR networks [87]. With recent developments in CR technology, it is now possible for these systems to simultaneously respect the rights of incumbent license holders while providing additional flexibility and access to spectrum.

To exploit the advantages of CR transceivers and enable unlicensed users to transmit in the presence of incumbents license holders, a flexible modulation technique based on multicarrier modulation that turns off subcarriers is widely used which would otherwise interfere with incumbent transmissions. This technique is known as non-contiguous multicarrier modulation, or NC-MCM [88]. Frequency division multiplexing (FDM) is a method of sending multiple independent signals simultaneously over different transmission center frequencies. Each of these independent signal can have their own modulation, such as M-ary quadrature amplitude modulation (QAM), M-ary phase shift keying (PSK), or others. Each of these signals are modulated onto its own unique sub-carrier [89]. Once modulated, these signals are then summed together and passed to the RF front-end in the case of wireless communication. OFDM is similar to FDM, but uses the principle of orthogonality between sub-carriers on different frequencies to space the carrier closer together. Each carrier is individually modulated using M-PSK or M-QAM to form a series of constellation points.

Although several techniques exist for implementing spectrally agile waveforms, one of the more efficient approaches is non-contiguous orthogonal frequency division multiplexing

(NC-OFDM), which leverages the divide-and-conquer capabilities of OFDM transmission in order to provide a suitably flexible data transmission candidate for DSA networks. In NC-OFDM, contiguous bands of sub-carriers cannot be used because their use would interfere with the primary user of a given portion of the radio spectrum, thus those carriers are left unused. Figure. 2.13 shows a set of carriers within an NC-OFDM transmission deactivated to minimize interference with the primary user. IEEE 802.11af, IEEE 802.22 and LTE-A CA DL all employ the same technology OFDM or NC-OFDM at PHY layer. The main implementation disadvantage of OFDM/NC-OFDM is the possibility of high PAPR. Since a multicarrier signal consists of a number of independent modulated subcarriers, that can cause a large PAPR when the subcarriers are added up coherently. When the OFDM/NC-OFDM signal with high PAPR passes through a non-linear device, such as a power amplifier working in the saturation region, the signal will suffer significant nonlinear distortion. This non-linear distortion will result in in-band distortion and OOB radiation. The in-band distortion causes system performance degradation and the OOB radiation causes adjacent channel interference that affects systems working in the neighbor bands [43, 90].

RF front-end of transmitters is a necessary enabler for delivery of wireless services, where a significant amount of the impairments and degradation of a wireless system are introduced in [91]. One of the most difficult engineering concerns in the RF portion of SDR/CR is the PA design, which is known for its nonlinearity. Hence, multicarrier transmission exhibits very large PAPRs which combined with the nonlinear intermodulation distortion (IMD) of the PA can generate severe spectral emissions into adjacent channels that potentially interfere with existing neighboring transmissions which can be observed from Figure. 2.13, and thereby deteriorate the reliability of the network. Recently it has been demonstrated that such IMD leads to increased unwanted emissions and can violate the given spectrum emission limits if not properly controlled in LTE-Advanced mobile transmitters with CA or multicarrier type transmissions [67].

To lessen the signal distortion, it requires a linear PA with large dynamic range. However, linear PA normally has poor efficiency and is very expensive. Consequently, in order to enable reliable spectrum pooling of secondary users operating with less cost, there is a need to mitigate these impairments using certain linearization technique.

2.4 Chapter Summary

In this chapter, details regarding the characteristics of reconfigurable multi-standard RF transmitters and the principal regulations in the approved CR-based networks were presented.

Section. 2.2 started with an introduction to two typical architectures of RF transceivers: the direct-up Tx paired with a zero-IF Rx and a two-step-up Tx with a low-IF Rx. The features and limitations of both structures are compared. As the main object this work is focusing on, the detailed knowledge of PA was described, including the signal clipping and saturation caused by its limitation of circuit design, classifications of PAs, main parameters to describe PAs and its resulted impairments: nonlinearity and memory effects. The unwanted IMDs and spectral emissions caused by PA nonlinearity were presented.

The concept and realization of CR networks were then presented in Section. 2.3. Starting with a brief introduction of the evolution from traditional wireless networks to CR networks, the realization of CR-based features were then covered. CA in 3GPP LTE-A network was introduced first in terms of its UL and DL aggregation operation and the properties of supported waveforms. Then the regulations for operating DSA in TVWS were covered in order to guarantee the coexistence between PUs and SUs, and also different SUs, including requirements of transmit power, distance, speed and synchronization to the database. Regarding to different SU operations, IEEE 802.11af and IEEE 802.22 are the two typical standards to operate on TVWS bands, both were briefly introduced in this section. Finally, the potential interference between different transmission operations were explained which is basically caused by nonlinearity of PA combined with high PAPR possessed by multicarrier transmissions. This type of interference is highly likely to deteriorate the reliability of DSA networks.

This chapter established the main problem to be solved in this research work, which is to improve the performance of RF front-end components, and led to the content of the next chapter: the techniques to linearize the RF front-end and thus to reduce the resulting unwanted spectrum emissions.

Chapter 3

Power Amplifier Linearization Techniques for Distortion Reduction

3.1 Chapter Introduction

There has been a substantial amount of research conducted into PA linearization techniques even since 1980s, Yoshihiko Akawa [14] and James K Cavers [12] are two of the most famous theories founders. Technologies proposed to linearize amplifiers can be categorized in various ways, such as analog approaches versus digital approaches, or feedback method versus feedforward method. Among all the methods, digital predistortion (DPD) is recognized as one of the most promising linearization technique and extensively used in industry especially for base station (BS) design, due to its good performance and cost-effectiveness. The goal of PA linearization is to correct unwanted impacts on transmitting signals, and DPD is to operate the correction from digital side before ADC.

In this chapter, all common techniques for PA linearization will be covered [16, 18–22, 92–94], and a comparison of advantages and disadvantages between these techniques will be provided. Since the proposed algorithms in this work is based on DPD schemes, half of this chapter will be contributed to explanation of fundamental knowledge of DPD algo-

rithm, including both current-of-the-art and insight to mathematical system identification procedures for adaptive DPD. In the end, the potential emissions at far out frequencies caused by employing conventional DPD methods are also presented, which are increasingly drawing more attention from researchers and industry recently.

3.2 An Overview of Common Techniques for Power Amplifier Linearization

As introduced in the previous chapter in this document, based on the nonideal performance exhibited highly likely by power amplifiers, a substantial amount of research has been conducted into PA linearization approaches even since 1980s, representative authors include Yoshihiko Akawa [14] and James K Cavers [12].

Linearization is a systematic procedure for reducing an amplifiers distortion. There are many different ways of linearizing an amplifier. One simplest way is to transmit the input waveform with its entire swing in the linear region of certain amplifier and back off from saturation level, but this causes low efficiency. Most of other important PA linearization methods that have been investigated in open literature are briefly discussed in the following subsections.

3.2.1 Feedback and Feedforward Method

Negative feedback is a basic concept behind both systems [95]. Polar feedback is done by sampling a portion of a PA's inverted waveform output, then adding it up with the input, this ended up partially canceling distortion products. The drawback is that the power gain is reduced, and the time delay introduced by the feedback signal path may limit the upper limit of frequency range. [18–20].

An alternate approach, well known as **Cartesian feedback**, separates the signal into in-phase and quadrature components as shown in Fig. 3.1. This eliminates the need for phase-shift components and still allows the correction of gain and phase by adjusting the amplitudes of two ortogonal components. An advantage of Cartesian feedback is that the bandwidths of the I/Q components are approximately equal, while in Polar feedback sys-

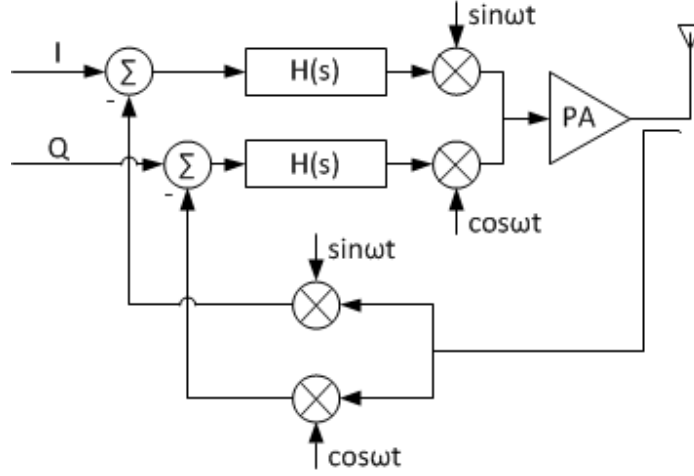


Figure 3.1: A typical Cartesian Feedback System.

tems, the bandwidths of the phase component is much greater than that of the amplitude component. [21, 22]. However, the drawback is that Cartesian feedback approach raises stability concerns.

Similar to feedback, there is a cancellation of the distorted output signal, but without the time delay of re-introducing an output sample at the input. Instead, there are two signal paths, one of which is highly linear, and carries a sample of the undistorted input signal. This signal is compared with a sample of the main signal path output, resulting in an error signal consisting (ideally) of only distortion products. This error signal is inverted and summed with the output signal, cancelling some of the distortion products. Delays are introduced to match the main signal and the error channels. There are numerous methods and topologies for acquiring the output sample, taking the difference with the undistorted signal, and recombining the error signal with the distorted output. [18] Feedforward approach is most useful for very high linearity applications. However, the concerns include matching and drift problems.

3.2.2 Predistortion Method

Pre-distortion is basically a method by which one first stimulates a non-linear PA with baseband samples and then observes the result of that stimulus at the PA output. Then, the

AM/AM and AM/PM effects of the PA are estimated. These estimated distortions are then removed from the PA by pre-distorting the input stimulus with their inverse equivalents [92]. Predistortion is among the more intuitive linearization techniques, and its implementation can be either analog or digital as shown in Fig. 3.2.

For the analog predistortion, linearity can be improved with some RF modules by employing a piecewise approximation of an amplitude transfer function that is opposite of the nonlinear amplifying device such as in [23]. The degree of improvement is limited by the accuracy and stability of the circuitry.

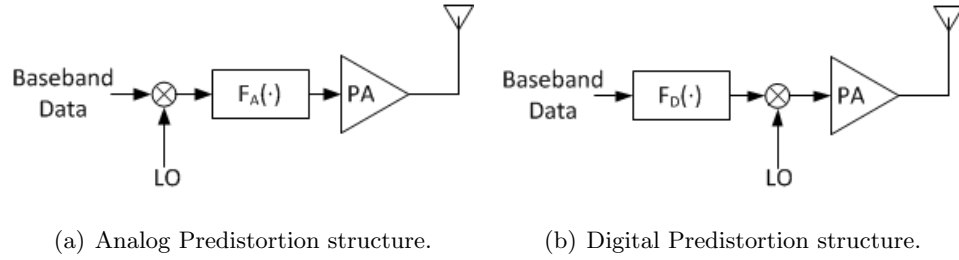


Figure 3.2: Illustration of Analog PD and DPD.

Comparing to analog implement, digital predistortion is widely preferred due to the accuracy that can be achieved in synthesizing the predistortion function with digital signal processors employed. Therefore, digital predistortion is, a cost-effective approach in the linearization of RF PAs.

For DPD, a fast digital signal processor (DSP) or FPGA that calculates the necessary correction to the transfer function of PA is used before ADC. For adaptive adjustment, samples of the power amplifier output can be routed back for digital signal processing, so that it is more sufficient to update the correction as operating parameters change due to thermal effects, aging, duty cycle and output power level in real time, and that is the concept of adaptive digital predistortion as in Fig. 3.3.

Variations in the envelope of the signal produce rapid changes in temperature in the active device of the amplifier caused by transistor temperature-dependent electrical parameters. Changes in the temperature of the active device affect its nonlinear gain, and it is unfortunately unavoidable.

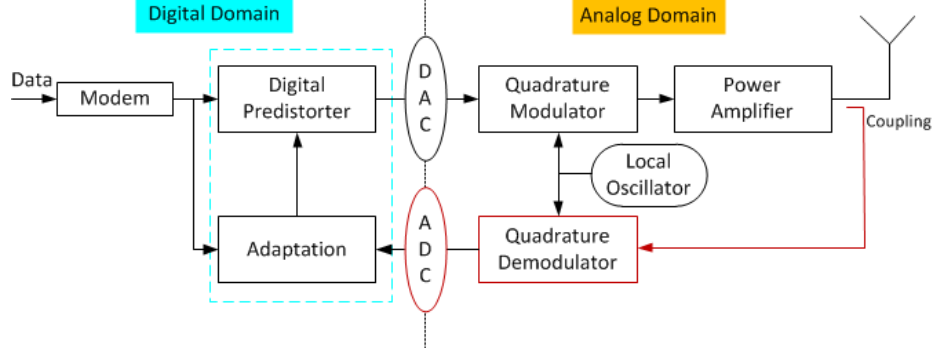


Figure 3.3: A typical Adaptive DPD System.

After first brought to attention by early researchers like James K Cavers [12, 13, 15–17], DPD method especially adaptive DPD method is being extensively used, and steadily improved at the same time, in current wireless communication systems.

The approach proposed in this research work is based on adaptive DPD method, more information of adaptive DPD can be found in the next section.

3.2.3 Outphasing PA System

The outphasing power amplification, also called linear amplification using nonlinear components (LINC), was proposed as another solution that may offer high efficiency with good linearity. LINC combines two nonlinear RF PAs into a linear RF PA system. The two PAs are driven with signals of same amplitude, different phases, and the phases are controlled so that the addition of the PA outputs produces a system output of the desired amplitude [93, 94].

I/Q (Inphase/Quadrature) $S_{IN}(t) = S_I(t) + jS_Q(t)$ and polar $S_{IN}(t) = |S_{IN}(t)| \cdot e^{j\phi(t)}$ are two basic complex signal representations, where $S_I(t)$ and $S_Q(t)$ stand for I- and Q-branch of the complex signal, and $|S_{IN}(t)|$ and $\phi(t)$ denote amplitude and phase of the same signal, respectively. I/Q and polar representation can be related by $|S_{IN}(t)| = \sqrt{S_I(t)^2 + S_Q(t)^2}$ and $\phi(t) = \arctan(S_Q(t)/S_I(t))$. With the proposal of outphasing power amplifier, another signal representation LINC [53] is used as a sum of two constant amplitude, phase modulated signals as $S_{IN}(t) = S_1(t) + S_2(t)$ as shown in Fig. 3.4. Basically, an

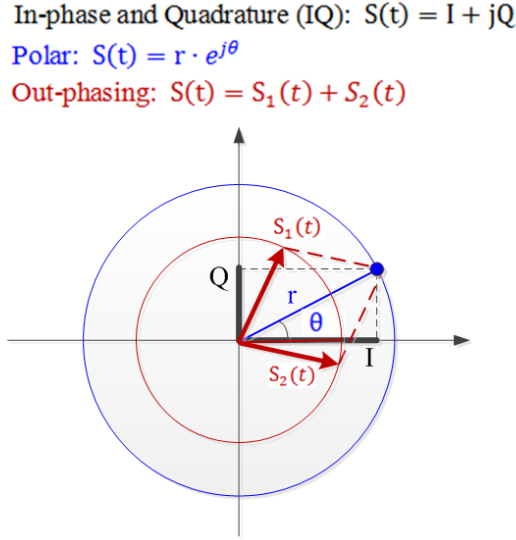


Figure 3.4: Illustration of different complex signal representations.

amplitude modulated signal is first decomposed into two constant amplitude, phase modulated signals that can be amplified using two high efficiency switching power amplifiers. The two outputs are then recombined to restore the original amplitude modulated signal. The derivation of LINC representation is based on:

$$\cos(\theta) \times e^{j\phi(t)} = \frac{1}{2}(e^{j(\phi(t)+\theta(t))} + e^{j(\phi(t)-\theta(t))}). \quad (3.1)$$

Assume that the maximum value of $|S_{IN}(t)|$ is A ($A = \max(|S_{IN}(t)|)$), the complex signal can be written as:

$$\begin{aligned} S_{IN}(t) &= |S_{IN}(t)| \times e^{j\phi(t)}, \\ &= A \times \frac{|S_{IN}(t)|}{A} \times e^{j\phi(t)}, \end{aligned} \quad (3.2)$$

where some θ can be found that satisfies $\cos(\theta) = \frac{|S_{IN}(t)|}{A}$. Hence, according to Eq. 3.1, Eq. 3.2 can be rewritten as:

$$S_{IN}(t) = \frac{1}{2} \times A \times e^{j(\phi(t)+\theta(t))} + \frac{1}{2} \times A \times e^{j(\phi(t)-\theta(t))}. \quad (3.3)$$

Now that we separated $S_{IN}(t)$ into $S_1(t)$ and $S_2(t)$ as:

$$\begin{aligned} S_1(t) &= \frac{1}{2} \times A \times e^{j(\phi(t)+\theta(t))}, \\ S_2(t) &= \frac{1}{2} \times A \times e^{j(\phi(t)-\theta(t))}. \end{aligned} \quad (3.4)$$

The amplitudes of $S_1(t)$ and $S_2(t)$ are both half of maximal amplitude of $S_{IN}(t)$, but the phases are different. Now we reach the conclusion [94] of representing $S_{IN}(t)$ as:

$$S_{IN}(t) = S_1(t) + S_2(t). \quad (3.5)$$

3.2.4 Summary of PA linearization methods

After introducing all common existing PA linearization methods, a summary of advantages and drawbacks of the approaches is given in Table. 3.1. Power backoff is the simplest way of linearizing a PA at the cost of low efficiency. The outphasing PA can achieve high efficiency, but it is very sensitive to amplitude and phase mismatches, and thus requires very high-end and expensive RF components. Digital predistortion technique offers a good balance of nonlinearity correction and cost, although it is limited by sampling rate of the system.

Table 3.1: Summary of common PA linearization methods.

Methods	Advantages	Disadvantages
Power Backoff	Simplicity	Low power efficiency
Cartesian Feed-back	Simplicity, robust to poor PA model	Stability concerns
Feedforward	No stability worries	Matching and drift concerns
Analog Predistortion	Conceptually clear	Requires good PA model, limited accuracy
Digital Predistortion	Easy to modify and update	Correction bandwidth limited by sampling rate
Adaptive Digital Predistortion	No drift problem	Introduces complexity
Outphasing PA	Enable high efficiency nonlinear PAs	Sensitive to amplitude and phase mismatches, and the combining technique

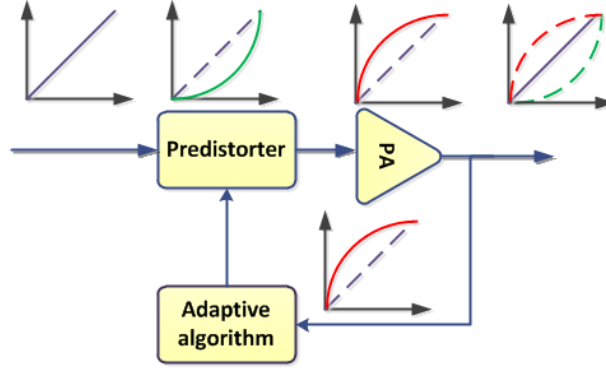


Figure 3.5: General architecture of PA with Digital Pre-distortion employed.

3.3 Adaptive Digital Pre-distortion

Digital Pre-distortion is a technique to improve the performance of radio transmitter PAs including nonlinearity and memory effects in a digital manner, and we really mean adaptive DPD in this section when speaking of DPD. Basically, the first step is to stimulate a PA with baseband signals, and then observe the result at the PA output. After that, the AM/AM and AM/PM effects of the PA are estimated [56]. By pre-distorting the input stimulus with their inverse equivalents, these estimated distortions can be reduced or minimized from the PA characteristics.

Fig. 3.5 illustrates a simple block diagram of a pre-distortion algorithm. We assume a linear gain at the start of pre-distorter, after that for each input baseband sample the pre-distorter generates a error signal based on the difference between the PA output distorted signal and its corresponding undistorted input sample. The pre-distortier gain (and phase) are set such that the overall combination response of the PA and the pre-distorter becomes a linear system, what this means is that the pre-distorter is acting as an inverse of the PA.

In the subsequent sections of this chapter, we analyze digital predistortion technique from the perspective of nonlinear system identification. Dynamic system identification aims at searching for a mathematical model representation best describing system dynamics using input-output data. It is normally concerned with a black-box model or a gray-box model. A gray-box model is constructed based on both a priori knowledge of the system and the

observed data, despite the fact that insight into the actual system is not entirely available. On the other hand, a black-box model is constructed only from system input and output data without knowing any knowledge of the insight. In order to identify a nonlinear system using a gray-box model, the system identification strategies can be subdivided further into two categories [96]:

- **Structure-identification.** This deals with the problem of searching for an optimal mathematical model structure and the optimal number of parameters that best fit a specific nonlinear system. It typically leads to a optimization problem, the complexity of which grows rapidly with the problem size.
- **Parameter-identification.** Having the nonlinear model structure decided including its type and size, it remains to find reasonable parameter values through curve-fitting approaches.

We expand our discussion on these two categories in the following two subsections in terms of representative approaches for nonlinear dynamic behavioral digital PD models and parameter estimation, respectively.

3.3.1 DPD Structure-identification

The existing DPD structure identification techniques mostly employ memory polynomials (MPs) for PA behavioral modeling. A Volterra series, which is the combination of linear convolution and a memoryless nonlinear power series for modelling, can be written as:

$$y(n) = \sum_{k=1}^K \sum_{l_1=0}^{L-1} \cdots \sum_{l_p=0}^{L-1} h_k(l_1, \dots, l_k) \prod_{i=1}^k x(n - l_i), \quad (3.6)$$

where $x(n)$ and $y(n)$ represents the input and output, respectively, and $h_k(l_1, \dots, l_k)$ is called the l_{th} order *Volterra kernel*. However, while the Volterra series can represent any nonlinear operations, under a range of conditions like causality, stability, convergence, time-invariance and fading-memory, the achieved accuracy is limited given a finite computational complexity for practical applications [97]. Hence, taking into account both computational complexity and the need for compensating for static nonlinearities as well as memory effects,

the most common models employed for digital PD are simplified Volterra series such as the Wiener model, the Hammerstein model and structures consisting of a parallel connection of these two models.

Using the Volterra series, two major models have been developed to perform nonlinear signal processing: nonorthogonal model and orthogonal model. Nonorthogonal model and is the most commonly used. which is also called the Volterra model. The advantage is that there is basically no preprocessing needed before the parameter identification (adaptation) [98]. The idea of orthogonal model is to use some orthonormal bases or orthogonal polynomials to represent the Volterra series. The benifit is that it alleviates the numerical sensitivity in nonlinear model parameter identification.

Nonorthogonal Nonlinear Models

Typically Volterra models are implemented by interconnections of linear time-invariant (LTI) subsystems and nonlinear, memory-less subsystems.

1. **Wiener model:** The Wiener model (see Fig. 3.6(a)) consisits of a linear time-invariant (LTI) system/a linear filter followed by a memoryless nonlinearity. The two subsystems are given by

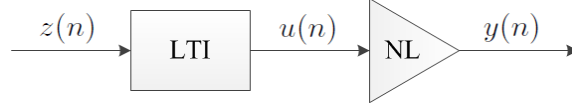
$$u(n) = \sum_{l=0}^{L-1} a_l x(n-l), \quad (3.7)$$

$$y(n) = \sum_{k=1}^K b_k u(n) |u(n)|^{k-1}, \quad (3.8)$$

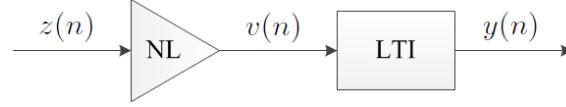
where a_l 's are the impulse response values of the LTI block and b_k 's are the coefficients of odd-order nonlinear polynomial. Substitution of (3.7) into (3.8) leads to:

$$y(n) = \sum_{k=1}^K b_k \left[\sum_{l=0}^{L-1} a_l x(n-l) \right] \left| \sum_{l=0}^{L-1} a_l x(n-l) \right|^{k-1}. \quad (3.9)$$

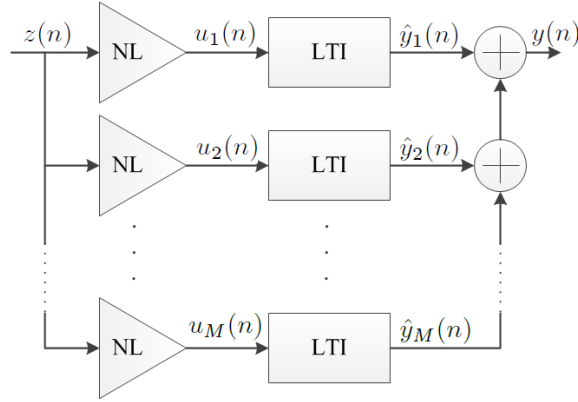
The Wiener model has replaced the memoryless polynomial model to model PA with memory effects to improve modeling accuracy.



(a) Wiener model.



(b) Hammerstein model.



(c) parallel Hammerstein (PH) model.

Figure 3.6: Some common nonlinear nonorthogonal models.

2. **Hammerstein Model:** The Hammerstein model (see Fig. 3.6(b)) is a reverse of Wiener model, i. e. a memoryless nonlinearity followed by an LTI system. Similarly, the two sub systems in this model can be described by:

$$v(n) = \sum_{k=1}^K b_k x(n) |x(n)|^{k-1}, \quad (3.10)$$

$$y(n) = \sum_{l=0}^{L-1} c_l v(n-l), \quad (3.11)$$

where b_k 's are the coefficients of odd-order nonlinear polynomial and c_l 's are the impulse response values of the LTI system. Substituting (3.10) into (3.11) gives:

$$y(n) = \sum_{l=0}^{L-1} c_l \sum_{k=1}^K b_k x(n-l) |x(n-l)|^{k-1}. \quad (3.12)$$

3. Parallel Hammerstein (PH) Model: As an extension of Hammerstein model, the parallel Hammerstein (PH) model, also known as memory polynomial [99] (see Fig. 3.6(c)), has its output equal to the sum of outputs from several independent Hammerstein model branches

$$y(n) = \sum_{p=1}^P \hat{y}_p(n), \quad (3.13)$$

where $\hat{y}_p(n)$ represents the output of the p_{th} parallel branch. This structure is advantageous to a single model branch when it serves as a means to represent the behavior of a PA at different envelope frequencies [25, 100].

In a PA DPD PH system, the branch nonlinearities are normally polynomials of different odd orders, which are considered to represent odd orders of IMD products (refer to Section ??), with $k \in I_k$ where $I_k = \{1, 3, 5, \dots, 2P + 1\}$.

Orthogonal Nonlinear Models

Orthogonal polynomials are introduced to reduce numerical errors in the direct inversion of memoryless nonlinearities, which can improve numerical stability in parameter extraction for baseband models, as well as to simplify spectral regrowth analysis [35, 98].

Take PH structure for example as shown in Fig. 3.6(c), assume that $\hat{y}_i(n)$ and $\hat{y}_j(n)$ are orthogonal functions, it is true if and only if:

$$E [\hat{y}_i^*(n) \hat{y}_j(n)] = \delta_{ij}, \quad (3.14)$$

where $*$ stands for complex conjugation, δ_{ij} is the Dirac delta function and $E[\bullet]$ denotes statistical expectation. For example authors in [35] present a set of orthogonal polynomials ($E[f^*(z)g(z)] = 0$) in order to alleviate the numerical sensitivity in nonlinear model parameter identification.

3.3.2 DPD Parameter-identification

After the first step of system identification - structural identification has already been taken, it leaves the parameters of a fixed type of model to be determined. Parametric system identification is also called parametric adaptive control. The parameters of the model are adjusted during the operation of the plant as the amount of data available for identification increases. When the number of parameters is larger than several, and they vary with time, automatic adjustment is needed.

There are two popular approaches to adaptive control, including model reference controllers and self-tuning regulators. The only real difference between them is that model reference schemes are direct adaptive control schemes, whereas self-tuning regulators are indirect. The self-tuning regulator first identifies the plant parameters recursively, and then uses these estimates to update controller parameters through some fixed transformations. The model reference adaptive schemes update the controller parameters directly, more details can be found in [101]. In this document, we distinguish between direct and indirect schemes for digital predistortion parameter identification.

1. *Direct Learning Architecture*: In the direct learning architecture in Fig. 3.7, firstly, the PA model is modeled by some MP such as the ones introduced in Section 3.3.1. And then the inverse of the PA model is calculated (or pre-inverting the PA model [102]). DPD function can be solved by defining z_n . Since the parameters of the pre-distortion approach are obtained directly based on its input and reference error, the direct learning approach outperforms indirect learning architecture in terms of measurement noise control. However, there are still distinct drawbacks to this solution, such as computational complexity, the local minima problem and the nonlinear effect on the convergence speed [103]. Although the proposed methods in [103] substantially reduces the computational complexity, the latter two problems remain for further investigation [104].
2. *Indirect Learning Architecture (ILA)*: Two identical polynomial-based nonlinearities are employed in ILA scheme for both pre-distortion and post-distortion [27], as shown in Fig. 3.8. In post-distortion, an inverse PA model is identified by using the output

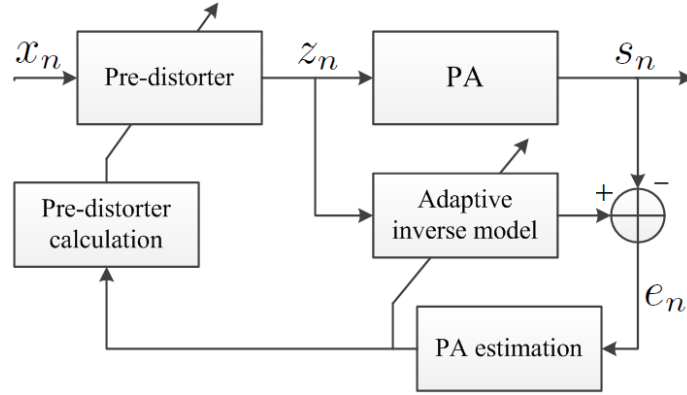


Figure 3.7: Direct Learning Architecture (DLA).

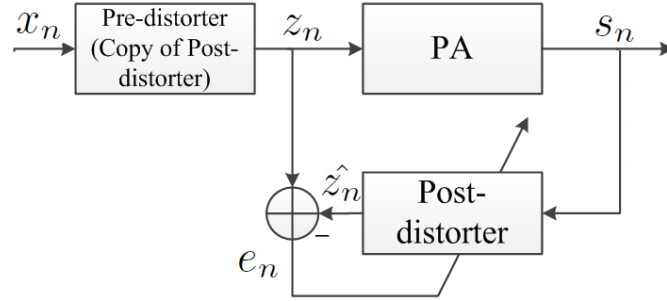


Figure 3.8: Indirect Learning Architecture (ILA).

of the PA to predict its input, and then the estimated parameters are copied to the identical pre-distortion. Comparing to direct learning scheme, the most appealing feature of the ILA is that it enables the estimation of the predistortion coefficients directly without finding and inverting the PA model and hence simplify the computation. However, measurement noise in ILA is more problematic than in direct learning [25, 42, 103].

The predistorter parameters can be defined by using linear estimation approaches in linear adaptive filter theory, such as the least squares (LS) method, recursive least square (RLS) and least mean square (LMS). It is possible because the model is linear in the unknown parameters.

1. *Least Square (LS) method.* The 'best' fit of LS method is obtained by minimizing the

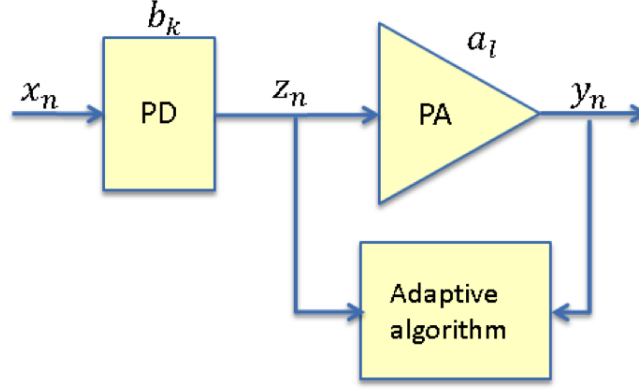


Figure 3.9: A general DPD parameter identification architecture.

sum of the squares of the difference between the input data and its estimate, such as z_n and \hat{z}_n in Fig. 3.8. In computational terms, it is a block-processing approach, where it is designed by processing a block of input data. The filter is adapted to nonstationary data by repeating the computation on a block-by-block basis, which makes its computational complexity much more demanding than its recursive counterpart RLS.

2. *Recursive Least Square (RLS)*. RLS is a recursive algorithm as an extension of LS. Basically, given the LS estimate at iteration $n - 1$, we may compute the updated estimate of the vector at iteration n upon the arrival of new data. An important feature of RLS (filter) is that its rate of convergence is typically an order of magnitude faster than that of the simple LMS method (filter).
3. *Least Mean Square (LMS)*. The LMS algorithm is a linear adaptive filtering algorithm to find the filter coefficients by producing the least mean squares of the error signal which is defined as the difference between the desired and the actual signal., which is normally composed of two basic processes: a filter process and an adaptive process. And a combination of the two processes constitutes a feedback loop. A significant feature of LMS algorithm is its simplicity and it doesn't require matrix inversion as for block LS [105].

With an ILA approach selected, the goal is to find a mathematical model that serves exactly as the inverse of the PA model, which also means that taking in the output vector of the unit gain PA \mathbf{y}_n as shown in Fig. 3.10, ideally the adaptive algorithm for DPD should produce the output samples exactly the same as the PA input \mathbf{z}_n . With \mathbf{b} denoting the coefficient vector of DPD, the error signal between the input of PA and the output of DPD can be represented as:

$$\mathbf{e}_n = \mathbf{z}_n - \mathbf{y}_n^T \mathbf{b}, \quad (3.15)$$

and thus after taking the square of Eq. (3.15) we have:

$$\mathbf{e}_n^2 = \mathbf{z}_n^2 - 2 \mathbf{z}_n \mathbf{y}_n^T \mathbf{b} + \mathbf{b}^T \mathbf{y}_n \mathbf{y}_n^T \mathbf{b}, \quad (3.16)$$

The solution we are seeking for is the **Wiener solution**, which represents the minimum mean-square error (MSE) solution. The MSE can be defined as:

$$\begin{aligned} \xi &\triangleq E[\mathbf{e}_n^2] \\ &= E[\mathbf{z}_n^2] - 2E[\mathbf{z}_n \mathbf{y}_n^T] \mathbf{b} + \mathbf{b}^T E[\mathbf{y}_n \mathbf{y}_n^T] \mathbf{b}. \end{aligned} \quad (3.17)$$

As we can observe, this solution depends on the input signal correlation matrix $E[\mathbf{y}_n \mathbf{y}_n^T]$ as well as on the the cross-correlation between the elements of the input signal vector and the reference signal $E[\mathbf{z}_n \mathbf{y}_n^T]$. The values of these correlations form the parameters of the MSE surface, which is a quadratic function of the adaptive-filter coefficients. Thus, referring to Fig. 3.10(a) and Eq. (3.18), after taking derivative of the surface function with respective of \mathbf{b} , the Wiener solution \mathbf{b}_0 can be located when the derivative function is set to 0:

$$\begin{aligned} \frac{\partial \xi}{\partial \mathbf{b}} &= -2E[\mathbf{z}_n \mathbf{y}_n^T] + 2E[\mathbf{y}_n \mathbf{y}_n^T] \mathbf{b} \\ &= 0. \end{aligned} \quad (3.18)$$

After solving Eq. (3.18), the Wiener solution \mathbf{b}_0 is given by:

$$\mathbf{b}_0 = E[\mathbf{y}_n \mathbf{y}_n^T]^{-1} E[\mathbf{z}_n \mathbf{y}_n^T] \quad (3.19)$$

In practice the parameters that determine the MSE surface shape are not available. What is left is to directly or indirectly estimate these parameters using the available data

and to develop adaptive algorithms that use these estimates to search the MSE surface, such that the adaptive-filter coefficients converge to the Wiener solution in some sense [106].

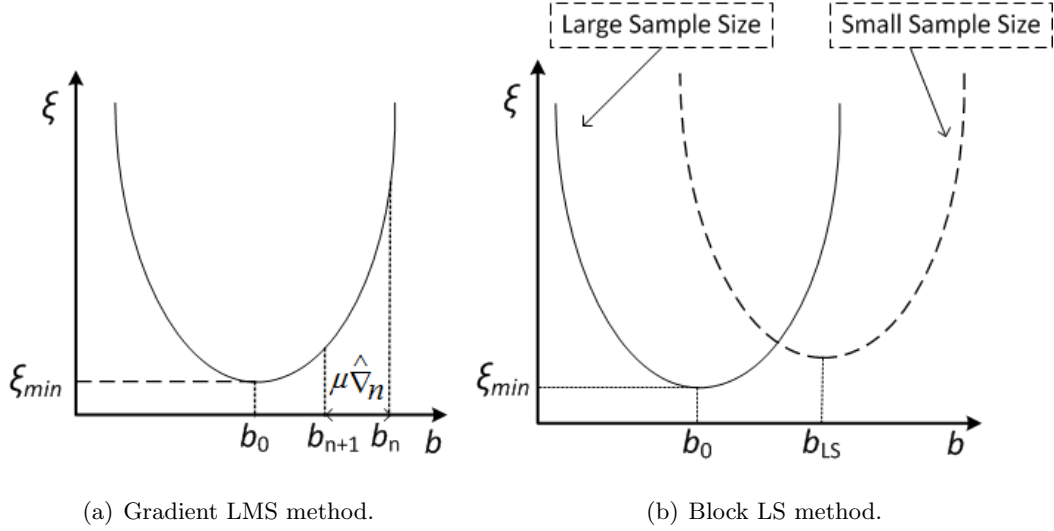


Figure 3.10: Illustration of MSE surface of LMS and block LS methods.

With gradient LMS method as shown in Fig. 3.10(a), the approximate DPD coefficients are dependent on the last sets of coefficients:

$$\mathbf{b}_{n+1} = \mathbf{b}_n - \mu \hat{\nabla}_n, \quad (3.20)$$

where $\hat{\nabla}_n$ is defined as:

$$\begin{aligned} \hat{\nabla}_n &= -2(\mathbf{z}_n - \mathbf{y}_n^T \mathbf{b}) \mathbf{y}_n \\ &= -2 \mathbf{e}_n \mathbf{y}_n, \end{aligned} \quad (3.21)$$

and thereby Eq. (3.20) can be rewritten as:

$$\mathbf{b}_{n+1} = \mathbf{b}_n + 2\mu \mathbf{e}_n \mathbf{y}_n. \quad (3.22)$$

By choosing the weight vector μ carefully, ideally the estimated coefficients should converge to Wiener solution eventually. However, the convergence time of the gradient LMS method is much longer than the block LS method, the results of which are only based on a block of samples. The coefficient approximate by block LS method can be:

$$\mathbf{b}_{LS} = (\mathbf{y}_n \mathbf{y}_n^T)^{-1} \mathbf{z}_n \mathbf{y}_n^T. \quad (3.23)$$

We can observe that instead of requiring statistical information of the data, the result of LS method is determined by the available data samples. As shown in Fig. 3.10(b), the larger sample size taken for each computation, the closer the result approaches the Wiener Solution.

3.3.3 Iterative Steps for DPD System Identification

System identification is a procedure with analysis, synthesis, selection and optimization. It can be carried out off-line or on-line recursively. Generally, system identifications are considered related with process control, so that the identification and control criterion will be done at the same time. Hence, on-line recursive identification methods are more significant, the results of which will be verified and improved iteratively until certain requirement are satisfied. Specifically for DPD system identification under assumption of ILA, it can be identified with the following iterative steps [96] with reference to Fig. 3.11:

1. *Optimal experiment design and data collection.* Select excitation signal pattern, signal processing parameters such as sampling rate and measure both input and output of certain PA model.
2. *Model structure selection.* Select a proper polynomial model structure with suitable order for post-distorter.
3. *Model estimation.* Having a model structure, measured data, along with a parameter identification method and some optimal algorithm like ILA and LS algorithm, the parameters in the model structure can be estimated by optimizing certain criterion.
4. *Model validation.* After several simulation iterations of estimation with different data, verify if the model is valid by checking whether performance of the output of PA with DPD is improved. For example, if linearity and memory effects are reduced to under certain level, or if spectrum regrowth is suppressed effectively.

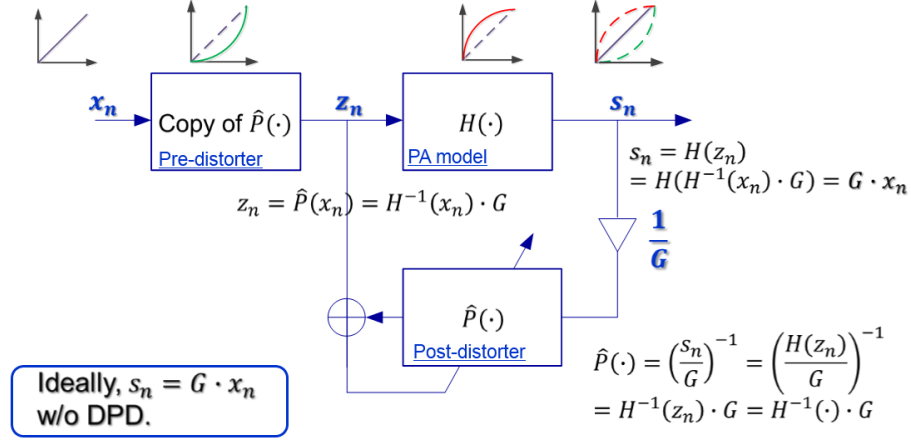
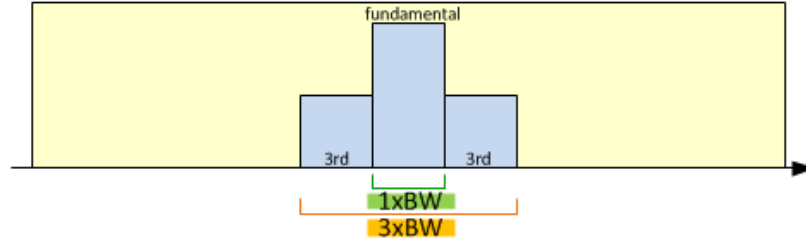


Figure 3.11: Illustration of iterative steps in ILA structure.

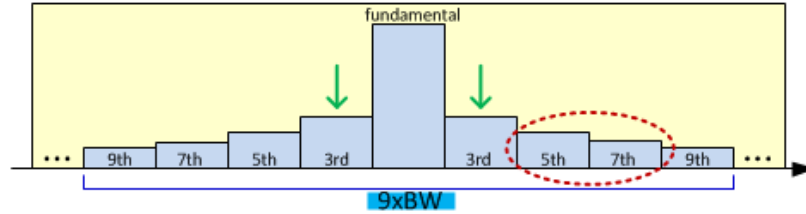
3.3.4 Features and Drawbacks of Current DPD techniques

The conventional DPD methods are proved to be able to effectively reduce the OOB emissions that fall within adjacent channels, however the implementation of DPD results in the far out spurious emission and thus expands the transmission bandwidth, which means that there is a trade-off between OOB at adjacent channels and spurious emissions further away from fundamental carrier. Moreover, when deploying FDD [44], one challenge is also to protect its own receiving band which can be impacted by the spurious emissions from the transmitter. One solution is to employ RF duplex filter, but the defect is that it suppresses its own receiving band as well.

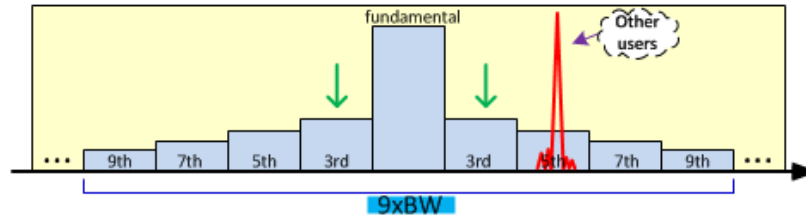
As shown in Fig. 3.12, we put a 3rd order polynomial DPD to correct a 3rd order polynomial PA model, from Fig. 3.12(a), it can be observed that without DPD, the output spectrum of PA is expanded to 3 times its bandwidth by carrying large OOB at both side. After implementing DPD as shown in Fig. 3.12(b), the bandwidth is expanded to 9 times bandwidth for the reason that applying DPD is equivalent to feeding a nonlinear signal (DPD) to another nonlinear system (PA), such that the final order of the nonlinearity becomes 9th in this example, and thus it results in 9 times the bandwidth. Consequently, even though the DPD technique can effectively suppress the OOB leakage at adjacent channels, the spurious emissions located further away from the fundamental carrier grow.



(a) PA output spectrum without DPD.



(b) PA output spectrum with DPD.



(c) Potential interference caused by DPD.

Figure 3.12: Illustration of possible spectrum interference caused by employing DPD.

In the cases when other users are operating in the far-away band with spectrum regrowth or its own receiver is receiving on that band as illustrated in Fig. 3.12(c), it may potentially result in interference.

Although emissions at the adjacent channel are usually still higher than those at far-away frequencies, a wireless system usually sets different power limits for allowable spectral emissions at OOB band and spurious domain [67]. Therefore, there is a need to investigate on an enhancement to conventional DPD approach that can keep both OOB emissions and spurious emissions under the corresponding emission limits. There has been a few work on this topic, for example, [45, 46] proposed enhanced DPD method to reduce the OOB emissions more effectively, the work in [47] was with the objective of generally suppressing

IMDs in LTE-A network [48].

3.4 Chapter Summary

In this chapter, common PA linearization techniques were introduced, with extensive discussions on adaptive DPD method.

Section 3.2 started with an overview of PA linearization methods, methods including power backoff, feedback, feedforward, analog and digital PD and outphasing PA system were covered, in terms of their structures and mathematical derivations. At the end of the section, a summary of the pros and cons of mentioned linearization approaches were provided.

In Section 3.3, an extensive study of adaptive DPD techniques based on author's understanding was provided. First, an overview of system identification for DPD was presented, including two steps: structure identification and parameter identification. The DPD structure identification is to find proper mathematical models for DPD and sometimes for PA too, two kind of mathematical models were covered including memoryless nonlinear model and memory-based nonlinear model, and the basis functions of both can be either non-orthogonal or orthogonal with extra processing. In the DPD parameter identification part, both DLA and ILA architecture were covered, and estimation of parameters can be done with LS method or LMS method to approximate the Wiener solution. The discussion on both approaches were expanded. Finally, the potential emissions caused by implementation of conventional DPD methods were highlighted, which serves as the goal of one task in the proposed work.

Up to this chapter, all the fundamental knowledge and maths that are closely related to the proposed DPD methods in this work have been covered.

Chapter 4

Proposed DPD Method for OOB Emission Reduction

4.1 Chapter Introduction

As introduced in Chapter 2, to enable more efficient use of wireless spectrum, DSA [10] has been proposed as a means of permitting SUs to temporarily occupy PUs' frequency bands with no interference directed towards the latter. One candidate approach for SU transmission is spectrally agile transmission [108], where the SU broadcasts data across several noncontiguous frequency bands at the same time such that they avoid interfering with the primary user transmissions while simultaneously obtaining the benefits of a substantial aggregate transmission bandwidth. One form of spectrally agile transmission is NC-OFDM, which leverages the “divide-and-conquer” capabilities of OFDM transmission in order to provide flexible data transmission within the context of DSA networks [109, 110]. This spectral flexibility is achieved by deactivating subcarriers based on dynamic spectrum sensing measurements [111]. Although the NC-OFDM transmission scheme is efficient in filling spectral gaps left vacant by the licensed users, high OOB emissions remain a challenging technical problem when using NC-OFDM to realize DSA.

The work presented in this chapter has been submitted in parts at [P1], [P3] and [P4]. The algorithm in [107] is identical to the one proposed in [P1].

Several effective algorithms to eliminate OOB sidelobe spectral leakage have been presented in the literature [112, 113]. Furthermore, as covered in Chapter 3, quite a few work of distortion reduction has been done with RF front-end impairments being accounted for. The primary issue associated with the PA is its nonlinear distortion characteristic, which combined with a high PAPR [114] that is often associated with multicarrier transmissions, generates large OOB sidelobe spectral leakage that can potentially interfere with existing neighboring transmissions, thus severely deteriorating the reliability of the DSA network. On the other hand, the I/Q modulator in direct-conversion radio transmitter architecture is potentially responsible for problems such as I/Q mismatch and LO leakage [41, 115]. Consequently, there is a need to mitigate these impairments using a DPD technique in order to enable reliable spectrum pooling of secondary users operating with primary spectrum.

A number of techniques have been proposed in the open literature that attempt to modify the PA characteristics in order for them to become more linear. For example, several techniques focus on a polynomial-based DPD approach [25, 32, 35, 100]. More recently, several DPD approaches were proposed for multicarrier transmission schemes [116, 117]. Furthermore, under I/Q imbalance and LO leakage, the PA predistorter coefficient estimates are heavily biased and PD can potentially make the spectral regrowth even worse. The techniques in [17, 41] focus only on I/Q modulator errors. There are several publications that discuss these problems together, such as in [26, 42] that focus on joint PA and I/Q modulator calibration in wideband direct-conversion transmitters, assuming frequency-dependent behavior for PA nonlinearities and modulator I/Q imbalance. However, these work did not take into account spectrally agile transmission, which potentially possesses narrow-band signals and broad-band signals at the same time.

In the work presented in this chapter, we investigate both PA only, and joint PA and I/Q modulator effects for an NC-OFDM transceiver when sidelobe suppression algorithms are employed. Moreover, we propose a novel DPD technique that simultaneously compensates for PA and I/Q modulator impairments. The proposed DPD method is presented, which builds upon the previous work of the authors in [42] with similar mathematical models employing QAM signals. We then explore an orthogonal basis approach and combine it with the predistorter structure such that the new method is better suited for NC-OFDM

transmission. In the end, the performance analysis of our proposed method is presented to support the theoretical explanation.

4.2 Proposed DPD System Identification Solutions

In this section, we introduce a simplified DPD structure for PA, I/Q modulator and LO, based on PH memory polynomial (MP) model, with ILA structure and LS for adaptive parameter estimation. The major benefit of the simplified architecture is that it largely cut the number of coefficients (parameters) that are to be estimated.

Table 4.1 summarizes most frequently used notations in this chapter to show the parameter identification procedures.

Table 4.1: Principal notations used in the chapter

Principal notations used in this chapter	
$x(n)$	Baseband digital pre-distorter (PD) input
$y(n)$	I/Q imbalance PD input/PA PD output in PD structure
$z(n)$	Digital Pre-distorter output
$\phi(\cdot)$	Basis functions of memoryless nonlinearities
$\psi(\cdot)$	Orthogonal polynomial functions of memoryless nonlinearities
\star	Convolution
$(\cdot)^*$	Complex-conjugation
$(\cdot)^T$	Matrix transpose
$(\cdot)^H$	Conjugate transpose

4.2.1 DPD Structure for PA

In this section, the estimation of post-distorter (and thus pre-distorter) parameters based on ILA (Fig. 3.8) and block LS estimation are selected (see Section. 3.3.1). With memory polynomial (PH structure) applied to post-distorter (see Fig. 3.6(c)), the post-distorter uses the PA output $s(n)$ as its input signal and the MSE between the post-distorter output $\hat{z}(n)$ and the PA input $z(n)$ is minimized (referring to Section. 3.3.2). While k only taking odd

numbers, we define the vector notations as follows:

$$\begin{aligned}\mathbf{z}' &= [z'(1), z'(2), \dots, z'(n)]^T \\ \Phi(\mathbf{s}) &= [\phi_1, \phi_3, \dots, \phi_K] \\ \mathbf{a} &= [a_1, a_3, \dots, a_K]^T\end{aligned}\tag{4.1}$$

z' can also be written as $\mathbf{z}' = \Phi(\mathbf{s})\mathbf{a}$. Also for simulation purposes, we define each ϕ_k after pre-windowing in vector-matrix (4.2), where we denote the training signal length by N , filter length by L and the order of nonlinear polynomial by K :

$$\phi_k = \begin{bmatrix} s_0 |s_0|^{k-1} & 0 & 0 & \dots & 0 \\ s_1 |s_1|^{k-1} & s_0 |s_0|^{k-1} & 0 & \dots & 0 \\ s_2 |s_2|^{k-1} & s_1 |s_1|^{k-1} & s_0 |s_0|^{k-1} & \dots & 0 \\ \vdots & \vdots & \vdots & & \vdots \\ s_{N-1} |s_{N-1}|^{k-1} & s_{N-2} |s_{N-2}|^{k-1} & s_{N-3} |s_{N-3}|^{k-1} & \dots & s_{N-L} |s_{N-L}|^{k-1} \end{bmatrix}.\tag{4.2}$$

Assuming the PA input signal vector is defined by $\mathbf{z} = [z(1), z(2), \dots, z(n)]^T$, then we may express the estimation error in the matrix form:

$$\boldsymbol{\varepsilon} = \mathbf{z} - \Phi(\mathbf{s})\mathbf{a}.\tag{4.3}$$

The sum of error squares can thus be written in terms of $\boldsymbol{\varepsilon}$ as :

$$\xi(\mathbf{a}) = \boldsymbol{\varepsilon}^H \boldsymbol{\varepsilon}.\tag{4.4}$$

Substituting $\boldsymbol{\varepsilon}$ in (4.4) with (4.3) and differentiating $\boldsymbol{\varepsilon}$ with respect to \mathbf{a} , we have the gradient vector $\frac{\partial \xi(\mathbf{a})}{\partial \mathbf{a}} = -2\Phi(\mathbf{s})^H \mathbf{z} + 2\Phi(\mathbf{s})^H \Phi(\mathbf{s})\mathbf{a}$. To minimize $\boldsymbol{\varepsilon}$, the gradient vector $\partial \xi(\mathbf{a})/\partial \mathbf{a}$ is set to zero, then the LS estimate of \mathbf{a} based on PA output measurements \mathbf{s} and the PA input \mathbf{z} becomes:

$$\hat{\mathbf{a}}_{LS} = (\Phi(\mathbf{s})^H \Phi(\mathbf{s}))^{-1} \Phi(\mathbf{s})^H \mathbf{z}.\tag{4.5}$$

With reference to Fig. 3.8, we use the term *ILA iteration* [25] to denote a single simulation cycle, in which we take N -sample PA input $\mathbf{z}_{N \times 1}$ along with $\Phi(\mathbf{s})$ as input signals of post-distorter, and plugin its output $\hat{\mathbf{a}}_{LS}$ into the pre-distorter for the next cycle:

$$\mathbf{z} = \Phi(\mathbf{x})\hat{\mathbf{a}}_{LS},\tag{4.6}$$

where \mathbf{x} represents the input of pre-distorter. With the pre-distorter turned off in the first ILA iteration, it typically takes two to three iterations to fully converge, the simulation results of which are illustrated and analyzed in the next section.

4.2.2 Parameter Identification with Proposed Orthogonal Basis Functions

The LS estimator has a unique solution given that the data matrix has full column rank. Full rank is guaranteed with all practical communications waveforms. However, even if the data matrix is of full rank, the sensitivity of the solution can depend on the condition number of the data matrix. Condition number is a measure of the linear dependency of the columns of the data matrix, and is generally related to the power spectral density (PSD) of the used signal waveform, as well as the dimensionality of the problem. If both the data matrix and the observation vector are perturbed by noise, then the error in the LS solution is proportional to the square of the condition number. Orthogonal polynomials can alleviate the problem of LS solution misalignment by decreasing the condition number of the data matrix. Therefore, by use of orthogonal polynomials, the LS solution should be robust against measurement noise.

The basic structure of the simplified joint PA and I/Q modulator predistorter proposed in [42] is adopted in this paper, and is generalized and improved upon with our proposed approach. The predistorter considering both nonlinearities and memory effects can be modeled mathematically with a memory polynomial, which is composed of an odd order memoryless nonlinearity followed by a linear filter. First, the nonlinearity can be represented by the polynomials $\mu(s) = \sum_{k=1}^K b_k \phi_k(s)$, where $\phi_k(s) = s(n) |s(n)|^{k-1}$ is the k^{th} basis function of the nonlinearity ($k \in \{1, 3, 5, \dots, K\}$), b_k is the coefficient associated with the k^{th} basis, and $s(n)$ represents the n^{th} sample of the input signal to the predistorter. And then combining with M^{th} order memory, the new memory polynomial model becomes:

$$\hat{z}(n) = \sum_{m=1}^M h_m \sum_{k=1}^K b_k \phi_k(s(n-m)), \quad (4.7)$$

where M is the order of the linear filter and h_m is the m^{th} order coefficient of the filter.

Eq. (4.7) can also be written in the form of a PH model [24]:

$$\hat{z}(n) = \sum_{k=1}^K b_k \phi_k(s(n-m)) \sum_{m=1}^M h_m. \quad (4.8)$$

As discussed in [107], when using the LS solution for the predistorter it is necessary to solve $(\Phi^H \Phi)^{-1}$ (Eq. (4.5)), where Φ is a matrix composed of ϕ , which introduces the numerical instability problem of inverting a matrix that is not guaranteed to be nonsingular. To solve this problem, several orthogonal polynomial approaches are proposed to replace conventional polynomials [35, 118]. However, these approaches are based on the assumptions of knowing the statistics of the input signal. In fact, the distribution of the input waveform to the PA or predistorter is not always known, here we propose an orthogonal polynomial method to work around the statistics of the signal by pre-processing the signal before it goes to the LS predistorter.

With $\psi_k(s)$ denoting the k^{th} orthogonal basis function, instead of finding $\psi_k(s)$'s that satisfy:

$$E[\psi_i(s)^* \psi_j(s)] = 0, \quad (4.9)$$

where $i \neq j$, i and j are odd numbers, $*$ denotes complex conjugation, and $E[\cdot]$ stands for statistical expectation. We collect a block of N samples of the input signal $s(n)$, where N is the block size of the LS solution, and write the new set of orthogonal polynomials as:

$$\psi_k(s) = \sum_{l=1}^k a_{l,k} \phi_l(s), \quad (4.10)$$

with $a_{1,k} = 1$ for all k 's and it satisfies:

$$\int \psi_i^*(s) \psi_j(s) ds = 0, \quad (4.11)$$

where $i \neq j$, i and j are odd numbers. All the coefficients $a_{l,k}$'s can be calculated by solving $\binom{K+1}{2}$ times of (4.11) for different combinations of i and j . Then, the new matrix $(\Psi^H \Psi)^{-1}$ for LS estimation becomes diagonal with the diagonal entries $\int \psi_k^2(s) ds$ with $k = 1, 3, \dots, K$, which is non-singular and thus solves the numerical instability problem.

Combining the orthogonal polynomial method with the PH structure, (4.8) can be rewritten as:

$$\hat{z}(n) = \sum_{k=1}^K c_k \psi_k(s(n-m)) \sum_{m=1}^M h_m, \quad (4.12)$$

and the proposed predistorter for PA can be structured as shown in Fig. 4.1, which consists of $(K + 1)/2$ parallel branches, with $\psi_k(s)$ denoting the k^{th} orthogonal polynomial basis function and $H_k(\cdot)$ representing the transfer function of the linear filter on the k^{th} branch.

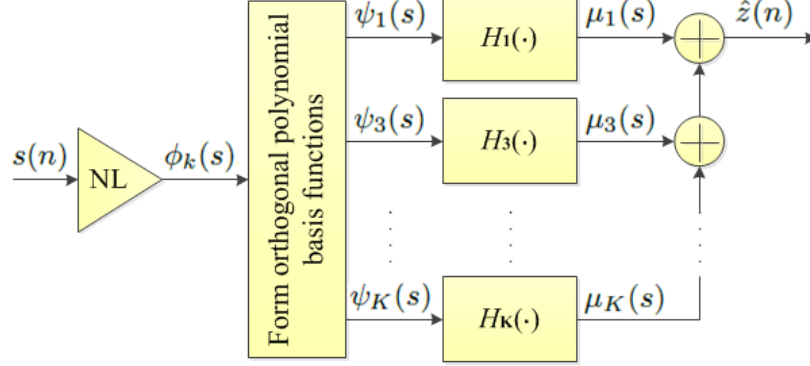


Figure 4.1: Proposed parallel Hammerstein predistorter structure based on orthogonal polynomials.

Taking a fifth order nonlinear DPD for example ($K = 5$), $\mu(s)$ can be expanded as

$$\mu(s) = c_1 \psi_1(s) + c_3 \psi_3(s) + c_5 \psi_5(s), \quad (4.13)$$

where following (4.10), $\psi_k(s)$ can be written as follows:

$$\begin{aligned} \psi_1(s) &= \phi_1(s) \\ \psi_3(s) &= \phi_1(s) - a_{3,3} \phi_3(s) \\ \psi_5(s) &= \phi_1(s) - a_{3,5} \phi_3(s) - a_{5,5} \phi_5(s) \end{aligned} \quad (4.14)$$

and (4.11) is then translated to the following three equations:

$$\begin{aligned} \int \psi_1^*(s) \psi_3(s) ds &= 0, \\ \int \psi_1^*(s) \psi_5(s) ds &= 0, \\ \int \psi_3^*(s) \psi_5(s) ds &= 0. \end{aligned} \quad (4.15)$$

After plugging (4.14) into (4.15), we have:

$$\begin{aligned}
\int |s|^2 ds - \int \alpha |s|^4 ds &= 0, \\
\int |s|^2 ds - \beta \int |s|^4 ds - \gamma \int |s|^6 ds &= 0, \\
\int |s|^2 ds - \beta \int |s|^4 ds - \gamma \int |s|^6 ds - \alpha \int |s|^4 ds + \alpha \beta \int |s|^6 ds + \alpha \gamma \int |s|^8 ds &= 0,
\end{aligned} \tag{4.16}$$

and then substitute the integrals of the squares of s with $\beta_k = \int |s|^k ds$ where $k = 2, 4, 6, 8$, the coefficients $a_{k,l}$'s become:

$$\begin{aligned}
a_{3,3} &= \frac{\beta_2}{\beta_4}, \\
a_{3,5} &= \frac{\beta_2 \beta_8 - \beta_4 \beta_6}{\beta_4 \beta_8 - \beta_6^2}, \\
a_{5,5} &= \frac{\beta_4^2 - \beta_2 \beta_6}{\beta_4 \beta_8 - \beta_6^2}.
\end{aligned} \tag{4.17}$$

With (4.17), referring to (4.14) and the known PA output $s(n)$, $\psi_1(s)$, $\psi_3(s)$ and $\psi_5(s)$ are solved. Moreover, with (4.15), the following matrix stands:

$$(\Psi^H \Psi) = \begin{bmatrix} \int \psi_1^2(s) ds & 0 & 0 \\ 0 & \int \psi_3^2(s) ds & 0 \\ 0 & 0 & \int \psi_5^2(s) ds \end{bmatrix}, \tag{4.18}$$

and since $(\Psi^H \Psi)$ is a diagonal matrix with non-zero diagonal entries, it is invertible as follows:

$$(\Psi^H \Psi)^{-1} = \begin{bmatrix} \frac{1}{\int \psi_1^2(s) ds} & 0 & 0 \\ 0 & \frac{1}{\int \psi_3^2(s) ds} & 0 \\ 0 & 0 & \frac{1}{\int \psi_5^2(s) ds} \end{bmatrix}, \tag{4.19}$$

which solved the numerical instability problem. Moreover, with (4.13) and (4.14), the orthogonal DPD coefficients c_1 , c_3 and c_5 can be translated to the non-orthogonal DPD coefficients by:

$$\begin{aligned}
b_1 &= c_1 + c_3 + c_5, \\
b_3 &= -c_3 a_{3,3} - c_5 a_{3,5}, \\
b_5 &= -c_5 a_{5,5}.
\end{aligned} \tag{4.20}$$

Although orthogonality holds for each memory-less element is diagonal, orthogonality does not hold for the different delayed elements, *i.e.*, is not exactly diagonal. However, we still expect the orthogonal memory polynomial model to be numerically more robust than the conventional memory polynomial model.

4.2.3 Simplified DPD Structure for Joint PA and I/Q Modulator

After the PA nonlinearities are modeled mathematically and optimized with the orthogonal approach introduced in Section. 4.2.2, I/Q imbalance compensator can be implemented in a manner of widely-linear transformation, given as:

$$z(n) = g_1(n) \star y(n) + g_2(n) \star y^*(n), \quad (4.21)$$

where \star denotes convolution, $y(n)$ and $z(n)$ indicate input and output of I/Q imbalance compensator respectively, and $g_1(n)$ and $g_2(n)$ are impulse responses of two filters, depending on phase mismatch, gain mismatch and impulse response mismatch of I/Q imbalance in transmitters [119].

As discussed in [42], the transfer functions of the two filters for both PA predistorter and I/Q modulator can be merged into:

$$F_p(x) = H_p(x) G_1(x), \quad (4.22)$$

$$\hat{F}_q(x) = H_q^*(x) G_2(x), \quad (4.23)$$

where $H_p(x)$ is filtering nonconjugate signal and $H_q(x)$ is filtering conjugate signal in the PA predistorter, $G_1(x)$ and $G_2(x)$ denote the transfer functions of the two filters in the I/Q imbalance compensator. This is illustrated in Fig. 4.2 with a dummy constant c for LO leakage compensator added to the end of the predistorter, such that the structure of the joint predistorter is simplified without violating properties of graph theory, and it deals with I- and Q- branch separately. For adaptive adjustment, samples of the RF front-end output are returned for baseband digital signal processing.

In the proposed approach, the parameter estimation for $F_p(x)$ and $F_q(x)$ is based on joint ILA structure as shown in Figure. 4.3 and the LS method. We denote the length of the training NC-OFDM signal by N . Lengths of the nonconjugate and conjugate linear

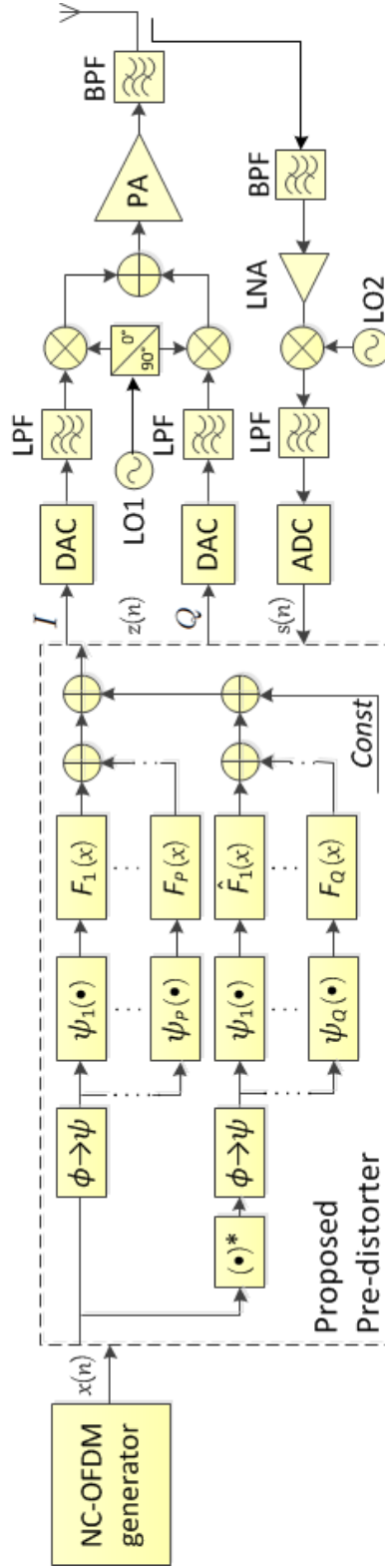


Figure 4.2: A general overview of the NC-OFDM transmitting system with proposed digital PD approach employed.

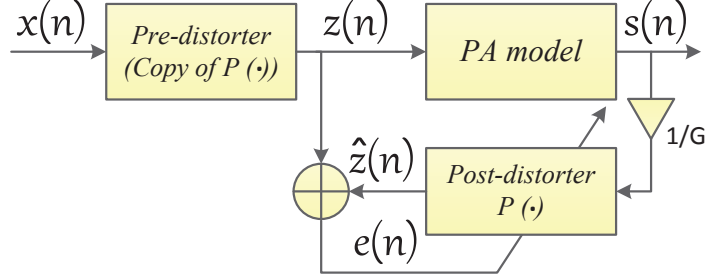


Figure 4.3: ILA for joint DPD parameter identification.

filters $H_p(z)$, $H_q(z)$ are denoted by L'_p and \hat{L}'_q respectively and that of the I/Q PD filters $G_1(s)$ and $G_2(s)$ is M . Such that in the simplified predistorter, lengths of $F_p(s)$ and $\hat{F}_q(s)$ become:

$$L_p = L'_p + M - 1, \quad (4.24)$$

$$\hat{L}_q = \hat{L}'_q + M - 1. \quad (4.25)$$

$$\mathbf{\Psi}_p = \begin{bmatrix} \psi_p(s(0)) & 0 & 0 & \cdots & 0 \\ \psi_p(s(1)) & \psi_p(s(0)) & 0 & \cdots & 0 \\ \psi_p(s(2)) & \psi_p(s(1)) & \psi_p(s(0)) & \cdots & 0 \\ \vdots & \vdots & \vdots & & \vdots \\ \psi_p(s(N-1)) & \psi_p(s(N-2)) & \psi_p(s(N-3)) & \cdots & \psi_p(s(N-L_p)) \end{bmatrix}. \quad (4.26)$$

The p^{th} orthogonal polynomial basis ψ_p on the nonconjugate path can be written into a matrix form (4.26) after pre-windowing [105], where the matrix $\mathbf{\Psi}_p$ has the dimension of $N \times L_p$. The conjugate matrix $\hat{\mathbf{\Psi}}_q$ can be similarly defined with the dimension of $N \times \hat{L}_q$. Then, we can define the filter impulse response with two column vectors \mathbf{f}_p and $\hat{\mathbf{f}}_q$, with the dimensions of $L_p \times 1$ and $\hat{L}_q \times 1$, respectively.

After collecting all orthogonal polynomial basis matrices into one block matrix $\mathbf{\Psi}$, add one column of all 1's for LO leakage compensation denoted by $\mathbf{1}$, we obtain a $N \times (L_p \times$

$P + \hat{L}_q \times Q + 1$) matrix:

$$\Psi = \begin{bmatrix} \Psi_1 & \Psi_2 & \cdots & \Psi_P & \hat{\Psi}_1 & \hat{\Psi}_2 & \cdots & \hat{\Psi}_Q & 1 \end{bmatrix}. \quad (4.27)$$

Similarly, stacking filter impulse response vectors as well as LO leakage compensation coefficients into one $(L_p \times P + \hat{L}_q \times Q + 1) \times 1$ vector as:

$$\mathbf{f} = \begin{bmatrix} \mathbf{f}_1^T & \mathbf{f}_2^T & \cdots & \mathbf{f}_P^T & \hat{\mathbf{f}}_1^T & \hat{\mathbf{f}}_2^T & \cdots & \hat{\mathbf{f}}_Q^T & c \end{bmatrix}^T. \quad (4.28)$$

Finally, following the linear LS estimation theory [105], the LS estimate of \mathbf{f} can be written as:

$$\hat{\mathbf{f}}_{LS} = (\Psi(s)^H \Psi(s))^{-1} \Psi(s)^H \mathbf{z}, \quad (4.29)$$

and the simplified PD operation is completed by plugging $\hat{\mathbf{f}}_{LS}$ into the pre-distorter.

$$\mathbf{z} = \Psi(x) \hat{\mathbf{f}}_{LS}. \quad (4.30)$$

4.3 Simulation and Measurement Results

4.3.1 Mathematical Simulation

The effects of employing previously discussed system identification and joint DPD techniques will be presented in this section in terms of illustration of simulation results. We use mathematic models to simulate the behavior of a direct conversion-transmitter: the PA is modeled by Wiener model with the same parameters from [24], transfer function of the filter is $(1 + 0.3z^{-2}) / (1 - 0.2z^{-1})$, and the memoryless nonlinearity is a fifth-order polynomial with reported coefficients $a_1 = 14.9740 + 0.0519j$, $a_3 = -23.0954 + 4.9680j$, and $a_5 = 21.3936 + 0.4305j$; the frequency-dependent I/Q imbalance [119] is modeled with following parameters: gain imbalance 3%, phase imbalance 3% and impulse response mismatch $h_{TX} = [1, -0.03]^T$ [41]. To present a clear view of possible impairments caused by transmitters, in this paper we are driving the PA model with the input power very close to its 1-dB compression point.

The post/pre-distorter consists of PH models with filter length of 5 in the orthogonal polynomial form proposed in [35] for both conjugate and nonconjugate branches. Noncon-

jugate branch is modeled by a seventh-order DPD and conjugate branch is by a fifth-order DPD.

We examine our joint DPD approach by employing two kinds of spectrally agile waveforms as input to in this section, including NC-OFDM signal and NC-OFDM signal with sidelobe suppression.

16-QAM Signal

We first examine the performance of the DPD method proposed in Section. 4.2.1 to correct only PA impairments, the PA is modeled by a Wiener model with the same parameters from [24] and both the pre-distorter and post-distorter are modeled by PH models, with each branch composed of a ninth-order nonlinearity ($K = 9$ and k is odd) with a linear filter of length five ($L = 5$). The input signal used in the simulation is a 16-QAM single-carrier signal with an oversampling rate of 12, and then passed to a raised-cosine pulse shaping filter, with 22% roll-off and oversampling rate of 12. 500 samples are generated at each ILA iteration for DPD training [107]. Without DPD employed, the ACPR of the PA output is driven to about 40 dBc.

Figure. 4.4 depicts the output PSD versus input PSD of PA model with and without DPD. As seen in the plot, for nonlinear PA model, gain compression is observed when approaching saturation level, and is considerably released after plugging in DPD.

Figure. 4.5 summarized the PSD of the PA output over 3 ILA iterations, with DPD structure. It's notable that the DPD is able to reduce the spectrum regrowth by approximately 30 dBc since from the second iteration.

Untreated NC-OFDM Signal

With 840 samples used at each ILA iteration for PD training, the NC-OFDM symbols are generated using a Differential Binary Phase Shift Keying (DBPSK) modulation scheme. Referring to plot (4) in Figure. 4.6, the number of subcarriers modulated orthogonally is 52, out of which 10 are deactivated, 8 to create a notch on the left and 2 to create a notch on the right. Furthermore, 10 null subcarriers are padded on either side of the NC-OFDM signal to avoid interference with the neighboring transmissions. Also, a cyclic prefix of length 14

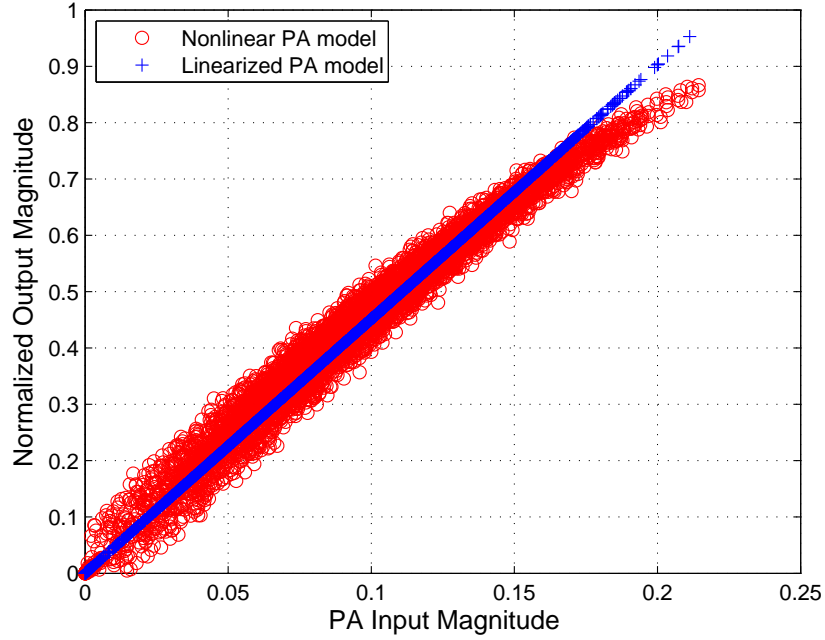


Figure 4.4: Normalized AM/AM for nonlinear and linearized PA model (16-QAM).

bits is added to counter the effects of intersymbol interference (ISI) [120]. The subcarrier bandwidth is kept constant over the entire simulation.

Figure. 4.6 displays the output PSD of the transmitter model without DPD technique, with PA DPD proposed in [107] and Section. 4.2.1, with joint PA and I/Q DPD discussed in Section. 4.2.2 and Section. 4.2.3 and an ideal linear transmitter model. As shown in the plots, the impairments caused by RF front-end component models can severely deteriorate signal quality with approximately 50 dBc OOB leakage by comparing plots (1) and (4). A significant release of OOB radiation is observed at plot (2) and (3) with joint PA and I/Q modulator DPD and orthogonal joint DPD employed (both at their third ILA iterations), 10 dBc and 30 dBc respectively. Comparatively, the compensation on in-band interference at the two notches are limited.

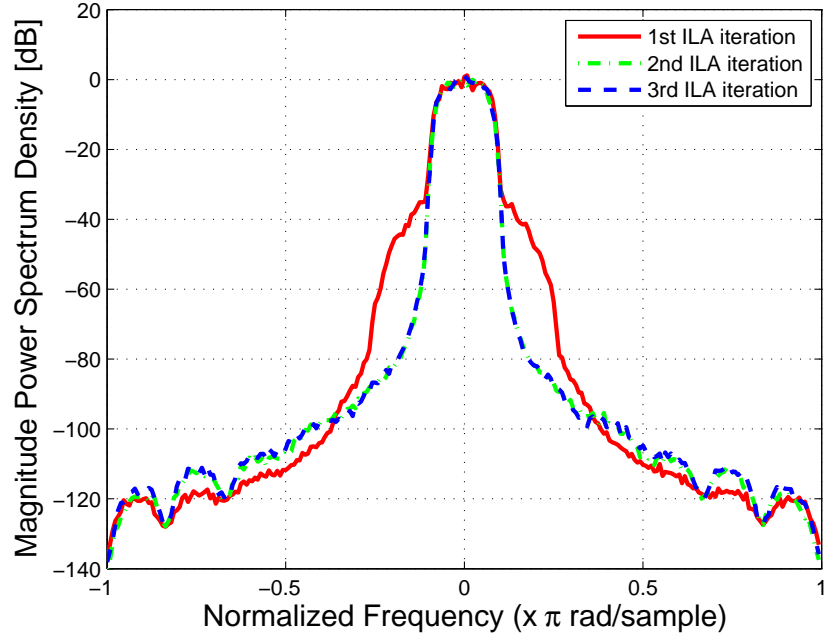


Figure 4.5: Output PSD of PA model with DPD employed tested on 16-QAM input signal.

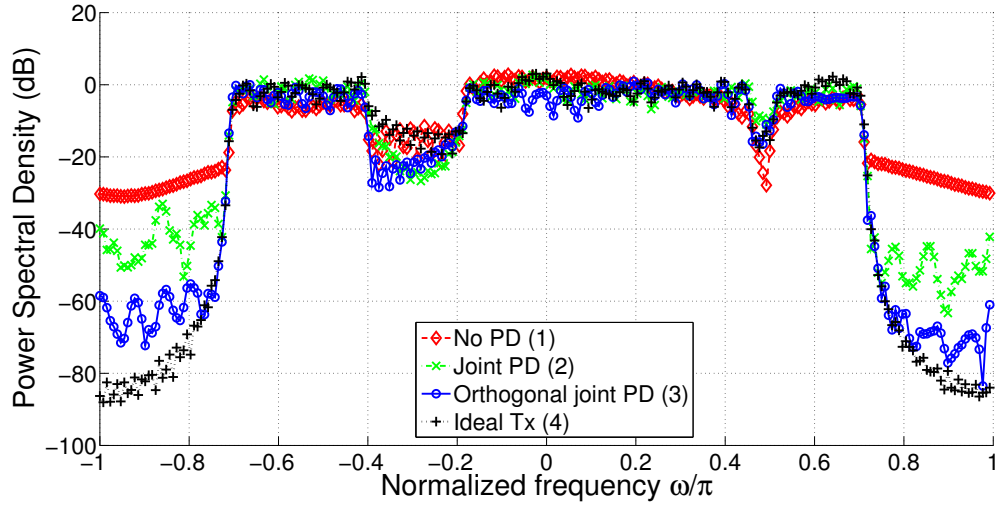


Figure 4.6: Output spectra of the direct-conversion transmitter model.

NC-OFDM Signal with Sidelobe Suppression

As shown in Figure. 4.7, in order to further suppress the notches in the untreated NC-OFDM signal, NC-OFDM signal is fed into a series of cascaded band reject filters (BRFs)

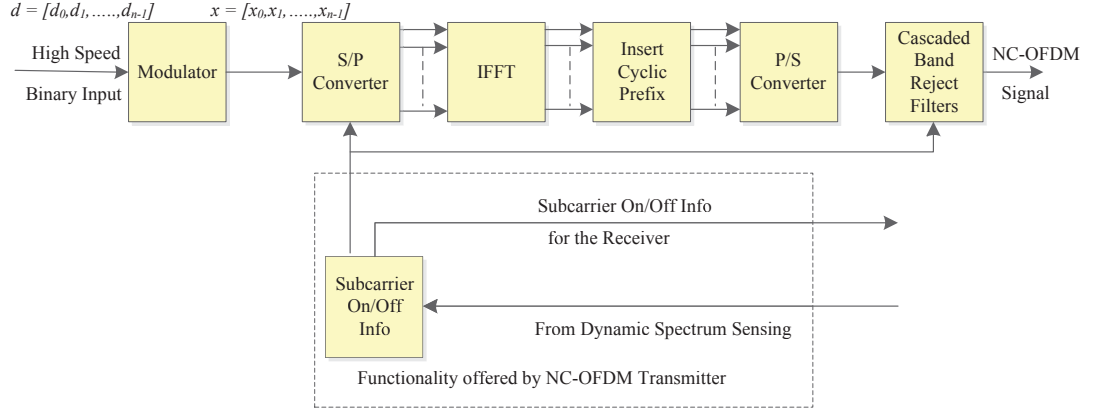


Figure 4.7: Schematic of NC-OFDM transmitter employing cascaded band reject filters

having the order of 251 to provide attenuation of the deactivated subcarriers, and then the filtered signal is passed through a raised-cosine pulse shaping filter with the roll-off factor of 20% and oversampling rate of 2. As shown in plot (4) of Figure. 4.8, the power level of the two inband notches is reduced by approximately 40 dBc comparing to untreated NC-OFDM.

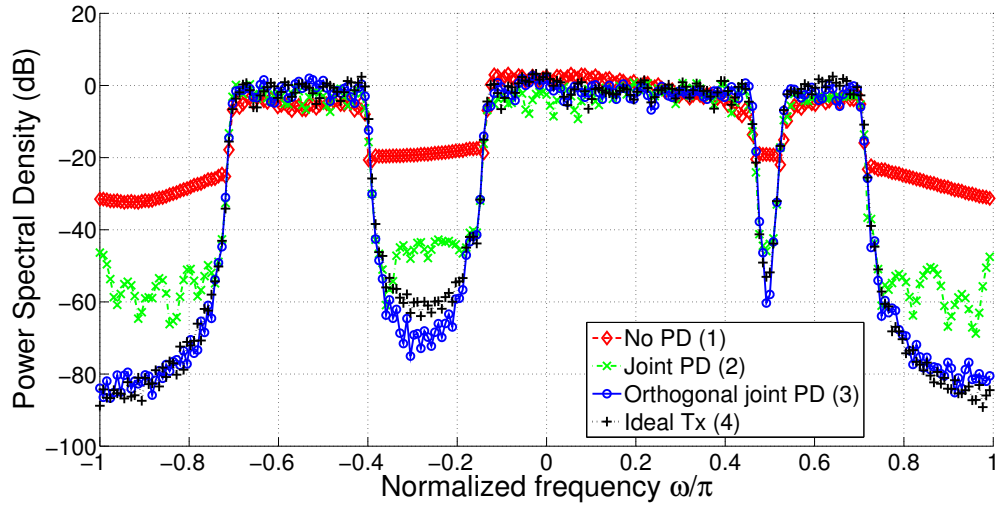


Figure 4.8: Output spectra of the direct-conversion transmitter model without DPD technique.

In Figure. 4.8, we show the results after testing our proposed DPD approach using

NC-OFDM signal with sidelobe suppression technique. The plots illustrate output PSD of the direct-conversion transmitter model without DPD technique, with joint DPD, with orthogonal joint DPD and an ideal linear transmitter model. As shown in plot (2) and (3), power levels of both OOB emissions and in-band notches are considerably suppressed with DPD approaches used, especially our proposed joint PA and I/Q DPD approach is able to almost completely counter the effects of impairments caused by the transmitter model.

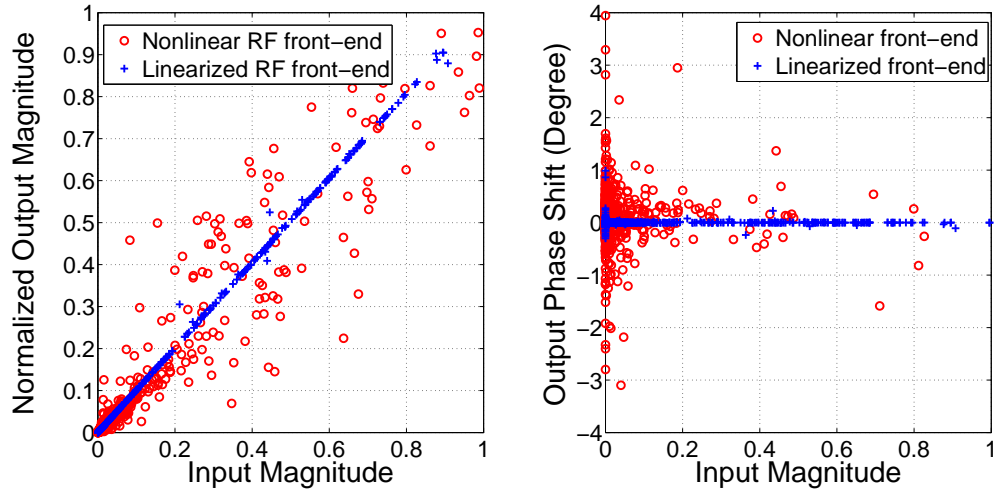


Figure 4.9: Normalized output magnitudes (AM/AM) and phase shift (AM/PM) versus input magnitudes. Including nonlinear and linearized direct-conversion transmitter models.

Furthermore, Figure. 4.9 show AM/AM and AM/PM plots of the direct-conversion transmitter model without and with proposed DPD technique employed, using NC-OFDM signal with sidelobe suppression. Without the pre-distorter, the output magnitude points are randomly distributed around the linear line, and become even more scattered while approaching saturation level in the AM/AM plot. Furthermore, similar behavior can be observed in AM/PM plot. On the other hand, both the magnitude and phase distortion are considerably released after plugging in the proposed DPD technique.

Simulation Summary

From the simulation results above, we can conclude that our proposed orthogonal DPD approach better fits non-contiguous multi-carrier signal with more obvious separations be-

tween different subcarriers in terms of power level, although it is also proved to effectively work on general NC-OFDM signal. Although the orthogonal joint method gives better performance, the trade-off is that additional signal pre-processing has to be done before the signal goes to the predistorter, and thus may cause delay in real-time signal processing.

4.3.2 Hardware Experiment

Characterization of RF Front-end of USRP2 Tx

A fully reconfigurable transceiver exhibiting a combined function of both transmitter and receiver, such as SDR, has been developed with the purpose of enabling the baseband processing entirely in software. USRP is a SDR platform developed by Ettus Research. In the implementation here, we set up two USRPs serving as Tx end and Rx end with their RF antenna ports connected by a SMA cable, as in Block ① and ② of Figure. 4.2. We set the Tx USRP on direct-conversion mode and Rx USRP on low-IF mode, so that we can only analyze the OOB radiation caused by Tx end temporarily without grasping features of RF impairments like I/Q mismatch on Rx end [102]. The XCVR2450 dual-band transceiver daughter cards are used on both Tx and Rx side. It can operate on a noncontiguous tuning range consisting of a high band (4.9 – 6.0 GHz) and a low band (2.4 – 2.5 GHz), with a maximum Tx power gain of 35 dB.

Figure. 4.10 shows the measured power levels on Rx end, by sweeping frequencies within supported range and by sweeping Tx power gain from 10 to 35 dB. Impairments especially nonlinearity can be observed, as well as the variation of characteristics at different frequencies. Furthermore, Table 4.2 lists the 1-dB compression points of several frequencies we tested on.

Table 4.2: 1-dB compression points of RF frequencies supported by XCVR2450

Tx Freq.	2.4 GHz	2.425 GHz	2.45 GHz	2.475 GHz	2.5 GHz
1-dB Comp.	-3.76 dB	-4.76 dB	-7.76 dB	-5.76 dB	-3.76 dB
Tx Freq.	4.9 GHz	5.15 GHz	5.4 GHz	5.65 GHz	5.9 GHz
1-dB Comp.	-3.76 dB	-6.76 dB	-5.76 dB	-3.76 dB	-4.76 dB

1-dB compression point indicates the input power where the output power drops by 1-dB from the linear level. In Table 4.2, different 1-dB compression points are observed for

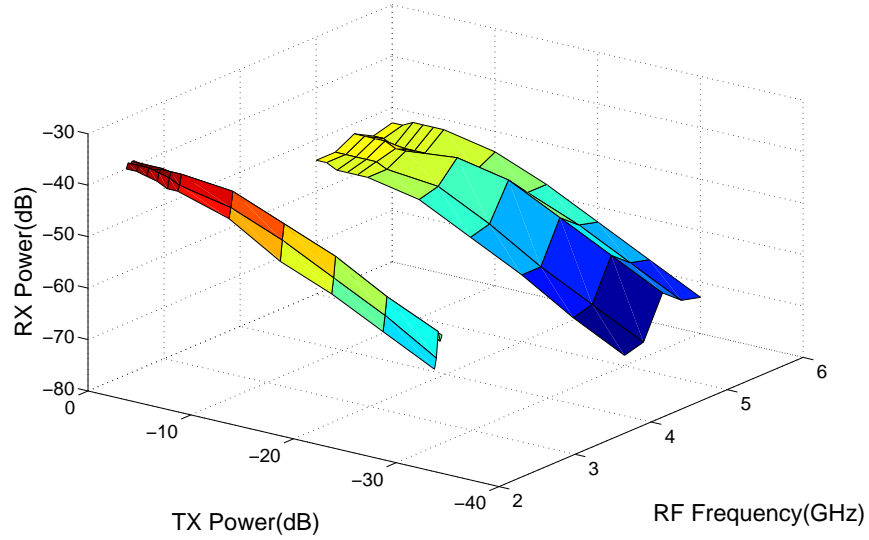


Figure 4.10: Measured power levels on Rx end by sweeping Tx power gain from Tx end, over a range of frequencies supported by XCVR2450 dual-band transceiver daughter cards.

different Tx frequencies. This further proves the need for separate calibrations of DPD for different Tx frequencies, so that more accurate DPD models are obtained for signals with wide bandwidth.

Hardware Experimental Results of Proposed DPD Algorithm

As one type of Software-Defined-Radio (SDR) prototyping platforms, the Universal Software Radio Peripheral (USRP) platform enables researchers to rapidly prototype software radio systems using a combination of both a digital motherboard and an daughterboard providing flexible, fully integrated RF frontend functionality. A block diagram of the main elements on the USRP2 boards is shown in Figure. 4.11. Focusing on the data flow of the transmitting path the digital modulated signals from MATLAB are received through Gigabit Ethernet port on the motherboard, after which signal filtering function is implemented in a Spartan 3 field programmable gate array (FPGA).

The resulting output is connected directly to a D/A converter and the converted analog signal is fed from the digital card to the RF daughterboard. The analog signal is fed through the transceiver, filters, and then the power amplifier, prior to being routed to the

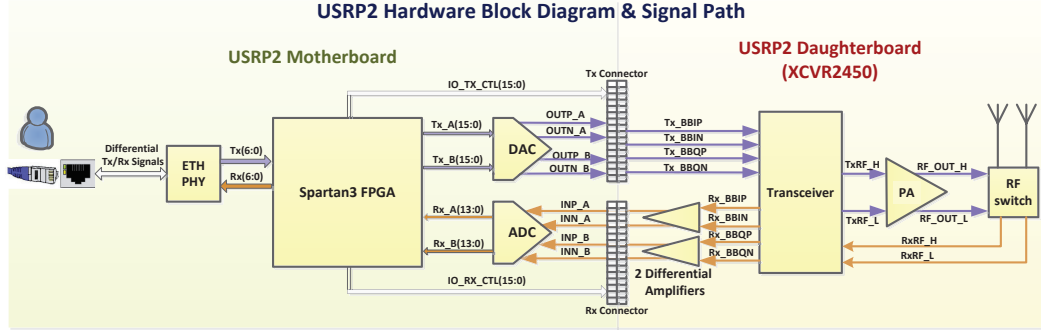


Figure 4.11: Block diagram of elements on USRP 2 hardware.

TX antenna by a RF switch component. The power amplifier on the particular type of RF board we are using is a dual-band power amplifier designed for 2.4 GHz and 5 GHz operating at 3.3 V supply. Additionally, the nominal saturated power is 28 dBm with typical power gain of 30 dB [107].

In the implementation for this research, we set up two USRPs serving as Tx end and Rx end with their RF antenna ports connected by a SMA cable. We set the Tx USRP on direct-conversion mode and Rx USRP on low-IF mode, so that we can only analyze the OOB radiation caused by Tx end temporarily without grasping features of RF impairments like I/Q mismatch on Rx end [102].

The test-bed we set up is composed of two major components: a USRP 2 SDR platform and an Agilent CSA spectrum analyzer as shown in Figure. 4.12. The USRP 2 transmitter and receiver blocks in MATLAB support communication between Simulink/MATLAB and a USRP 2 platform, with the benefit of real-time signal I/O for the SDR, allowing the simulation and development of various SDR applications. Regarding the signal path of our measurement, the digital signals originate from digital signal generating models in MATLAB, passing through attenuators followed by USRP 2, ultimately going to the spectrum analyzer for observation. Note that 10 dB attenuators are employed in order to restrict the maximum power applied to the spectrum analyzer input.

With test-bed setup as shown in Figure. 4.12 and untreated NC-OFDM signal transmitting at 2.43GHz from the USRP2, we first estimated PA model parameters, and then

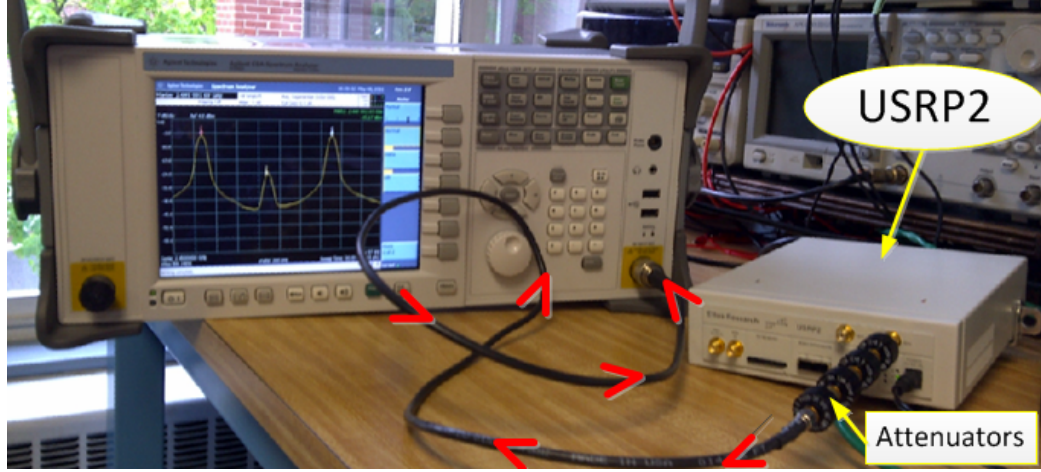


Figure 4.12: Hardware test-bed setup for experimental measurements on USRP 2.

plugged these parameters into the PA model in the simulation script in order to obtain the corresponding LS estimate \hat{a}_{LS} . We then applied the constant vector \hat{a}_{LS} to the predistorter. The transmit-signal is de-multiplexed into 128 subcarriers, with the data on each subcarrier modulated into an 16-QAM symbol, and then NC-OFDM is transmitted after we deactivate 20 subcarriers on each side.

Finally, results of laboratory radio signal measurements are presented in Figure. 4.13, which captures the spectra both with and without DPD from a spectrum analyzer. From Figure. 4.13 performance improvement in terms of approximately $5dB$ suppression of OOB is observed with DPD employed, comparing with the PA output without DPD. At this stage, we can conclude that our DPD scheme improved the RF performance of USRP2. Note that in Figure. 4.13 the transmit-signal seems to contain a carrier component at 2.43 GHz, this is due to the roll-off factor of the interpolation filter during the up-conversion processing of the USRP2.

4.4 Chapter Summary

In this chapter, we proposed joint DPD techniques for not just PA but I/Q modulator effects in spectrally agile waveforms.

In Section 4.2, mathematical presentations of a proposed DPD method for PA [107],

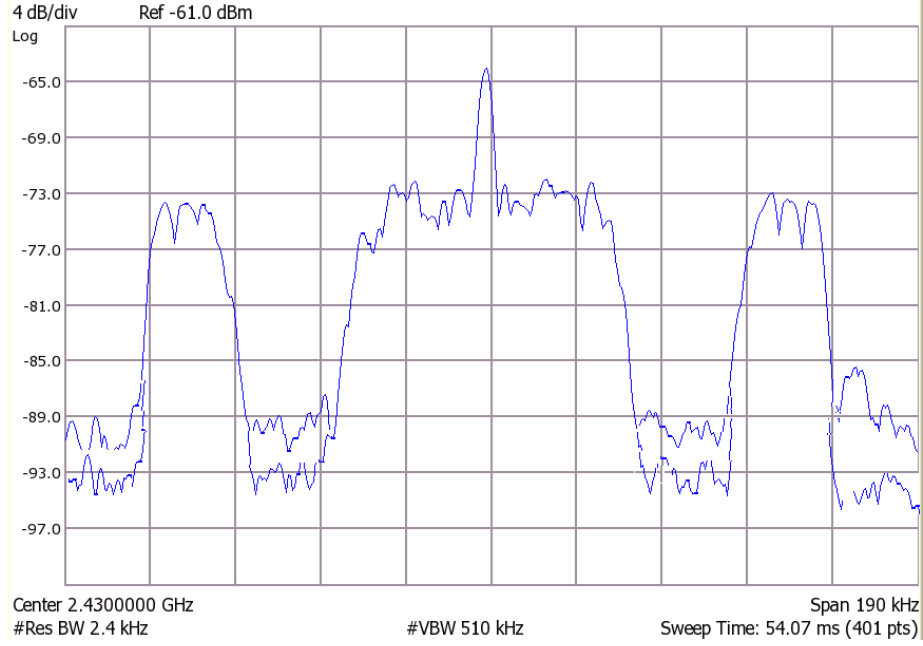


Figure 4.13: PSD of NC-OFDM signals output from USRP2 with and without DPD.

and an orthogonal basis joint DPD technique for joint PA and I/Q modulator effects in spectrally agile waveforms were covered. The simulation and measurement results provided in Section 4.3 show that our proposed DPD approaches can efficiently suppress the OOB emission based on both QAM and several spectrally agile waveforms, including untreated NC-OFDM signals and NC-OFDM signals processed using sidelobe suppression algorithms. It was also shown that the proposed technique achieves relatively better interference mitigation performance in the case of the NC-OFDM signal processed using sidelobe suppression algorithms.

Chapter 5

Proposed DPD method for Spurious Emission Reduction

5.1 Chapter Introduction

The conventional DPD methods, including the algorithm proposed in Chapter 4, are proven to be able to effectively reduce the out-of-band (OOB) emissions that fall within adjacent channels, however the implementation of DPD expands the transmission bandwidth and gives rise to spurious emissions further away from the carrier. Moreover, when deploying frequency division duplexing (FDD) [44], one challenge is also to protect its own receiving band which can be impacted by the spurious emissions from the transmitter. This becomes especially problematic in the case of multiple carrier or carrier aggregation transmissions, in which case the duplexing gap is usually smaller than in regular single carrier transmissions.

Although emissions at the adjacent channel are usually still higher than those at the spurious domain, a wireless system usually sets different power limits for allowable spectral emissions at OOB band and spurious domain [67]. Therefore, there is a need to investigate on an enhancement to conventional DPD approach that can keep both OOB emissions and spurious emissions under the corresponding emission limits. There have been a few

The work presented in this chapter has been submitted in parts at [P5] and [P6].

works on this topic, for example, [45] proposed enhanced DPD method to reduce the OOB emissions more effectively, the work in [47] was with the objective of generally suppressing intermodulation distortion (IMD) in LTE-Advanced network [48], and [46] focuses on DPD technique for IMD reduction in two-tone experiments.

In this chapter, we propose a novel frequency-selective DPD method that can reduce the spectral regrowth at any pre-specified component in the spurious domain of the output RF spectrum. Specifically, the proposed algorithm can optimize the DPD coefficients in a intuitive way, such that spurious emissions around certain frequency in the PA output spectrum can be minimized, while at the same time maintaining the OOB under its emission limit. To the best of the authors' knowledge, no similar work has been done on this topic.

5.2 Problem Statement and Motivation

The transmitter output spectrum usually consists of three components: The emissions within the occupied channel bandwidth, the OOB emissions, and the spurious emission domain. Fig. 5.1 illustrates the output spectrum of a multicarrier transmitter. Occupied bandwidth is defined as the bandwidth containing 99% of the total integrated mean power of the transmitted spectrum on the assigned channel. The OOB emissions are unwanted emissions immediately outside the assigned channel bandwidth resulting from the non-linearity in the transmitter but excluding spurious emissions. This OOB emission is specified and measured in terms of the spectrum emission mask (Δf_{OOB}) and Adjacent Channel Leakage power Ratio (ACLR), which is the ratio of the filtered mean power centered on the assigned channel frequency to the filtered mean power centered on an adjacent channel frequency. Spurious emissions are located at far-away frequencies, outside the OOB region [67].

Conventional DPD methods are proven to be able to reduce ACLR at the adjacent frequency bands, but at the same time produce higher order intermodulation products (IMPs), which results in increased bandwidth as shown in Fig. 5.2(b). This is due to the predistorter usually being modeled by the nonideal inverse of the nonlinearity possessed by PA, and when placed in front of the PA, the two nonlinearities in serial result in less power

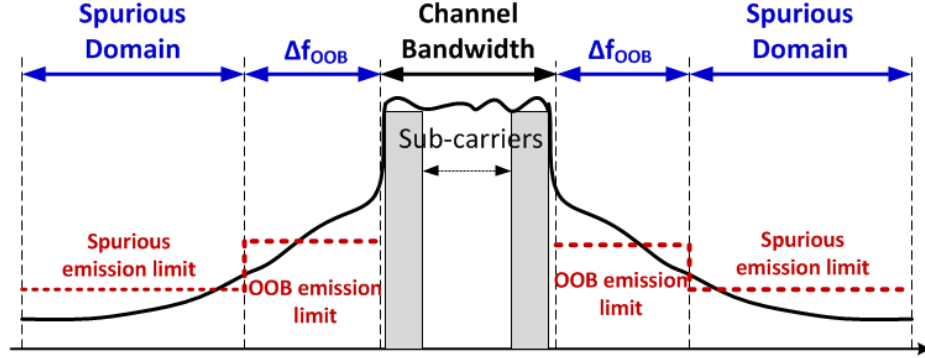


Figure 5.1: Transmitter RF spectrum. It is composed of channel bandwidth, OOB emissions and the spurious domain.

at low order IMPs but more of higher order nonlinear terms. The mathematical analysis will be shown in Section 5.3.

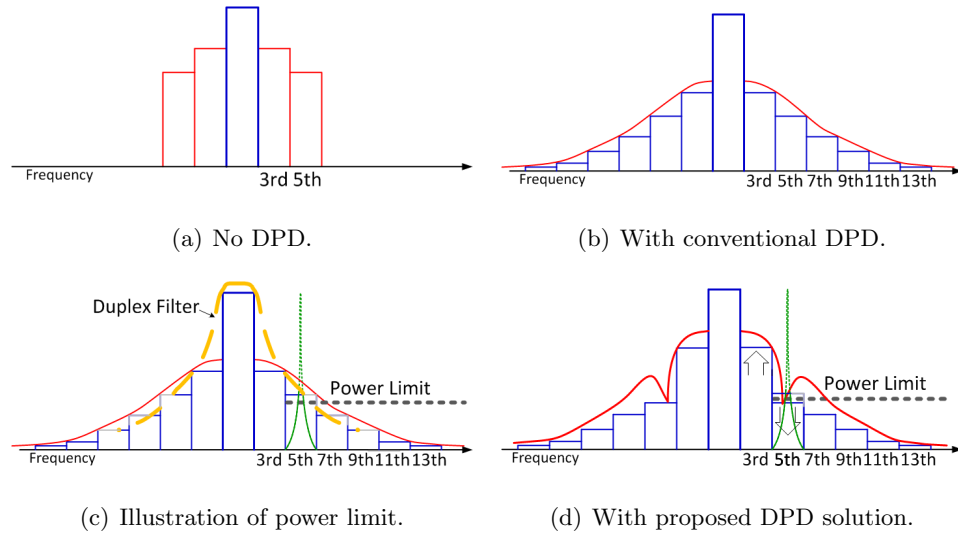


Figure 5.2: Output spectrum of a transmitter (a) with no DPD, (b) with conventional DPD, (c) employing FDD mode with power limit and (d) with proposed DPD.

Despite the fact that emissions at adjacent channels are usually still higher than those at spurious domain after applying DPD, standards for wireless systems usually set different power limits for allowable emissions in the spurious domain of the output RF spectrum. Either with or without applying DPD, in general it can be asserted that the closer the frequency band is located to the fundamental carrier, the frequency band will experience a

higher power level (please refer to Fig. 5.2(a) and Fig. 5.2(b)), and thereby be at higher risk of violating power limit in the spurious domain. Moreover, for wireless systems deployed in FDD mode [68], the power limit designed to protect its own receiver is even tighter than the spurious emission limit. Although a duplex filter is usually implemented to provide adequate rejection of transmitter noise occurring at the receive frequency, one challenge is to obtain sufficient attenuation for the emissions on the receiver band when the duplexing gap is small.

For instance, in band 20 of Evolved Universal Terrestrial Radio Access (E-UTRA) operating bands [67], the uplink frequencies, *i.e.*, user equipment (UE) to base station (BS), and the downlink frequencies, *i.e.*, BS to UE, are specified as 832 MHz - 862 MHz and 791 MHz - 821 MHz, respectively. The duplex gap for this configuration is given as 41 MHz. When a fully allocated 20 MHz LTE uplink is transmitted, the downlink will fall on top of the 5th order IM band (IM5 band) of the uplink transmission, which is very close to each other in frequency. As shown in Fig. 5.2(c), the green spike represents the received waveform, which falls on the IM5 band of the transmitter with DPD deployed. As shown in Fig. 5.2(c), although a bandpass filter is implemented in the duplexer to protect its receiver band, in this example the assumed power limit of the receiver band is still violated on IM5 band due to the small duplexing gap.

Our proposed method aims to suppress the emissions at any pre-specified frequency in spurious domain with a DPD-based method. Ideally, the proposed method is able to generate a notch at any pre-specified frequencies in the spurious domain by manipulating DPD coefficients, such that the spurious emissions can be kept under the power limit. As shown in Fig. 5.2(d), a notch is generated at IM5 band, so the power limit is not violated any more at the receiving frequency. The trade-off is that the OOB at IM3 band increases, but it is not an issue as long as it still following the ACLR requirement.

5.3 Mathematical Analysis of the Proposed Digital Predistortion Solutions

Both PA and DPD can be modeled as truncated complex power series. The coefficients of the power series are complex so that they can represent the AM-AM and AM-PM conversion accurately. The ‘DPD + PA’ system can then be modeled by two memoryless odd order polynomials in serial. The DPD model, where $z(t)$ represents the output of DPD, $x(t)$ denotes the input waveform and b_{2l-1} is the coefficient of the $(2l-1)^{\text{th}}$ odd order term in the predistorter, is given as:

$$z(t) = \sum_{l=1}^L b_{2l-1} x(t) |x(t)|^{2l-2} \quad (5.1)$$

$$= \sum_{l=1}^L b_{2l-1} x(t)^l x^*(t)^{l-1}, \quad (5.2)$$

where the form in (5.2) is used in the subsequent derivation steps. Similarly, PA can be modeled as:

$$y(t) = \sum_{p=1}^P a_{2p-1} z(t) |z(t)|^{2p-2} \quad (5.3)$$

$$= \sum_{p=1}^P a_{2p-1} z(t)^p z^*(t)^{p-1}, \quad (5.4)$$

where $y(t)$ denotes the output of PA model and a_{2p-1} represents the coefficient of the $(2p-1)^{\text{th}}$ odd order term in the PA model. After plugging (5.2) into (5.4), we obtain

$$y(t) = \sum_{k=1}^{L \times P} c_{2k-1} x(t)^k x^*(t)^{k-1} \quad (5.5)$$

$$= \sum_{k=1}^{L \times P} c_{2k-1} x(t) |x(t)|^{2k-2}, \quad (5.6)$$

where the coefficients c_{2k-1} consist of PA and DPD coefficients a_{2p-1} and b_{2l-1} . Since we are aiming to suppress the emissions in the spurious domain, which covers intermodulation

products (IMPs) with the orders higher than 3rd, only 5th and higher order nonlinear terms in (5.6) contribute to the power regrowth in the corresponding IM region. In other words, only the N^{th} and higher than N^{th} order nonlinear terms contribute to the emissions located at the N^{th} order IM region. In order to reduce the N^{th} order IM emission, we can truncate $y(t)$ as in the following equation and use the truncated signal for the subsequent analysis

$$y_{\text{trunc}}(t) = \sum_{k=N}^{L \times P} c_{2k-1} x(t) |x(t)|^{2k-2}. \quad (5.7)$$

Based on Wiener-Khinchin theorem [121], autocorrelation function and power spectral density (PSD) form a Fourier Transform pair as follows

$$\begin{aligned} R(\tau) &= \int_{-\infty}^{\infty} S(f) e^{j2\pi f \tau} df, \\ S(f) &= \int_{-\infty}^{\infty} R(\tau) e^{-j2\pi f \tau} d\tau. \end{aligned} \quad (5.8)$$

With $\phi_{2k-1}(t)$ denoting $x(t) |x(t)|^{2k-2}$ in the case of memoryless nonlinear model, the autocorrelation function of the truncated signal y_{trunc} can then be derived as

$$\begin{aligned} R_{y_{\text{trunc}}}(\tau) &= E[y_{\text{trunc}}(t) y_{\text{trunc}}^*(t - \tau)] \\ &= E\left[\left(\sum_{k_1=N}^{L \times P} c_{2k_1-1} \phi_{2k_1-1}(t)\right) \left(\sum_{k_2=k_1}^{L \times P} c_{2k_2-1} \phi_{2k_2-1}(t - \tau)\right)^*\right] \\ &= \sum_{k_1=N}^{L \times P} \sum_{k_2=k_1}^{L \times P} c_{2k_1-1} c_{2k_2-1}^* E[\phi_{2k_1-1}(t) \phi_{2k_2-1}(t - \tau)] \\ &= \sum_{k_1=N}^{L \times P} \sum_{k_2=k_1}^{L \times P} c_{2k_1-1} c_{2k_2-1}^* R_{\phi_{2k_1-1} \phi_{2k_2-1}}(\tau), \end{aligned} \quad (5.9)$$

where $(\cdot)^*$ denotes complex conjugation. As it can be observed, the autocorrelation function is simplified to double summation of the cross-correlation of odd order power terms of the input signal $x(t)$ multiplied by coefficients c_{2k-1} and c_{2k-1}^* . Note that the second summation starts from k_1 instead of N in the expression, which is simplified by only collecting terms associated with the emissions on the right hand side within the PSD. The corresponding

PSD of the truncated signal can then be derived as:

$$\begin{aligned}
S_{y_{trunc}}(f) &= \int_{-\infty}^{\infty} \sum_{k_1=N}^{L \times P} \sum_{k_2=k_1}^{L \times P} c_{2k_1-1} c_{2k_2-1}^* R_{\phi_{2k_1-1} \phi_{2k_2-1}}(\tau) e^{-j2\pi f \tau} d\tau \\
&= \sum_{k_1=N}^{L \times P} \sum_{k_2=k_1}^{L \times P} c_{2k_1-1} c_{2k_2-1}^* \int_{-\infty}^{\infty} R_{\phi_{2k_1-1} \phi_{2k_2-1}}(\tau) e^{-j2\pi f \tau} d\tau \quad (5.10) \\
&= \sum_{k_1=N}^{L \times P} \sum_{k_2=k_1}^{L \times P} c_{2k_1-1} c_{2k_2-1}^* S_{\phi_{2k_1-1} \phi_{2k_2-1}}(f),
\end{aligned}$$

which shows that suppression of power emission at certain frequency f can be achieved by manipulating c_{2k-1} and c_{2k-1}^* to minimize the output of (5.10). With the pre-knowledge of the PA coefficients a_{2p-1} and input signal $x(t)$, it remains to find the optimal combination of DPD coefficients b_{2l-1}

5.4 Parameter Estimation of the Proposed Predistorter

In this section, the implementation of the proposed DPD method combined with the conventional predistorter is introduced with the purpose of keeping a suitable balance between OOB and spurious emissions.

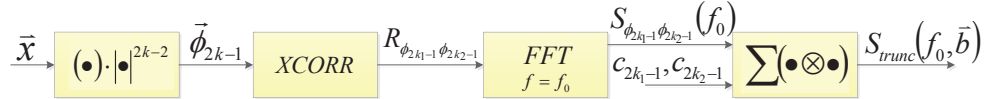


Figure 5.3: Block diagram showing signal processing procedures in the proposed DPD method.

The proposed signal processing procedure discussed in Section 5.3 is shown in Fig. 5.3 with a block-based approach adopted. The input \vec{x} is an n -dimensional vector composed of N samples, and is transformed to the basis functions of a memoryless nonlinear model and becomes K of n -dimensional vector $\phi_{2\mathbf{k}-1}$. Then, based on the pre-specified frequency f_0 , around which we aim to minimize the spurious emissions, only the $\phi_{2\mathbf{k}-1}$ values associated with the truncated signal are fed to the cross-correlation function block as shown in (5.7) and (5.9). The vectors $R_{\phi_{2k_1-1} \phi_{2k_2-1}}$ are then sent to the Fast Fourier Transform (FFT)



The next step is to optimize the parameter vector \mathbf{b} of the predistorter to find $\min(S_{trunc}(\vec{b}))$. This is an optimization problem, which aims to seek values for certain design or control variables in order to minimize an objective function. In this study, the *Newton-Raphson* method is employed, which seeks the minimum of $F(x)$ using both first and second derivatives. In its simplest form, it can be described as follows:

where x_0 is an initial estimate of the minimum of $F(x)$, and (5.11) executed in a loop until $|F'(x_i)|$ is sufficiently small [122]. Specifically, the implementation of Newton-Raphson method to $\min(S_{trunc}(\vec{b}))$ is shown in Fig. 5.4. In most cases, we are optimizing multiple parameters of b_{2l-1} 's in the vector form \vec{b} instead of a scalar. The proposed predistorter is based on the ‘indirect learning Architecture (ILA)+ least square (LS)’ scheme discussed in [107], which produces \vec{b}_{LS} in order to reduce the OOB emissions. In this study, we take $\mathbf{b}_{\mathbf{LS}}$ as the initial estimate of \mathbf{b} , *i.e.*, $\vec{b}_0 = \vec{b}_{LS}$. Furthermore, since b_3 plays a key role in suppression of OOB emissions, $b_3 = b_{LS3}$ is kept unchanged to avoid negatively affecting

ACLR. Thus, it leaves $\mathbf{b} = [b_5 \ b_7 \ \dots \ b_{2K-1}]^T$ to be optimized using Newton-Raphson method for a multi-variable function.

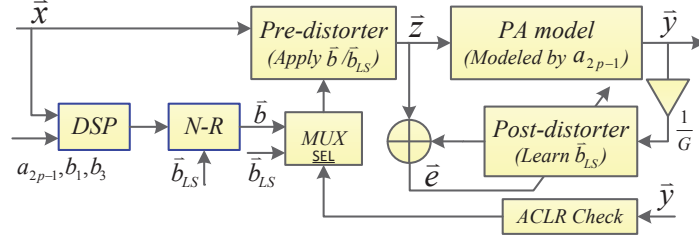


Figure 5.5: The proposed combined predistorter based on ILA. A multiplexer is used to determine whether the parameters of the proposed DPD algorithm or the conventional LS method is selected for the next ILA iteration.

As shown in Fig. 5.4, iterative structure is given as:

$$\mathbf{b}_{i+1} = \mathbf{b}_i - \mathbf{J}_f^{-1}(\mathbf{b}_i) S'_{trunc}(\mathbf{b}_i), \quad (5.12)$$

where $S'_{trunc}(\mathbf{b})$ is defined as:

$$S'_{trunc}(\mathbf{b}) = \left[\frac{\partial S_{trunc}(\mathbf{b})}{\partial b_5} \quad \frac{\partial S_{trunc}(\mathbf{b})}{\partial b_7} \quad \dots \quad \frac{\partial S_{trunc}(\mathbf{b})}{\partial b_{2K-1}} \right]^T, \quad (5.13)$$

and $\mathbf{J}_f(\mathbf{b})$ is the Jacobian of $S'_{trunc}(\mathbf{b})$, namely:

$$\mathbf{J}_f(\mathbf{b}) = \begin{bmatrix} \frac{\partial^2 S_{trunc}(\mathbf{b})}{\partial^2 b_5} & \frac{\partial^2 S_{trunc}(\mathbf{b})}{\partial b_5 \partial b_7} & \dots & \frac{\partial^2 S_{trunc}(\mathbf{b})}{\partial b_5 \partial b_{2K-1}} \\ \frac{\partial^2 S_{trunc}(\mathbf{b})}{\partial b_7 \partial b_5} & \frac{\partial^2 S_{trunc}(\mathbf{b})}{\partial^2 b_7} & \dots & \frac{\partial^2 S_{trunc}(\mathbf{b})}{\partial b_7 \partial b_{2K-1}} \\ \vdots & \vdots & \dots & \vdots \\ \frac{\partial^2 S_{trunc}(\mathbf{b})}{\partial b_{2K-1} \partial b_5} & \frac{\partial^2 S_{trunc}(\mathbf{b})}{\partial b_{2K-1} \partial b_7} & \dots & \frac{\partial^2 S_{trunc}(\mathbf{b})}{\partial^2 b_{2K-1}} \end{bmatrix}. \quad (5.14)$$

If the initial estimate is close enough to the root, the Newton-Raphson Method converges very fast, usually within 3-4 iterations.

In the parameter estimation stage, the ILA explained in [107] is also utilized in this study with modifications. The baseband equivalent operation is shown in Fig. 5.5, where the function blocks ‘DSP’ and ‘N-R’ represent the operations shown in Fig. 5.3 and Fig. 5.4, respectively. The fundamental idea behind the ILA is to find the inverse of the PA nonlinear

function with unit gain in the post-predistorter, and use it as the predistorter. In the ILA, the inverse technique of nonlinear functions is not explicitly employed, but an inverse model \mathbf{b}_{LS} that produces the least square error is calculated. In this chapter, we integrate the proposed method with the ILA, and an modified ILA iteration is defined as a single cycle of the following operations:

- Transmitting a signal of length N to the predistorter followed by the PA model, and at the same time to the function block ‘DSP’ to prepare the data for the subsequent procedures in the proposed method. Note that, in the first ILA iteration, the predistorter is turned off, such that the signal is transmitted directly to the PA model;
- Measuring the signal in the feedback loop and identifying the post-inverse parameter of the PA \mathbf{b}_{LS} , and at the same time calculating the ACLR of the PA output;
- Sending the \mathbf{b}_{LS} to the function block ‘N-R’ as the initial estimate of \mathbf{b} , and after 4 sub-iterations of Newton-Raphson operations in each ILA cycle, the stabilized \mathbf{b} is obtained;
- Inputting both \mathbf{b}_{LS} and \mathbf{b} to a multiplexer (‘MUX’) with the result after the comparing the ACLR with a pre-set threshold as the select line, in other words, if the ACLR is higher than the threshold, then \mathbf{b} is selected, and otherwise \mathbf{b}_{LS} is selected;
- Plugging the selected parameter estimates into the predistorter.

When applying the proposed DPD algorithm, Fig. 5.5 and the described operations can be simplified by removing the multiplexer and always applying \mathbf{b} to \mathbf{x} in the predistorter.

5.5 Examples and Simulation Results

In this section, examples of applying the proposed method to certain specific PA models are described along with simulation results. The assumption is that the PA model is known, and a conventional predistorter based on ILA [27] and LS parameter identification [106, 123] is up and running [107], which reduces the OOB emissions in the PA output spectrum. The combined DPD scheme with multiple ILA iterations discussed in Section 5.4

are simulated. The PA modeled by a quasi-memoryless nonlinearity is a fifth-order polynomial with complex coefficients $a_1 = 14.9740 + 0.0519j$, $a_3 = -23.0954 + 4.9680j$, and $a_5 = 21.3936 + 0.4305j$. The proposed method in this study is tested in order to reduce the emissions that fall within the 5th order IM band with a 9th order DPD quasi-memoryless nonlinear model, since the closer the band is located to the fundamental carrier the more emissions it usually carries, and thus higher probability in violation of the power limit. Three forms of baseband transmit signal are simulated, including 16-QAM, 20 MHz LTE and non-contiguous orthogonal frequency division multiplexing (NC-OFDM).

Starting with the break-down of ‘9th order DPD plus a 5th order PA’ scheme, it can be defined mathematically as follows:

$$z(t) = 1 x(t) + b_3 |x(t)|^2 x(t) + b_5 |x(t)|^4 x(t) + b_7 |x(t)|^6 x(t) + b_9 |x(t)|^8 x(t), \quad (5.15)$$

$$y(t) = a_1 z(t) + a_3 |z(t)|^2 z(t) + a_5 |z(t)|^4 z(t). \quad (5.16)$$

And after combining these two equations, the output of PA can be represented as:

$$y(t) = c_1 x(t) + c_3 |x(t)|^2 x(t) + c_5 |x(t)|^4 x(t) + \dots + c_{45} |x(t)|^{44} x(t). \quad (5.17)$$

With the purpose of reducing the power regrowth at f_0 MHz, which falls within the IM5 band of the input waveform, (5.7) is truncated again and becomes:

$$y_{trunc}(t) = c_5 |x(t)|^4 x(t) + c_7 |x(t)|^6 x(t) + c_9 |x(t)|^8 x(t) + c_{11} |x(t)|^{10} x(t), \quad (5.18)$$

with only the parts left that contribute the most to the results in terms of order of magnitude. By doing this, the computation complexity is reduced by a huge amount.

After taking cross-correlation of the y_{trunc} , the resulting correlation function and the corresponding PSD are given as:

$$R_{y_{trunc}}(\tau) = c_5 c_5^* R_{x^5 x^5}(\tau) + c_5 c_7^* R_{x^5 x^7}(\tau) + c_5 c_9^* R_{x^5 x^9}(\tau) + c_5 c_{11}^* R_{x^5 x^{11}}(\tau) + c_7 c_7^* R_{x^7 x^7}(\tau) + c_7 c_9^* R_{x^7 x^9}(\tau), \quad (5.19)$$

$$\begin{aligned}
S_{ytrunc}(f) = & c_5 c_5^* S_{x^5 x^5}(f) + c_5 c_7^* S_{x^5 x^7}(f) + c_5 c_9^* S_{x^5 x^9}(f) \\
& + c_5 c_{11}^* S_{x^5 x^{11}}(f) + c_7 c_7^* S_{x^7 x^7}(f) + c_7 c_9^* S_{x^7 x^9}(f).
\end{aligned} \tag{5.20}$$

Specifically, the PSD at f_0 can be written as

$$\begin{aligned}
S_{ytrunc}(f_0) = & c_5 c_5^* S_{x^5 x^5}(f_0) + c_5 c_7^* S_{x^5 x^7}(f_0) + c_5 c_9^* S_{x^5 x^9}(f_0) \\
& + c_5 c_{11}^* S_{x^5 x^{11}}(f_0) + c_7 c_7^* S_{x^7 x^7}(f_0) + c_7 c_9^* S_{x^7 x^9}(f_0),
\end{aligned} \tag{5.21}$$

where c_5 , c_7 , c_9 and c_{11} can be expanded and represented by the coefficients as:

$$\begin{aligned}
c_5 = & a_1 b_5 + 2a_3 b_3 + a_5 + a_3 b_3^*, \\
c_7 = & 2a_3 b_3 b_3^* + a_3 b_3^2 + 2a_5 b_3^* + a_1 a_7 \\
& + 2a_3 b_5 + 3a_5 b_3 + a_3 b_5^*, \\
c_9 = & a_3 b_3^2 b_3^* + a_5 (b_3^*)^2 + 2a_3 b_5 b_3^* + 6a_5 b_3^* b_3 + 2a_3 b_3 b_5^*, \\
& + 2a_3 b_3 b_5 + 3a_5 b_3^2 + 2a_5 b_5^* + a_1 b_9 + 2a_3 b_7 \\
& + 3a_5 b_5 + a_3 b_7^*, \\
c_{11} = & 3a_5 (b_3^*)^2 b_3 + 2a_3 b_3 b_5 b_3^* + 6a_5 b_3^* b_3^2 + a_3 b_3^2 b_5^* + a_5 b_3^3 \\
& + 2a_3 b_3 b_7^* + 2a_5 b_3^* b_5^* + 2a_3 b_7 b_3^* + 6a_5 b_3^* b_5 + 2a_3 b_5 b_5^* \\
& + 6a_5 b_5^* b_3 + 2a_3 b_3 b_7 + a_3 b_5^2 + 6a_5 b_3 b_5 + 2a_5 b_7^* \\
& + 2a_3 b_9 + 3a_5 b_7 + a_3 b_9.
\end{aligned} \tag{5.22}$$

Three characteristic are used to evaluate the performance of the DPD methods: ACLR is used to estimate reduction of OOB emissions, which is defined as the ratio of the mean power within the channel bandwidth to the mean power within IM3 band; Spurious emission ratio (SER) at f_0 is defined as ratio of the mean power within channel bandwidth to the PSD at f_0 , which is used to evaluate the power regrowth at f_0 ; Error Vector Magnitude (EVM) is defined in order to determine the in-band noise as $EVM = \sqrt{P_{error}/P_{ideal}} \times 100\%$, where P_{error} denotes the power of noise within the bandwidth and P_{ideal} represents the power of the ideally amplified signal within the transmitting band. The ACLR threshold for the combined method are set to be about 50 dBc, which is 10 dB higher than the ACLR requirement for LTE.

First, this proposed approach is verified on a 16-QAM single-carrier signal. The baseband transmit waveform is a 16-QAM signal with root-raised cosine pulse, 22% roll-off and 1 MHz bandwidth. The ACLR of the PA output is driven to 38.69 dBc, with the frequency mask of ACLR ranges from 0.5 MHz to 1.5 MHz. 5000 samples of the baseband input signal are used at each iteration. After every 5000 samples are generated, they are fed to all of the three ILA structures, including conventional LS method, the proposed method and a combined method of both the conventional and the proposed methods as shown in Fig. 5.5. The proposed method in this case is designed to reduce the emissions located around 2 MHz which falls within the IM5 band.

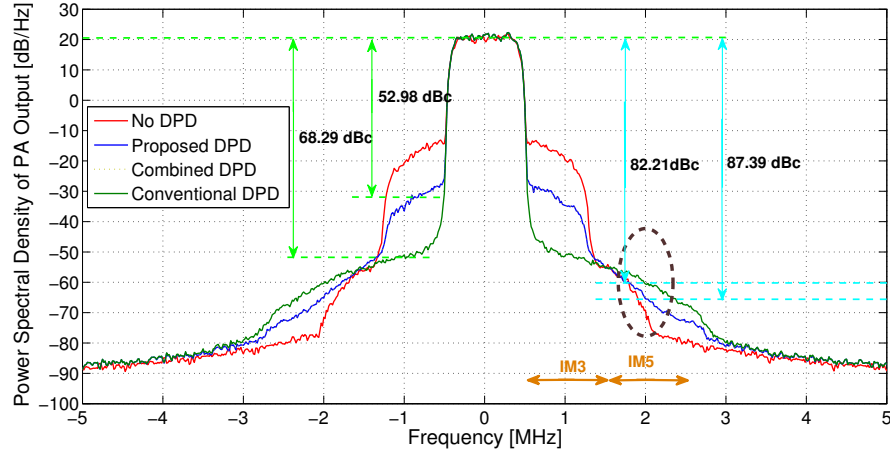


Figure 5.6: PA output PSD plots of 16-QAM baseband waveform in the fourth ILA iteration with no DPD, proposed DPD, combined DPD and conventional DPD methods employed.

Fig. 5.6 shows the PA output PSD plots of the fourth iteration employing no DPD, the proposed DPD, conventional DPD and the combined DPD structure. About 18 dB reduction of OOB emissions in IM3 band can be observed with the conventional DPD employed together with a rise of spurious emissions in IM5 band. On the other hand, for the proposed DPD and the combined method, less reduction of OOB emissions are produced comparing to the conventional predistorter, but the ACLR values are both kept around the 50 dBc ACLR threshold. Moreover, the spurious emissions at 2 MHz in IM5 band are about 6 dB less than the conventional DPD. From the simulation, the conventional DPD is able to significantly reduce the emissions in the adjacent channel band, namely IM3 band, and the

proposed method and the combined method can both produce a suitable balance of OOB emissions in IM3 band and the spurious emissions at 2 MHz in IM5 band as expected.

Table 5.1: Values of SER at 2 MHz and ACLR with Different DPD Methods Employed on Quasi-memoryless Models and 16-QAM Baseband Waveform.

Spec	No DPD	Conventional DPD	Proposed DPD	Combined DPD
ACLR [dBc]	37.95	68.29	52.98	52.99
SER [dBc]	90.43	82.21	87.39	87.39
EVM [%]	7	0.1	0.75	0.75

Table. 5.1 quantifies the results of all the three cases by comparing the ACLR, SER and EVM values for the fourth iteration. The conventional method provides the best ACLR improvement as expected, which is around 30 dB higher than with no DPD employed and 18 dB higher than the threshold, at the cost of worst control of spurious emissions. On the other hand, the proposed DPD method is able to almost suppress the spurious emissions at 2 MHz (SER= 87.39 dBc) down to the case with no DPD employed (SER= 90.43 dBc). However, the expense is less suppression of OOB emissions by only maintaining the ACLR about the ACLR threshold. The proposed DPD and the combined method behave similarly when the ACLR is higher than the threshold. Once the ACLR of the PA output becomes less than 50 dBc, the conventional DPD approach will be activated for the next iteration in the combined method. Furthermore, from the EVM results, the conventional DPD produces the least in-band noise, but both the other methods can reduce the EVM down to 0.75%.

We then simulated the case of a 20 MHz LTE waveform being transmitted, with a measurement bandwidth of 18 MHz. All 100 of the resource blocks (RBs) are fully allocated, and each of them is modulated on a 16-QAM symbol. The waveform is then properly scaled on the amplitude before being fed to the PA model. The proposed algorithm is executed with the purpose of minimizing PSD at $f_0 = 34\text{MHz}$, which falls within the IM5 band of the baseband LTE waveform. The ACLR of the PA output is driven to 42.84 dBc, with the frequency mask of IM3 band ranges from 9 MHz to 27 MHz.

Fig. 5.7 shows the PA output PSD plots of the fourth iteration with no DPD, the proposed DPD, conventional DPD and the combined DPD structure employed. About 25 dB reduction of OOB emissions in IM3 band can be observed with the conventional DPD employed together with more spurious emissions in IM5 band. On the other hand, for the

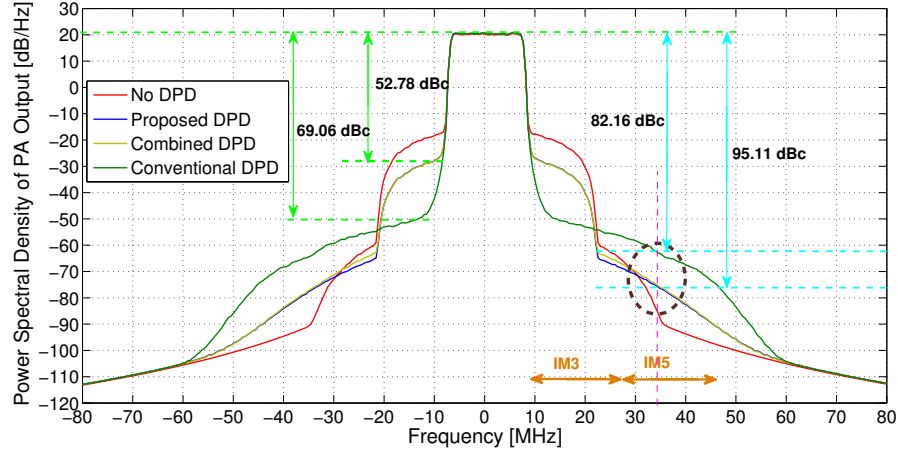


Figure 5.7: PA output PSD plots of 20 MHz baseband LTE waveform in the fourth ILA iteration with no DPD, proposed DPD, combined DPD and conventional DPD methods employed.

proposed DPD and the combined method, less reduction of OOB emissions are produced comparing to the conventional predistorter, but the ACLR values are both maintained under the 52 dBc ACLR threshold. Moreover, the spurious emissions at 34 MHz in IM5 band are about 10 dB less than the conventional DPD. In sum, the conventional DPD is able to significantly reduce the emissions in the IM3 band, and the proposed method and the combined method can produce a suitable balance of OOB emissions in IM3 band and the spurious emissions at 34 MHz in IM5 band, which is consistent with the expectation. If the RF transmitter is working in FDD mode with a receiver band configured to be located around 34 MHz, then less noise is produced at the receiver band with the propose approaches employed.

Table 5.2: Values of SER at 34 MHz and ACLR with Different DPD Method Employed on Quasi-memoryless Models and 20 MHz baseband LTE waveform.

Spec	No DPD	Conventional DPD	Proposed DPD	Combined DPD
ACLR [dBc]	42.84	69.06	52.78	52.87
SER [dBc]	102.21	82.16	95.11	94.51
EVM [%]	4	0.17	0.83	0.84

Table. 5.2 quantifies the results of all the three cases by comparing the ACLR, SER and EVM values for the fourth iteration. The conventional method provides ACLR values

about 17 dB higher than the threshold, at the cost of around 12 dB less of SER values in comparison the the other two methods. Again, the proposed method is able to provide an ACLR value above the ACLR threshold, while reducing the power regrowth at the pre-specified frequency in spurious domain. From the EVM results, the conventional DPD produces the least in-band noise, but both the other methods can reduce the EVM down to less than 1%.

Finally, the 1 MHz NC-OFDM waveform is simulated. The number of subcarriers modulated orthogonally is 52, out of which 15 are deactivated forming a notch. The proposed algorithm is executed with the purpose of minimizing PSD at $f_0 = 2\text{MHz}$, which is located in the IM5 band of the baseband NC-OFDM waveform. The ACLR of the PA output is driven to 41.53 dBc, with the frequency mask of ACLR ranges from 0.5 MHz to 1.5 MHz.

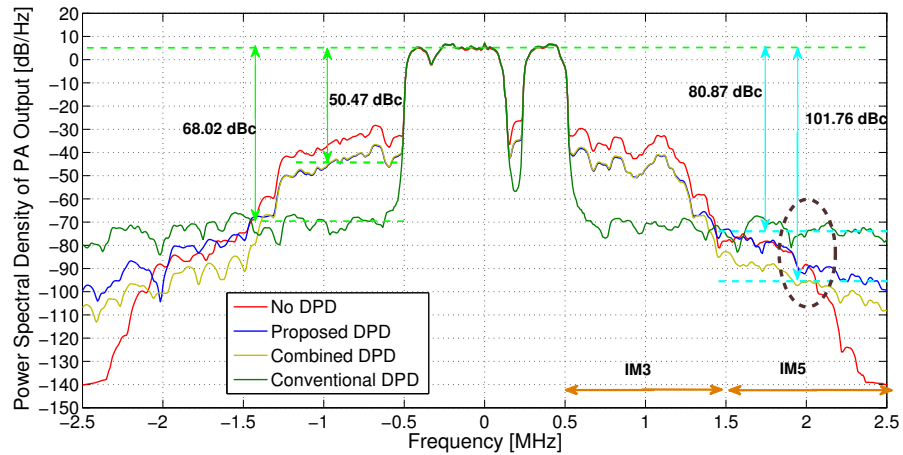


Figure 5.8: PA output PSD plots of baseband NC-OFDM waveform in the fourth ILA iteration with no DPD, proposed DPD, combined DPD and conventional DPD methods employed.

Fig. 5.8 shows the PA output PSD plots of the fourth iteration with no DPD, the proposed DPD, conventional DPD and the combined DPD structure employed. About 30 dB suppression of OOB emissions in IM3 band can be observed with the conventional DPD employed. For the proposed DPD and the combined method, OOB emissions can be reduced by 10, and the spurious emissions at 2 MHz in IM5 band are 16 - 20 dB less than the conventional DPD. Hence, in the DSA case scenario, if another user is transmitting

2 MHz away from the NC-OFDM signal, less interference will be caused with proposed method employed.

Table 5.3: Values of SER at 2 MHz and ACLR with Different DPD Method Employed on Quasi-memoryless Models and 1 MHz baseband NC-OFDM waveform.

Spec	No DPD	Conventional DPD	Proposed DPD	Combined DPD
ACLR [dBc]	41.53	68.02	50.47	50.05
SER [dBc]	93.72	80.87	96.95	101.76
EVM [%]	5	0.2	0.9	0.96

Table. 5.3 quantifies the results of all the three cases by comparing the ACLR, SER and EVM values for the fourth iteration. The conventional method provides ACLR values about 27 dB higher than the threshold, at the cost of upto 21 dB less of SER values in comparison with the other two methods. Hence, the proposed method is able to provide an ACLR value above the ACLR threshold, while reducing the power regrowth at the pre-specified frequency in spurious domain. From the EVM results, the conventional DPD produces the least in-band noise, but both the other methods can reduce the EVM from 5% to less than 1%.

5.6 Chapter Summary

The goal of the proposed method is to achieve a good balance of both OOB emissions and spurious emissions at any specified frequency in the PA output spectrum. The mathematical derivation procedures of our proposed DPD solution have been presented for both memoryless nonlinear model and memory-based nonlinear model. The systematic procedures of applying the combined DPD scheme of the proposed algorithm and the conventional ILA are explained. Simulation results of examining the proposed model with both single carrier and multicarrier transmit waveforms are shown and compared in terms of ACLR and SER improvement. From the simulation results, the proposed method can successfully reduce the emissions at the pre-specified frequency in the spurious domain as expected. However, from the results of analyzing complexity of the simulation program, the necessary operations of doing FFT and cross-correlation of basis functions in the proposed method consume $\frac{1}{3}$ of the overall running time.

There are things to be improved in the future work, for instance, the iterative coefficient optimization operations are only examined on quasi-memoryless models, which can be verified on memory-based models in the future work.

Chapter 6

Conclusion

6.1 Research Achievements

In this dissertation, several contributions have been made in the area of DPD for RF front-end impairments in DSA networks. The research achievements of this thesis are the following:

- A DPD mechanism that can compensate for impairments from either a PA only structure or a joint PA + I/Q modulator structure in direct-conversion radio transmitters. The proposed method has effectively reduced the OOB emissions that occur during the transmissions of both untreated NC-OFDM waveforms and NC-OFDM waveforms with sidelobe suppression algorithms applied.
- A set of orthogonal polynomial basis functions proposed for DPD modeling that alleviates the numerical instability problem associated with non-orthogonal polynomials. Moreover, this algorithm doesn't require any pre-knowledge of statistical information on the transmit signal.
- A novel DPD method that can reduce the spectral regrowth in the far out frequency range. A good balance of both OOB emissions and spurious emissions at any specified frequency in the PA output spectrum has been achieved by applying the proposed algorithms.

6.2 Future Work

There also exists several topics resulted from this research that could be continued.

- The joint DPD method proposed in Section 4.2.3 works better for the NC-OFDM signal with sidelobe suppression algorithms applied, the possible reasons were not fully studied.
- Although the algorithms proposed in Chapter 5 can effectively suppress the spurious emissions, there are still things that could be improved. For instance, the optimization method employed only supports real-valued numbers, which can be replaced by some other methods allowing complex-valued numbers.
- Both the orthogonal polynomial proposed in Section 4.2.2 and the frequency-selective DPD algorithms proposed in Chapter 5 were tested out in simulation, hardware implementation should be carried out in the future.

6.3 List of Publications

The work presented in this thesis is based on the following articles:

- [P1] Zhu Fu, Lauri Anttila, Mikko Valkama, and Alexander M. Wyglinski. “Digital pre-distortion of power amplifier impairments in spectrally agile transmissions,” in *Sarnoff Symposium (SARNOFF)*, 2012 35th IEEE, pages 16, May 2012.
- [P2] Zhu Fu, and Alexander M. Wyglinski. “Digital Pre-distortion of Radio Frequency Front-end Impairments in the Design of Spectrally Agile Multicarrier Transmission,” 2013 *Conference Record of the Forty Seventh Asilomar Conference on Signals, Systems and Computers (ASILOMAR)*, Nov. 2013
- [P3] Zhu Fu, and Alexander M. Wyglinski. “Digital Pre-distortion of Power Amplifier Impairments on Software-defined Radio Platforms”, *Electronics Letters, IET*, Dec 2013 [Submitted]

- [P4] Zhu Fu, Amit Sail, and Alexander M. Wyglinski. “Digital pre-distortion for power amplifier and I/Q modulator impairments in spectrally agile transmissions”, *EURASIP Journal on Wireless Communications and Networking*, Jan 2014 [Submitted]
- [P5] Zhu Fu, Lauri Anttila, Mikko Valkama, and Alexander M. Wyglinski. “Frequency-Selective Digital Predistortion for Spectrum Emission Reduction”, *IEEE Transactions on Communications*, April 2014 [Submitted]
- [P6] Zhu Fu, Lauri Anttila, Mahmoud Abdelaziz, Mikko Valkama, and Alexander M. Wyglinski. “On Digital Predistortion for Next Generation Wireless Networks: Improving Emission Mitigation in Spectrally Agile Waveforms”, *IEEE Communications Magazine*, April 2014 [Submitted]

Bibliography

- [1] Encyclopedia. (2014) Definition of: 802.11. [Online]. Available: <http://www.pcmag.com/encyclopedia/term/37204/802-11>
- [2] I. S. Association. (2014, Mar.) IEEE 802.11: Wireless lans. [Online]. Available: <http://standards.ieee.org/about/get/802/802.11.html>
- [3] C. Murariu. (2012, Sep.) Everything will be wireless, says intel. [Online]. Available: <http://news.softpedia.com/news/Everything-Will-Be-Wireless-Says-Intel-292335.shtml>
- [4] “IEEE standard for information technology– telecommunications and information exchange between systemslocal and metropolitan area networks– specific requirements– part 11: Wireless lan medium access control (mac) and physical layer (phy) specifications–amendment 4: Enhancements for very high throughput for operation in bands below 6 ghz.” *IEEE Std 802.11ac-2013 (Amendment to IEEE Std 802.11-2012, as amended by IEEE Std 802.11ae-2012, IEEE Std 802.11aa-2012, and IEEE Std 802.11ad-2012)*, pp. 1–425, Dec 2013.
- [5] CISCO. (2014, Mar.) 802.11ac: The fifth generation of Wi-Fi technical white paper. [Online]. Available: http://www.cisco.com/c/en/us/products/collateral/wireless/aironet-3600-series/white_paper_c11-713103.pdf
- [6] “IEEE standard for information technology - telecommunications and information exchange between systems - local and metropolitan area networks - specific requirements - part 11: Wireless lan medium access control (MAC) and physical layer (PHY)

- specifications - redline," *IEEE Std 802.11-2007 (Revision of IEEE Std 802.11-1999)* - *Redline*, pp. 1–1238, June 2007.
- [7] Federal Communications Commission Office of Engineering and Technology Policy and Rules Division. (2013, Apr.) FCC online table of frequency allocation. [Online]. Available: <http://transition.fcc.gov/oet/spectrum/table/fcctable.pdf>
 - [8] Federal Communications Commission (FCC), "Promoting more efficient use of spectrum through dynamic spectrum use technologies," November 2010.
 - [9] —, "Additional spectrum for unlicensed devices below 900 MHz and in the 3 GHz band," November 2010.
 - [10] S. Pagadarai, A. Wyglinski, and R. Rajbanshi, "A novel sidelobe suppression technique for ofdm-based cognitive radio transmission," in *3rd IEEE Symposium on New Frontiers in Dynamic Spectrum Access Networks, 2008. DySPAN 2008.*, oct. 2008, pp. 1–7.
 - [11] A. Wyglinski, "Physical layer loading algorithms for indoor wireless multicarrier systems," Ph.D. dissertation, McGill University, 2004.
 - [12] J. K. Cavers, "Amplifier linearization by adaptive predistortion," Sep. 17 1991, uS Patent 5,049,832.
 - [13] —, "Amplifier linearization using a digital predistorter with fast adaptation and low memory requirements," *IEEE Transactions on Vehicular Technology*, vol. 39, no. 4, pp. 374–382, 1990.
 - [14] Y. Akaiwa and Y. Nagata, "Highly efficient digital mobile communications with a linear modulation method," *IEEE Journal on Selected Areas in Communications*, vol. 5, no. 5, pp. 890–895, 1987.
 - [15] J. K. Cavers and M. W. Liao, "Adaptive compensation for imbalance and offset losses in direct conversion transceivers," *IEEE Transactions on Vehicular Technology*, vol. 42, no. 4, pp. 581–588, 1993.

- [16] J. K. Cavers, "The effect of quadrature modulator and demodulator errors on adaptive digital predistorters for amplifier linearization," *IEEE Transactions on Vehicular Technology*, vol. 46, no. 2, pp. 456–466, 1997.
- [17] ———, "New methods for adaptation of quadrature modulators and demodulators in amplifier linearization circuits," *IEEE Transactions on Vehicular Technology*, vol. 46, no. 3, pp. 707–716, 1997.
- [18] G. Breed, "An overview of common techniques for power amplifier linearization," *High Frequency Electronics*, pp. 44–46, 2010.
- [19] T. Arthanayake and H. Wood, "Linear amplification using envelope feedback," *Electronics Letters*, vol. 7, no. 7, pp. 145–146, 1971.
- [20] V. Petrovic and W. Gosling, "Polar-loop transmitter," *Electronics Letters*, vol. 15, no. 10, pp. 286–288, 1979.
- [21] A. Katz, "Linearizing high power amplifiers," *Application Note from Linearizer Technology, Inc*, 2001.
- [22] J. Dawson and T. Lee, "Automatic phase alignment for a fully integrated cartesian feedback power amplifier system," *Solid-State Circuits, IEEE Journal of*, vol. 38, no. 12, pp. 2269–2279, 2003.
- [23] J. Yi, Y. Yang, M. Park, W. Kang, and B. Kim, "Analog predistortion linearizer for high-power rf amplifiers," *IEEE Transactions on Microwave Theory and Techniques*, vol. 48, no. 12, pp. 2709–2713, 2000.
- [24] L. Ding, "Digital predistortion of power amplifiers for wireless applications," Ph.D. dissertation, Georgia Institute of Technology, 2004.
- [25] D. Morgan, Z. Ma, J. Kim, M. Zierdt, and J. Pastalan, "A generalized memory polynomial model for digital predistortion of rf power amplifiers," *IEEE Transactions on Signal Processing*, vol. 54, no. 10, pp. 3852–3860, oct. 2006.

- [26] L. Anttila, P. Händel, O. Mylläri, and M. Valkama, "Recursive learning based joint digital predistorter for power amplifier and I/Q modulator impairments," *International Journal of Microwave and Wireless Technologies*, vol. 2, no. 2, pp. 173–182, 2010.
- [27] H. Paaso and A. Mammela, "Comparison of direct learning and indirect learning predistortion architectures," in *IEEE International Symposium on Wireless Communication Systems. 2008. ISWCS '08.*, oct. 2008, pp. 309–313.
- [28] E. Biglieri, S. Barberis, and M. Catena, "Analysis and compensation of nonlinearities in digital transmission systems," *IEEE Journal on Selected Areas in Communications*, vol. 6, no. 1, pp. 42–51, 1988.
- [29] M. Schetzen, "Theory of pth-order inverses of nonlinear systems," *IEEE Transactions on Circuits and Systems*, vol. 23, no. 5, pp. 285–291, 1976.
- [30] A. Katz, "Linearization: Reducing distortion in power amplifiers," *IEEE Microwave Magazine*, vol. 2, no. 4, pp. 37–49, 2001.
- [31] W.-J. Kim, S. P. Stapleton, J. H. Kim, and C. Edelman, "Digital predistortion linearizes wireless power amplifiers," *IEEE Microwave Magazine*, vol. 6, no. 3, pp. 54–61, 2005.
- [32] M. Schetzen, "The volterra and wiener theories of nonlinear systems," 1980.
- [33] D. R. Morgan, Z. Ma, J. Kim, M. G. Zierdt, and J. Pastalan, "A generalized memory polynomial model for digital predistortion of RF power amplifiers," *IEEE Transactions on Signal Processing.*, vol. 54, no. 10, pp. 3852–3860, 2006.
- [34] H. Ku, M. D. McKinley, and J. S. Kenney, "Extraction of accurate behavioral models for power amplifiers with memory effects using two-tone measurements," in *Microwave Symposium Digest, 2002 IEEE MTT-S International*, vol. 1. IEEE, 2002, pp. 139–142.
- [35] R. Raich and G. Zhou, "Orthogonal polynomials for complex gaussian processes," *IEEE Transactions on Signal Processing*, vol. 52, no. 10, pp. 2788 – 2797, oct. 2004.

- [36] H. W. Kang, Y. S. Cho, and D. H. Youn, "On compensating nonlinear distortions of an ofdm system using an efficient adaptive predistorter," *IEEE Transactions on Communications*, vol. 47, no. 4, pp. 522–526, 1999.
- [37] H. Yang, P. F. Smulders, and E. Fledderus, "Comparison of single-and multi-carrier block transmissions under the effect of nonlinear hpa," in *14th IEEE Symposium on Communications and Vehicular Technology in the Benelux, 2007*. IEEE, 2007, pp. 1–7.
- [38] C. D. Presti, D. F. Kimball, and P. M. Asbeck, "Closed-loop digital predistortion system with fast real-time adaptation applied to a handset wcdma pa module," *IEEE Transactions on Microwave Theory and Techniques*, vol. 60, no. 3, pp. 604–618, 2012.
- [39] P. L. Gilabert, G. Montoro, E. Bertran, and J. A. García, "Fpga-based set-up for rf power amplifier dynamic supply with real-time digital adaptive predistortion," in *2010 IEEE Radio and Wireless Symposium (RWS)*. IEEE, 2010, pp. 248–251.
- [40] O. Sharifi-Tehrani, "Novel hardware-efficient design of lms-based adaptive fir filter utilizing finite state machine and block-ram," *Przegląd Elektrotechniczny*, vol. 87, pp. 240–244, 2011.
- [41] L. Anttila, M. Valkama, and M. Renfors, "Frequency-selective I/Q mismatch calibration of wideband direct-conversion transmitters," *IEEE Transactions on Circuits and Systems II: Express Briefs*, vol. 55, no. 4, pp. 359–363, 2008.
- [42] L. Anttila, P. Handel, and M. Valkama, "Joint mitigation of power amplifier and I/Q modulator impairments in broadband direct-conversion transmitters," *IEEE Transactions on Microwave Theory and Techniques*, vol. 58, no. 4, pp. 730–739, april 2010.
- [43] S. Pagadarai, *Sidelobe suppression for OFDM based cognitive radios in dynamic spectrum access networks*. ProQuest, 2007.
- [44] P. Chan, E. Lo, R. Wang, E. Au, V. Lau, R. Cheng, W.-H. Mow, R. Murch, and K. Letaief, "The evolution path of 4g networks: FDD or TDD?" *IEEE Communications Magazine*, vol. 44, no. 12, pp. 42–50, Dec 2006.

- [45] B. Laki and C. Kikkert, "Adaptive digital predistortion for wideband high crest factor applications based on the WACP optimization objective: A conceptual overview," *IEEE Transactions on Broadcasting*, vol. 58, no. 4, pp. 609–618, Dec 2012.
- [46] P. Roblin, S. K. Myoung, D. Chaillot, Y.-G. Kim, A. Fathimulla, J. Strahler, and S. Bibyk, "Frequency-selective predistortion linearization of rf power amplifiers," *IEEE Transactions on Microwave Theory and Techniques*, vol. 56, no. 1, pp. 65–76, Jan 2008.
- [47] M. Abdelaziz, A. Ghazi, L. Anttila, J. Boutellier, T. Lahteensuo, X. Lu, J. R. Cavallaro, S. S. Bhattacharyya, M. Juntti, and M. Valkama, "Mobile transmitter digital predistortion: Feasibility analysis, algorithms and design exploration," in *Signals, Systems and Computers (ASILOMAR), 2013 Conference Record of the Forty Seventh Asilomar Conference on*, Nov 2013.
- [48] T. L  hteensuo, "Linearity requirements in lte-advanced mobile transmitter," 2013.
- [49] M. Rahman, C. Tang, and B. Xu, "Systems and methods for spurious emission cancellation," Jun. 19 2012, uS Patent 8,204,456.
- [50] P.-i. Mak, P.-I. Mak, U. Seng-Pan, U. Seng-Pan, and R. Martins, "Transceiver architecture selection: review, state-of-the-art survey and case study," *IEEE Circuits and Systems Magazine*, vol. 7, no. 2, 2007.
- [51] A. Baschiroto, R. Castello, F. Campi, G. Cesura, M. Toma, R. Guerrieri, R. Lodi, L. Lavagno, and P. Malcovati, "Baseband analog front-end and digital back-end for re-configurable multi-standard terminals," *IEEE Circuits and Systems Magazine*, vol. 6, no. 1, pp. 8–28, 2006.
- [52] J.-M. Park, B.-J. Ku, Y.-S. Kim, and D.-S. Ahn, "Technology development for wireless communications system using stratospheric platform in korea," in *The 13th IEEE International Symposium on Personal, Indoor and Mobile Radio Communications, 2002.*, vol. 4. IEEE, 2002, pp. 1577–1581.

- [53] S. C. Cripps, *RF Power Amplifiers for Wireless Communications*, (Artech House Microwave Library (Hardcover)). Artech House, Inc., 2006.
- [54] M. Och. (2012, Nov.) Chapter 12. power amplifiers. [Online]. Available: <http://highered.mcgraw-hill.com/sites/dl/free/007297527x/329094/malvinoch12.pdf>
- [55] R. Ludwig, *RF Circuit Design: Theory & Applications*, 2/e. Pearson Education India, 2000.
- [56] M. K. Nezami, “Fundamentals of power amplifier linearization using digital pre-distortion,” *High Frequency Electronics*, pp. 54–59, 2004.
- [57] A. S. Sappal, M. S. Patterh, and S. Sharma, “Mitigation of non-linear impairments of w-cdma power amplifier.”
- [58] L. Butler, “Intermodulation performance and measurement of intermodulation components,” *Amateur Radio*, August, 1997.
- [59] P. M. Cabral, J. C. Pedro, and N. B. Carvalho, “Modeling nonlinear memory effects on the am/am, am/pm and two-tone imd in microwave pa circuits,” *International Journal of RF and Microwave Computer-Aided Engineering*, vol. 16, no. 1, pp. 13–23, 2006.
- [60] S. Boumaiza, T. Liu, and F. M. Ghannouchi, “On the wireless transmitters linear and nonlinear distortions detection and pre-correction,” in *Canadian Conference on Electrical and Computer Engineering, 2006. CCECE'06*. IEEE, 2006, pp. 1510–1513.
- [61] G. Xing, M. Shen, and H. Liu, “Frequency offset and I/Q imbalance compensation for direct-conversion receivers,” *IEEE Transactions on Wireless Communications*, vol. 4, no. 2, pp. 673–680, 2005.
- [62] “Evolved universal terrestrial radio access (EUTRA) and evolved universal terrestrial radio access network (EUTRAN) overall description, stage 2, 3GPP TS 36.300 v10.6.0.”

- [63] A. Wyglinski, “Cognitive radio communications and networks [guest editorial],” *IEEE Communications Magazine*, vol. 46, no. 4, pp. 30–31, April 2008.
- [64] “FCC 12-36 before the federal communications commission washington, D.C. 20554,” Federal Communications Commission , Tech. Rep., April 2012.
- [65] “IEEE standard for information technology– local and metropolitan area networks– specific requirements– part 22: Cognitive wireless ran medium access control (MAC) and physical layer (PHY) specifications: Policies and procedures for operation in the TV bands,” *IEEE Std 802.22-2011*, pp. 1–680, July 2011.
- [66] H. Holma and A. Toskala, *LTE for UMTS-OFDMA and SC-FDMA based radio access*. John Wiley & Sons, 2009.
- [67] “Radio transmission and reception (release 9)., 3GPP TS 36.101 version 9.3. 0 3GPP. 3rd generation partnership project.”
- [68] A. Yonis, M. Abdullah, and M. Ghanim, “LTE-FDD and LTE-TDD for cellular communications,” *Proc. Prog. Electromagn. Res. Sym*, pp. 1467–1471, 2012.
- [69] M. Al-Shibly, M. Habaebi, and J. Chebil, “Carrier aggregation in long term evolution-advanced,” in *2012 IEEE Control and System Graduate Research Colloquium (ICS-GRC)*, July 2012, pp. 154–159.
- [70] C. Herranz, V. Osa, J. Monserrat, D. Calabuig, N. Cardona, and X. Gelabert, “Cognitive radio enabling opportunistic spectrum access in lte-advanced femtocells,” in *Communications (ICC), 2012 IEEE International Conference on*, June 2012, pp. 5593–5597.
- [71] C. Park, L. Sundstrom, A. Wallen, and A. Khayrallah, “Carrier aggregation for lte-advanced: design challenges of terminals,” *IEEE Communications Magazine*, vol. 51, no. 12, pp. 76–84, December 2013.
- [72] Federal Communications Commission and others, “Spectrum policy task force report, FCC 02-155,” 2002.

- [73] —, “Unlicensed operation in the tv broadcast bands,” *ET Docket*, no. 04-186, 2004.
- [74] Federal Communications Commission (FCC), “Unlicensed operation in the tv broadcast bands,” November 2008.
- [75] —, “Unlicensed operation in the tv broadcast bands,” 2010.
- [76] C. Stevenson, G. Chouinard, Z. Lei, W. Hu, S. Shellhammer, and W. Caldwell, “IEEE 802.22: The first cognitive radio wireless regional area network standard,” *IEEE Communications Magazine*, vol. 47, no. 1, pp. 130–138, January 2009.
- [77] A. Flores, R. Guerra, E. Knightly, P. Ecclesine, and S. Pandey, “Ieee 802.11af: a standard for tv white space spectrum sharing,” *IEEE Communications Magazine*, vol. 51, no. 10, pp. 92–100, October 2013.
- [78] “IEEE draft standard for information technology - telecommunications and information exchange between systems - local and metropolitan area networks - specific requirements - part 11: Wireless lan medium access control (MAC) and physical layer (PHY) specifications amendment 5: Tv white spaces operation,” *IEEE P802.11af/D4.0*, April 2013, pp. 1–326, Oct 2013.
- [79] D. Lekomtcev and R. Maršálek, “Comparison of 802.11 af and 802.22 standards—physical layer and cognitive functionality,” *Elektro Revue*, vol. 3, no. 2, pp. 12–18, 2012.
- [80] M. Beluri, E. Bala, Y. Dai, R. Di Girolamo, M. Freda, J. Gauvreau, S. Laughlin, D. Purkayastha, and A. Touag, “Mechanisms for lte coexistence in tv white space,” in *2012 IEEE International Symposium on Dynamic Spectrum Access Networks (DYS-PAN)*., Oct 2012, pp. 317–326.
- [81] S. Shellhammer, A. Sadek, and W. Zhang, “Technical challenges for cognitive radio in the tv white space spectrum,” in *Information Theory and Applications Workshop, 2009*, Feb 2009, pp. 323–333.
- [82] Federal Communications Commission (FCC), “Second memorandum opinion and order,” 2010.

- [83] D. Datla, R. Rajbanshi, A. M. Wyglinski, and G. Minden, "Parametric adaptive spectrum sensing framework for dynamic spectrum access networks," in *2nd IEEE International Symposium on New Frontiers in Dynamic Spectrum Access Networks, 2007. DySPAN 2007.*, April 2007, pp. 482–485.
- [84] D. Datla, A. M. Wyglinski, and G. Minden, "A spectrum surveying framework for dynamic spectrum access networks," *IEEE Transactions on Vehicular Technology*, vol. 58, no. 8, pp. 4158–4168, Oct 2009.
- [85] Federal Communications Commission and others, "Office of engineering and technology announces the approval of google, inc.s TV bands database system for operation," *Public Notice FCC*, 2013.
- [86] M. Rahman, A. Behravan, H. Koorapaty, J. Sachs, and K. Balachandran, "License-exempt LTE systems for secondary spectrum usage: Scenarios and first assessment," in *2011 IEEE Symposium on New Frontiers in Dynamic Spectrum Access Networks (DySPAN).*, May 2011, pp. 349–358.
- [87] A. M. Wyglinski, "Effects of bit allocation on non-contiguous multicarrier-based cognitive radio transceivers," in *Vehicular Technology Conference, 2006. VTC-2006 Fall. 2006 IEEE 64th.* IEEE, 2006, pp. 1–5.
- [88] M. P. Wylie-Green, "Dynamic spectrum sensing by multiband ofdm radio for interference mitigation," in *2005 First IEEE International Symposium on New Frontiers in Dynamic Spectrum Access Networks, 2005. DySPAN 2005.* IEEE, 2005, pp. 619–625.
- [89] K. M. Bobrowski, "Practical implementation considerations for spectrally agile waveforms in cognitive radio," Ph.D. dissertation, Worcester Polytechnic Institute, 2009.
- [90] P. K. Dubey and N. Kumar, "Introduction to papr reduction techniques in OFDM signals."
- [91] G. Fettweis, M. Löhning, D. Petrovic, M. Windisch, P. Zillmann, and W. Rave, "Dirty RF: a new paradigm," *International Journal of Wireless Information Networks*, vol. 14, no. 2, pp. 133–148, 2007.

- [92] M. K. Nezami, "Fundamentals of power amplifier linearization using digital pre-distortion," *High Frequency Electronics*, pp. 54–59, 2004.
- [93] F. Raab, "Efficiency of outphasing rf power-amplifier systems," *IEEE Transactions on Communications*, vol. 33, no. 10, pp. 1094–1099, Oct 1985.
- [94] K.-W. Kim, "A fully-integrated all-digital outphasing transmitter for wireless communications," 2009.
- [95] J. S. Mandeep, A. Lokesh, S. I. S. Hassan, M. F. Ain *et al.*, "Design of cartesian feedback rf power amplifier for l-band frequency range," *Progress In Electromagnetics Research B*, vol. 2, pp. 207–222, 2008.
- [96] F. Guo, "A new identification method for wiener and hammerstein systems," Ph.D. dissertation, Institut für Angewandte Informatik, 2003.
- [97] A. Zhu and T. Brazil, "An overview of volterra series based behavioral modeling of rf/microwave power amplifiers," in *Wireless and Microwave Technology Conference, 2006. WAMICON '06. IEEE Annual*, dec. 2006, pp. 1–5.
- [98] T. Ogunfunmi, *Adaptive nonlinear system identification: the Volterra and Wiener model approaches*. Springer, 2007.
- [99] H. Ku and J. Kenney, "Behavioral modeling of nonlinear rf power amplifiers considering memory effects," *IEEE Transactions on Microwave Theory and Techniques*, vol. 51, no. 12, pp. 2495–2504, Dec 2003.
- [100] H. Ku, M. Mckinley, and J. Kenney, "Extraction of accurate behavioral models for power amplifiers with memory effects using two-tone measurements," in *Microwave Symposium Digest, 2002 IEEE MTT-S International*, vol. 1, 2002, pp. 139–142.
- [101] S. Sastry and M. Bodson, *Adaptive control: stability, convergence and robustness*. Courier Dover Publications, 2011.
- [102] F.-L. Luo, *Digital Front-End in Wireless Communications and Broadcasting: Circuits and Signal Processing*. Cambridge University Press, 2011.

- [103] D. Zhou and V. E. DeBrunner, "Novel adaptive nonlinear predistorters based on the direct learning algorithm," *IEEE Transactions on Signal Processing*, vol. 55, no. 1, pp. 120–133, jan. 2007.
- [104] A. Nordsjo, "An algorithm for adaptive predistortion of certain time-varying nonlinear high-power amplifiers," in *RADAR 2002*, 2002, pp. 469–473.
- [105] S. Haykin, "Adaptive filter theory, 1996," 2000.
- [106] P. S. R. Diniz, *Adaptive filtering: algorithms and practical implementation*. Springer, 2013.
- [107] Z. Fu, L. Anttila, M. Valkama, and A. M. Wyglinski, "Digital pre-distortion of power amplifier impairments in spectrally agile transmissions," in *2012 35th IEEE Sarnoff Symposium (SARNOFF)*, May 2012, pp. 1–6.
- [108] A. M. Wyglinski, M. Nekovee, and Y. T. Hou, *Cognitive radio communications and networks: principles and practice*. Burlington, MA, USA: Academic Press, 2009.
- [109] H. Bogucka, A. M. Wyglinski, S. Pagadarai, and A. Kliks, "Spectrally agile multicarrier waveforms for opportunistic wireless access," *IEEE Communications Magazine*, vol. 49, no. 6, pp. 108–115, 2011.
- [110] R. Airoidi, O. Anjum, F. Garzia, A. M. Wyglinski, and J. Nurmi, "Energy-efficient fast fourier transforms for cognitive radio systems," *IEEE Micro*, vol. 30, no. 6, pp. 66–76, 2010.
- [111] Z. Yuan, S. Pagadarai, and A. M. Wyglinski, "Feasibility of NC-OFDM transmission in dynamic spectrum access networks," in *Proceedings of the IEEE Military Communications Conference*, Oct. 2009, pp. 1–5.
- [112] S. Pagadarai, R. Rajbanshi, A. M. Wyglinski, and G. J. Minden, "Sidelobe suppression for OFDM-based cognitive radios using constellation expansion," in *Proceedings of the IEEE Wireless Communications and Networking Conference*, 2008, pp. 888–893.

- [113] S. Pagadarai, A. M. Wyglinski, and R. Rajbanshi, "A sub-optimal sidelobe suppression technique for ofdm-based cognitive radios," in *Proceedings of the IEEE Military Communications Conference*, Nov. 2008, pp. 1–6.
- [114] R. Rajbanshi, A. M. Wyglinski, and G. Minden, "Peak-to-average power ratio analysis for NC-OFDM transmissions," in *Proceedings of the IEEE 66th Vehicular Technology Conference*, 2007, pp. 1351–1355.
- [115] Q. Zou, A. Tarighat, and A. H. Sayed, "Compensation of phase noise in OFDM wireless systems," *IEEE Transactions on Signal Processing*, vol. 55, no. 11, pp. 5407–5424, 2007.
- [116] H. W. Kang, Y. S. Cho, and D. H. Youn, "On compensating nonlinear distortions of an OFDM system using an efficient adaptive predistorter," *IEEE Transactions on Communications*, vol. 47, no. 4, pp. 522–526, Apr. 1999.
- [117] H. Yang, P. F. M. Smulders, and E. Fledderus, "Comparison of single- and multi-carrier block transmissions under the effect of nonlinear hpa," in *14th IEEE Symposium on Communications and Vehicular Technology in the Benelux, 2007.*, Nov 2007, pp. 1–7.
- [118] R. Raich, H. Qian, and G. T. Zhou, "Orthogonal polynomials for power amplifier modeling and predistorter design," *IEEE Transactions on Vehicular Technology*, vol. 53, no. 5, pp. 1468–1479, 2004.
- [119] M. Valkama, "Advanced I/Q signal processing for wideband receivers: Models and algorithms," *Tampereen teknillinen yliopisto. Julkaisu-Tampere University of Technology. Publication; 350*, 2001.
- [120] D. C. Shah, B. U. Rindhe, and S. K. Narayankhedkar, "Effects of cyclic prefix on OFDM system," in *Proceedings of the International Conference and Workshop on Emerging Trends in Technology*, 2010, pp. 420–424.
- [121] C. Chatfield, *The analysis of time series: an introduction*. CRC press, 2013.

- [122] M. Bartholomew-Biggs, *Nonlinear optimization with engineering applications*. Springer, 2008, vol. 19.
- [123] S. Haykin, “Adaptive filter theory,” *Prentice Hall*, vol. 2, pp. 478–481, 2002.